

Critical Analysis of Dry Storage Temperature Limits for Zircaloy-Clad Spent Nuclear Fuel Based on Diffusion Controlled Cavity Growth

T.A. Hayes

*University of California, San Diego
La Jolla, California 92093 USA*

R.S. Rosen

*Lawrence Livermore National Laboratory
Livermore, California 94550 USA*

M.E. Kassner

*Oregon State University
Corvallis, Oregon 97331 USA*

U.S. Department of Energy

Lawrence
Livermore
National
Laboratory

December 1999

DISCLAIMER

This document was prepared as an account of work sponsored by an agency of the United States Government. Neither the United States Government nor the University of California nor any of their employees, makes any warranty, express or implied, or assumes any legal liability or responsibility for the accuracy, completeness, or usefulness of any information, apparatus, product, or process disclosed, or represents that its use would not infringe privately owned rights. Reference herein to any specific commercial product, process, or service by trade name, trademark, manufacturer, or otherwise, does not necessarily constitute or imply its endorsement, recommendation, or favoring by the United States Government or the University of California. The views and opinions of authors expressed herein do not necessarily state or reflect those of the United States Government or the University of California, and shall not be used for advertising or product endorsement purposes.

Work performed under the auspices of the U. S. Department of Energy by the University of California Lawrence Livermore National Laboratory under Contract W-7405-Eng-48.

This report has been reproduced
directly from the best available copy.

Available to DOE and DOE contractors from the
Office of Scientific and Technical Information
P.O. Box 62, Oak Ridge, TN 37831
Prices available from (423) 576-8401
<http://apollo.osti.gov/bridge/>

Available to the public from the
National Technical Information Service
U.S. Department of Commerce
5285 Port Royal Rd.,
Springfield, VA 22161
<http://www.ntis.gov/>

OR

Lawrence Livermore National Laboratory
Technical Information Department's Digital Library
<http://www.llnl.gov/tid/Library.html>

Critical Analysis of Dry Storage Temperature Limits for Zircaloy-Clad Spent Nuclear Fuel Based on Diffusion Controlled Cavity Growth

T.A. Hayes¹, R.S. Rosen² and M.E. Kassner³

Summary

Upon removal from reactor, spent nuclear fuel (SNF) rods are placed in wet storage for a period of generally 5 years or more. Wet storage capacity at commercial nuclear power plants is inadequate to hold all fuel rods until a permanent disposal site becomes available. This has led to the development of interim dry storage, where SNF rods are placed inside of a canister, usually concrete with a stainless steel liner, in an inert atmosphere while awaiting permanent disposal. An increasing number of rods are now being placed into interim dry storage due to delays in the availability of a permanent disposal site (mined geologic repository). The ultimate duration of the interim dry storage period is unknown because acceptance of fuel into the repository is not scheduled to begin for at least another decade and an application for licensing approval of the repository has not yet been made. However, safe interim dry storage must be maintained for a minimum of twenty years according to Nuclear Regulatory Commission (NRC) licensing requirements and, therefore, dry interim storage of SNF rods is of critical concern.

The NRC has accepted two models to define the temperature limit, or maximum allowable initial temperature, for interim dry storage of SNF rods. These models are based on the diffusion controlled cavity growth (DCCG) failure mechanism as proposed by Raj and Ashby. DCCG is assumed to be the controlling failure mechanism based on current fracture theory of metals under conditions similar to dry storage. There is a lack

¹ Research Assistant, University of California, San Diego, La Jolla, California 92093-0418

² Lawrence Livermore National Laboratory, Livermore, California 94550

³ Northwest Aluminum Professor of Mechanical Engineering, Oregon State University, Corvallis, Oregon 97331

of experimental evidence either supporting or refuting this theory for zirconium, zirconium alloys (Zircaloy), or other alloys, as creep tests have not been performed to failure under conditions relevant to dry storage. Dry storage temperature limits are determined by using either the equations developed by Lawrence Livermore National Laboratory (LLNL) or temperature limit curves developed by Pacific Northwest National Laboratory (PNNL) based on deformation and fracture mapping. Though these two models are based on the same fundamental failure theory (DCCG), the two groups of researchers have made different assumptions, including selection of the most critical variables in the DCCG equation. These inconsistencies are discussed in this report.

Recently, some researchers have proposed using a strain-based failure model to predict maximum allowable SNF storage temperatures. The NRC is now accepting this approach and state that it should be used in place of the LLNL DCCG model (though they still feel that the DCCG based PNNL model is acceptable). The applicability of a strain-based approach is discussed in this report. Briefly, as DCCG is assumed to be the failure mechanism of Zircaloy, a strain-based failure model is not applicable since progression of damage by DCCG is *independent of strain*. This is true of both currently accepted models (by PNNL and LLNL) as they are both based on DCCG.

We determined that the most important variables in the currently accepted failure models are the equation for temperature decay of the fuel rods, $T(t)$, the activation energy for grain boundary diffusion of the Zircaloy cladding (which is coupled with temperature to determine the grain boundary diffusion coefficient), Q_{gb} , and the assumed cavity spacing, λ . In fact, one can, simply by changing Q_{gb} within the range of reported values, achieve a range of predictions from failure in a relatively short time to failure never occurring. The most critical parameter *that can be regulated* by the proposed licensee is the temperature of the rods.

Temperature is an exponential term in the DCCG fracture equation and, thus, small changes in temperature can have a significant effect on the resulting predicted failure

times and hence the maximum initial allowable temperature. Modeling has shown that the most accurate temperature decay model for fuel rods under dry storage conditions is a power-type temperature decay. Using a power temperature decay profile, however, results in a very strong sensitivity to the initial fuel temperature. We will show that the use of a linear temperature decay profile decreases the predicted failure time and decreases the sensitivity of the failure time to the initial temperature or fuel age. The sensitivity is reduced as a direct result of the difference in behavior of a linear function compared to a power function. We have evaluated the sensitivity of predicted failure times to changes in the initial temperature for various temperature profiles.

We recommend that the proposed dry storage licensees use one of two fuel rod temperature decay profiles in determining the maximum allowable storage temperature. The first choice would be for the individual vendor (licensee) to use an accurate profile measured under the proposed storage configuration. If the temperature profile is not accurately known for the proposed storage configuration, we recommend that a conservative linear decay profile be used instead of a power decay profile for reasons discussed below.

The lack of experimental data for the activation energy for grain boundary diffusion of the Zircaloy cladding (Q_{gb}), has led to an uncertainty of several orders of magnitude in values for grain boundary diffusion coefficients and hence predicted failure times. Only one study performed to date has directly measured the grain boundary diffusion coefficient of zirconium. We recommend that current models use the results of this study in place of previously chosen diffusion coefficients. Using this value reduces some of the uncertainty of current models. Further grain boundary diffusion studies should be carried out to verify these reported values and to measure the effects of alloying and irradiation on the grain boundary diffusion coefficient.

Current models assume that a fixed number of cavities exist along grain boundaries upon insertion into dry storage. These cavities are assumed to grow with time until the void area reaches a certain percentage of the grain boundary area, at which point

failure is assumed to occur, or at least the fuel is considered unsafe for post-dry-storage handling. It is not clear whether values chosen in the current models for the cavity spacing, λ , are conservative or realistic. Data on void nucleation in zirconium did not appear to indicate that void nucleation reaches a saturation point. Assuming a fixed number of cavities, therefore, may overestimate the distance between cavities. Also, many recent studies have shown that irradiation can result in void nucleation in the vicinity of, and possibly on, grain boundaries with cavity spacings more than an order of magnitude lower than values chosen for the current models. We recommend that a smaller, more conservative cavity spacing be chosen until further experimentation can more accurately determine the cavity spacing under conditions relevant to dry storage.

The shortcomings inherent in the current models result in temperature limits for dry storage that may be non-conservative. Since DCCG may be the operational fracture mechanism under dry storage conditions, the three key variables (T , Q_{gb} and λ) should be better defined through extensive experimentation. It is therefore recommended that grain boundary diffusion experiments and creep testing on pure zirconium, zirconium alloys and irradiated zirconium alloys under typical dry storage conditions be started immediately. The predicted failure times can be quite low under dry storage conditions, and these tests could verify if short predicted failure times such as these are reasonable. Creep testing followed by damage examination could help support or refine the current creep models. Long term testing could help determine whether or not the existing failure models are conservative. These tests would allow observance of failure in Zircaloy under conditions similar to dry storage. Observing failure would enable the relevant fracture mechanism for Zircaloy to be better quantified. Until these tests are completed, we feel that using the model suggested by LLNL, with input values for T , Q_{gb} and λ modified as mentioned above, is the most reasonable option.

Table of Contents

Summary	i
1 Introduction	1
2 Current Models	2
2.1 Lawrence Livermore National Laboratory Analysis [3]	4
2.2 Pacific Northwest National Laboratory Analysis [4]	4
2.3 Inconsistency between LLNL and PNNL	7
2.3.1 PNNL comparison between CSFM and LLNL models	8
2.3.2 Assumed fracture mechanism	12
2.3.3 Recovery factor	12
2.3.4 Material condition assumed to correspond to failure	14
2.3.5 Inconsistency in assumed inputs	15
2.4 Critical factors to be input by proposed dry storage licensee	15
2.4.1 Temperature	15
2.4.1.1 PNNL suggested temperature decay profile	16
2.4.1.2 Effect of changing the upper integration limit, t_i	19
2.4.1.3 Choosing a temperature decay profile	21
2.4.1.3.1 Method suggested by LLNL [3]	22
2.4.1.3.2 Method suggested by PNNL [4]	22
2.4.1.3.3 A more conservative approach: 5 year old SNF	25
2.4.1.3.4 A more conservative approach: older SNF	29
2.4.2 Cladding stress	34
2.5 Critical material parameters	35
2.5.1 Grain boundary diffusion coefficient	35
2.5.1.1 General discussion of diffusion in zirconium	35
2.5.1.2 Diffusion coefficient value chosen by PNNL [4]	36
2.5.1.3 Diffusion coefficient value chosen by LLNL	37
2.5.1.4 Discussion of the diffusion coefficient values chosen by LLNL and PNNL	38
2.5.1.5 Current grain boundary diffusion data	39
2.5.1.6 Irradiation effects	39
2.5.1.7 Differences between zirconium and zirconium alloys	40
2.5.2 Cavity spacing	41
2.6 Conclusions about current models	43
3 Rod Surveillance Testing	43
4 Discussion of Brookhaven National Laboratory 1989 [41] and 1994 [45] Reports	44
4.1 The BNL strain-based approach	45
4.2 Errors committed by BNL	46
4.3 Conclusions about the BNL work	48
5 Discussion of April 1999 LLNL report	48
6 Conclusions	50
7 Recommendations	51
7.1 Recommended model	51
7.2 Recommended SNF temperature decay profile	52
7.3 Recommended experiments	52

8	Acknowledgements	53
9	List of Symbols [3,36]	54
10	References	56
	Appendix A: Discussion of LLNL [3] Report	A-1
	A1.1 Raj and Ashby [36]	A-1
	A1.2 LLNL [3]	A-3
	A1.3 Derivation of Raj and Ashby f(A) equation	A-5
	Appendix B: Evaluation of and Comparison of LLNL and PNNL Suggested Constants	B-1
	B1.1 Input values suggested by PNNL	B-1
	B1.1.1 Chin 1983 [37]:	B-1
	B1.1.2 Chin 1986 [32]	B-2
	B1.1.3 Chin 1987 (PNNL) [4]:	B-3
	B1.1.4 Chin 1987 [28] and Chin 1989 [81]:	B-3
	B1.1.5 Chin 1992 [82]:	B-3
	B1.2 Comparison and discussion of LLNL and PNNL suggested input values	B-5
	B1.2.1 Atomic volume, Ω :	B-5
	B1.2.2 Grain boundary thickness, δ :	B-5
	B1.2.3 Average cavity spacing, λ :	B-6
	B1.2.4 Grain boundary diffusion, D_{gb} :	B-9
	B1.2.5 Other constants in the fracture equation:	B-11
	B1.2.6 Recovery Factor	B-11
	B1.3 Results:	B-13
	B1.4 Sensitivity of current models to the fracture equation input variables	B-13
	B1.4.1 LLNL model evaluated using the most conservative constants	B-14
	B1.4.2 LLNL model evaluated using the least conservative constants	B-15
	B1.4.3 Discussion	B-16
	B1.5 Model sensitivity using the grain boundary diffusion coefficient of Vieregge and Herzig [174]	B-16
	B1.5.1 Combination of most and least conservative input variables	B-17
	B1.5.2 Variability within range of error report by Vieregge and Herzig [174]	B-18
	Appendix C: Mathcad Documents Used to Evaluate the Failure Models	C-1

Figures

Figure 1 Fracture map for Zircaloy developed by PNNL [4]	5
Figure 2 Comparison of PNNL and LLNL “40 year” initial temperature limits for 5 year old fuel (based on Figure D.4 in the PNNL report [4])	11
Figure 3 Plot of power temperature decay function (T in °C and t in months) used by PNNL [4]	17
Figure 4 The value of the integral of G(t) as a function of the upper integration limit, t_r , for 5 year old fuel rods	18
Figure 5 Comparison of a 40 year, a 5 year and a 1 year failure line predicted using the LLNL criteria (assuming the atomic volume approximation reported by PNNL, b^3 , is equal to $3.37 \times 10^{-29} \text{ m}^3/\text{atom}$ [4])	20
Figure 6 Comparison of 1 year, 5 year and 40 year failure lines (temperature limits) as predicted by the PNNL model [4] (PNNL model reproduced using Mathcad – see Appendix C)	21
Figure 7 Comparison of power and linear temperature decrease profiles for 5 year old fuel rods	26
Figure 8 Fracture time as a function of initial storage temperature for linear and power temperature decay functions for 5 year old fuel rods with an initial cladding hoop stress of 100 MPa	28
Figure 9 Comparison of the value of the integral of $\int_0^{t_r} G(t)dt$ (from LLNL) as a function of the upper integration limit, t_r , for power and linear temperature decay functions for 5 year old fuel rods with an initial cladding hoop stress of 100 MPa	29
Figure 10 Comparison of power and linear temperature decrease profiles for 10 year old fuel rods suggested by PNNL [4] and BNL [45], respectively	32
Figure 11 Fracture time as a function of initial storage temperature for a linear and power temperature decay function for 10 year old fuel rods with an initial stress of 100 MPa	32

Figure 12 The value of the integral of $G(t)$ as a function of the upper integration limit, t , for 5, 10 and 15 year old fuel rods (normalized so that the time 0 on the abscissa corresponds to the time of insertion into dry storage) using an initial (start of dry storage) stress of 100 MPa and an initial (start of dry storage) temperature of 385°C _____ 33

Figure A-1 Void configuration assumed by Raj and Ashby [36] _____ A-9

Figure A-2 A more realistic configuration for a periodic array of voids in a grain boundary _____ A-10

Figure B-1 Creep cavity nucleation data for Zircaloy-2 at 350°C and 375°C [54] ____ B-7

Tables

Table 1 Peak (while under vacuum) temperatures and normal dry (helium gas) initial storage temperatures for rods under surveillance [50]	25
Table 2 Cumulative LWR (light water reactor) spent fuel inventory of all operating reactors in year 1986 [4]	30
Table B-1 Most conservative input values for the LLNL fracture time prediction	B-14
Table B-2 Least conservative input values for the LLNL fracture time prediction	B-15
Table B-3 Most conservative input values for the LLNL fracture time prediction based on the grain boundary diffusion coefficient of Vierrege and Herzig [174]	B-17
Table B-4 Least conservative input values for the LLNL fracture time prediction based on the grain boundary diffusion coefficient of Vierrege and Herzig [174]	B-18

1 Introduction

Interim dry storage of spent nuclear fuel (SNF) rods is of critical concern because a shortage of existing SNF wet storage capacity combined with delays in the availability of a permanent disposal repository has led to an increasing number of SNF rods being placed into interim dry storage. Safe interim dry storage must be maintained for a minimum of twenty years according to the Standard Review Plan for Dry Cask Storage Systems [1] and the Code of Federal Regulations, 10 CFR Part 72 [2]. Interim dry storage licensees must meet certain safety conditions when storing SNF rods to ensure that there is a “very low probability (e.g. 0.5%) of cladding breach during long-term storage” [1].

Commercial SNF typically consists of uranium oxide pellets surrounded by a thin cladding. The cladding is usually an α -zirconium based alloy known as “Zircaloy”. In dry storage, the SNF rods are confined in one of several types of cask systems approved by the Nuclear Regulatory Commission (NRC). “The cask system must be designed to prevent degradation of fuel cladding that results in a type of cladding breach, such as axial-splits or ductile fracture, where irradiated UO_2 particles may be released. In addition, the fuel cladding should not degrade to the point where more than one percent of the fuel rods suffer pinhole or hairline crack type failure under normal storage conditions [1].”

The NRC has approved two models [3,4] for use by proposed dry storage licensees to determine the maximum initial temperature limit for nuclear fuel rods in dry storage that supposedly meet the above criteria and yield consistent temperature limits. Though these two models are based on the same fundamental failure theory, different assumptions have been made including the choice of values for material constants in the failure equation. This report will examine and compare the similarities and inconsistencies of these two models. It will illustrate some of the shortcomings of the current models and suggest modifications as well as some experiments that should be started in the near future. This report will also discuss

changes in the current NRC standards with regard to the adoption of a strain-based model to be used to determine maximum allowable temperatures of the SNF.

2 Current Models

Currently, temperature limits, or the maximum allowable initial temperatures for interim dry storage of SNF rods, are determined using either the equations developed by Lawrence Livermore National Laboratory (LLNL) [3] or temperature limit curves developed by Pacific Northwest National Laboratory (PNNL) [4] based on fracture mapping. Individual storage licensees are given the option to evaluate dry storage temperature limits based on either model, as both models are currently believed to predict consistent results [1]. The PNNL fracture maps are used to determine the controlling mechanism (controlling fracture equation) under any given set of dry storage conditions. Although PNNL [4] reports that these two models yield nearly consistent temperature limits, this consistency appears unlikely as conflicting assumptions are utilized in developing the failure criteria (as will be discussed later). Both the PNNL and the LLNL models predict that cavitation failure under dry storage conditions may occur by diffusion controlled cavity growth (DCCG), which is associated with high temperature creep of some metals.

Many investigators [5-22] have suggested that under conditions similar to those relevant to dry storage, the creep-cavity growth mechanism may not be exclusively DCCG, but rather a coupled diffusion and power law creep mechanism. This coupled mechanism assumes that, under certain conditions, cavity growth proceeds by a combination of diffusion from the cavity walls to the surrounding grain boundary material and power law creep of the material surrounding the expanding cavities and associated diffusion zones. It is unclear, however, how this mechanism could operate in the case of Zircaloy under dry storage conditions. Without large far field strains (as is absent in the case of the creep of Zircaloy fuel rods [23-28]), cavity growth does not seem possible by power law creep as suggested in the coupling models. If large triaxial stresses are present or significant cavity-cavity interaction occurs (giving rise to local high triaxial stress-states) the plastic strain to failure

would, perhaps, be reduced in which case some sort of coupling model would, possibly, be appropriate. No evidence, however, has been found supporting cavity interaction resulting in enhanced triaxial stress states in Zircaloy. Also, there is no evidence that elastic incompatibility stresses across grain boundaries would significantly increase the triaxiality in Zircaloy [29-31]. Thus, we tentatively concluded that, in the absence of new experimental data, a diffusion controlled cavity growth model is most reasonable and is assumed to be applicable throughout this report. This is consistent with the PNNL and LLNL models and assumptions (though PNNL indicated in other documents that they believe in a coupled type mechanism [28,32,33]– see discussion below).

The NRC recently dismissed the LLNL model as “overly restrictive” and replaced it with a strain-based model [34] as suggested by a group at Brookhaven National Laboratory (the strain-based model is discussed below). They also state that “recently developed literature” (without specific reference) does not support the use of DCCG for zirconium-based metals. This position seems unsubstantiated, at least according to data available to the current authors. The suggestion to eliminate the LLNL model based on the premise that DCCG is not a relevant fracture mechanism while still accepting the PNNL model is inconsistent, as the PNNL model is also based on DCCG. When questioned on this position, the NRC stated [35] that they still accept DCCG as a possible fracture mechanism, but dismiss LLNL’s treatment of DCCG (treatment referring to what values used to evaluate the DCCG failure equation). They still accept PNNL’s treatment of DCCG because it was found to be more conservative than that by LLNL [35]. This is in conflict with calculations in this report (and those made by PNNL) which show that the LLNL model predicts a more conservative temperature limit for most stresses relevant to dry storage conditions (less than about 110 MPa). Since both models utilize DCCG and since DCCG is still an accepted fracture mechanism for Zircaloy under dry storage conditions, we will discuss both the LLNL and PNNL models in this report.

2.1 Lawrence Livermore National Laboratory Analysis [3]

LLNL uses the diffusion controlled cavity growth (DCCG) analysis by Raj and Ashby [36] to predict the time to failure of Zircaloy under dry storage conditions based on a 'limited damage' approach. LLNL supplies suggested values for the parameters in the Raj and Ashby failure equations and leaves the stress and temperature profiles of the Zircaloy SNF during dry storage to be supplied by the individual licensees depending on the specific storage conditions. The equations can be used to calculate initial SNF temperature limits for specified temperatures and stresses. It is shown in Appendix A that the LLNL solution results directly from the Raj and Ashby work. The principal contributions by LLNL were to suggest values for the constants to be substituted into the Raj and Ashby failure equation for the case of Zircaloy and establish a different failure criterion based on estimated post-dry-storage loading (this will be discussed in detail below). The conservatism of the values suggested by LLNL is evaluated in Appendix B.

2.2 Pacific Northwest National Laboratory Analysis [4]

PNNL predicted maximum initial dry storage temperatures (that, as will be shown, ultimately determine the fracture time) using a fracture map that accounts for various fracture mechanisms predicted to be active over the relevant range of stresses and temperatures. PNNL assumed that all fracture mechanisms act independently and that damage occurring by the independent mechanisms is additive. Failure times were calculated by summing (over the lifetime of the SNF) the amount of "damage" predicted to occur during each time increment based on the fracture mechanism predicted for the conditions associated with that time increment. Damage is calculated simply as a ratio of the time spent under the given conditions to the time necessary for fracture under those conditions. Fracture was assumed to occur when the summation of these time-incremental ratios reached 1. For example, if the ratio for 1st time increment were 0.5 based on DCCG and 0.5 for the 2nd time increment based on power law creep, the summation of the 1st and 2nd time increments would be 1 and the SNF would be predicted to fail.

Under dry storage conditions (stresses from 0-160 MPa and temperatures ranging from 200 to 450°C), the fracture map developed by PNNL indicates that either DCCG (approximately 0-110 MPa) or power law creep growth (approximately 110-160 MPa) controls failure (see Figure 1). PNNL called their model, which uses this fracture map to predict the initial dry storage temperature, the Commercial Spent Fuel Management (CSFM) model.

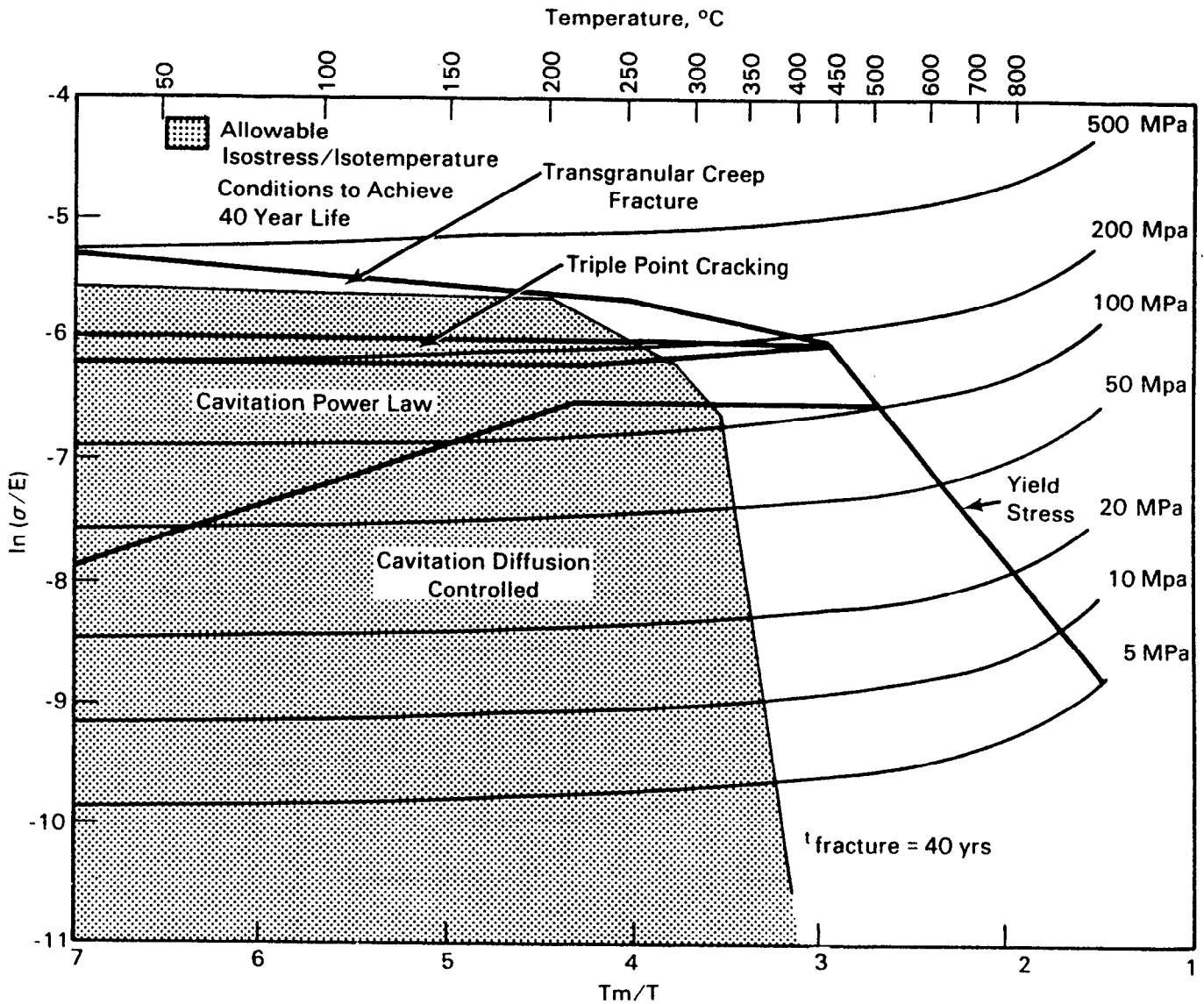


Figure 1 Fracture map for Zircaloy developed by PNNL [4]

The diffusion controlled cavity growth equation used by PNNL to develop the fracture maps is reported as

$$t_f = 2.525 \times 10^{-3} \frac{kT}{b^3 \left[D_{0gb} \exp\left(\frac{-Q_{gb}}{RT}\right) \right] \delta\sigma} l^3 \quad \text{Eq. (1)}$$

It is worth noting that this equation, which forms the basis for most temperature limit predictions under SNF dry storage conditions (below ~110MPa), is *not* strain dependent. Although PNNL states (when explaining the fracture map construction in other reports [28,32,33]) that cavitation should occur by a coupling of cavity growth by diffusion and power law creep, they use only a diffusion based fracture equation for this region. The power law fracture equation is assumed, according to the PNNL equations, to act independently and in a different stress regime than the DCCG fracture equation. The basis for choosing this equation to describe DCCG was not explicitly stated by PNNL, nor in any of the reports referenced by PNNL that were available to us, though two previous PNNL reports [32,37] referenced four sources [36,38-40] that they “considered” when developing the fracture equation for DCCG. A comparison of the fracture equation reported by PNNL (Equation 1) with the Raj and Ashby fracture equation [36] is useful to help determine the basis for Equation 1. The fracture equation given by Raj and Ashby is

$$t_f = \frac{3\pi^{1/2}}{32} \frac{f_v(\alpha)}{f_B(\alpha)^{3/2}} \int_{A_{min}}^{A_{max}} \frac{dA}{f(A)} \frac{kT}{\Omega D_{gb} \delta\sigma} \frac{1}{\rho^{3/2}} \quad \text{Eq. (2)}$$

or, simplifying by combining the constants [including the integral of the area function and functions of α (functions defined by Raj and Ashby based on energy angles of the grain boundary cavities)],

$$t_f = C \frac{kT}{\Omega D_{gb} \delta \sigma} \frac{1}{\rho^{3/2}} \quad \text{Eq. (3)}$$

where C is a condensed constant. Condensing the constant to allows for direct comparison with the PNNL DCCG equation, which contains a similar condensed constant (basis or “deconvolution” of the constant was not reported by PNNL).

Raj and Ashby use the cavity area density ρ instead of the half cavity spacing, l ($\lambda/2$), as shown in Equation 2. The cavity density can be expressed by

$$\rho = \frac{1}{\lambda^2} \quad \text{Eq. (4)}$$

or,

$$\lambda^3 = \frac{1}{\rho^{3/2}} \quad \text{Eq. (5)}$$

PNNL used the cube of the Burgers vector (b) as an approximation for the atomic volume (Ω). The cube of the cavity spacing (λ) is equivalent to the inverse of the cavity density (ρ) raised to the 3/2 power as shown above. It is apparent, then, that PNNL used the Raj and Ashby [36] DCCG model. This is the same conclusion made by BNL [41] upon examining the PNNL failure equations. The Raj and Ashby work is also the basis of the LLNL DCCG failure model.

2.3 Inconsistency between LLNL and PNNL

Assuming conditions that would indicate DCCG is operative, PNNL claims that the NRC [42] (the NRC report is apparently based on the work of LLNL [3] and thus will hereafter be referred to as LLNL) predicts temperature limits nearly consistent with those calculated by PNNL. At first, this appears to be a coincidence that occurred due to a misapplication of the LLNL failure equation. This apparent coincidence and

the true inconsistencies between the LLNL and PNNL models are discussed in the following sections.

2.3.1 PNNL comparison between CSFM and LLNL models

The equations used to calculate a failure time (initial temperature) as it appears in the NRC [42] report and the LLNL work [3] is

$$\int_{A_i}^{A_f} \frac{dA}{f(A)} = \int_0^{t_f} G(t)dt \quad \text{Eq. (6)}$$

The function $f(A)$ is defined by LLNL as

$$f(A) = \frac{\left[1 - \left(\frac{A_f}{A}\right)^{1/2}\right](1-A)}{A^{1/2} \left[\frac{1}{2} \ln\left(\frac{1}{A}\right) - \frac{3}{4} + A\left(1 - \frac{A}{4}\right) \right]} \quad \text{Eq. (7)}$$

The physical basis for these equations is discussed in Appendix A. In Equation 6, A_f is the area fraction of decohesion that occurs over the time t_f . The area fraction of decohesion is simply the ratio of the void area in the grain boundary to the total grain boundary area. Equation 7 is a function of the area fraction of decohesion, A , developed from the volumetric cavity growth rate, dV/dt (see reference [36]). Failure is assumed to occur, according to LLNL, when 15% area fraction of decohesion ($A = 0.15$) occurs. LLNL [3] claims that this is a conservative estimate, as the value of 15% was determined to be the maximum decohesion limit that would still allow safe handling at the end of dry interim storage based on the work of Chun et al. [43,44]. Post-dry-storage processing may be necessary to move the fuel rods to a permanent SNF storage facility.

PNNL reported [4] (Table D.1 in PNNL-87) that the NRC [42] (LLNL [3]) model uses the following equations to calculate failure times:

$$A_f = \int_0^{t_f} G(t) dt < 0.15 \quad \text{Eq. (8) PNNL}$$

$$G(t) = \frac{32 f_B^{3/2}(\alpha) \Omega \delta \sigma_\infty(t) D_{gb}(t)}{3\pi f_v(\alpha) k\lambda^3 T(t)} \quad \text{Eq. (9) PNNL}$$

Equation 9 varies from what is reported by LLNL (Equation (2-3) of reference 3) by only a minor factor in that the π term in the denominator appears in LLNL and Raj and Ashby as $\pi^{1/2}$. The reason for this difference is likely due to a typographical error in the NRC report [42] (which also reports the equation as π rather than $\pi^{1/2}$) as it is presumably based on the work of LLNL [3]. Equation 8, however, is incorrectly reported by PNNL. PNNL reports Equation 8 above and references the NRC [42] as the source of that equation. The PNNL authors have replaced the integral on the left hand side of Equation 6 with the value suggested by LLNL for the area fraction of decohesion limit of 0.15. The value of 0.15 should have been used as the integration limit, A_i , of the function $f(A)$ in Equation 6, not the value of the integral of $G(t)$ as shown in Equation 8. The error that PNNL committed is equivalent to assuming that the integral of $dA/f(A)$ is equal to A (the area fraction of decohesion), or,

$$\int_{A_i}^{A_f} \frac{dA}{f(A)} = 0.15 \quad \text{(Eq. 6 evaluated incorrectly)}$$

This error in Equation 8 is also made in the text where PNNL states in section D.1 that “this criterion is equivalent to specifying that the integral of $G(t)dt$ shall be less than 0.15 after 20 years in dry storage” [4].

The integrand of Equation 6, as defined by Equation 7, has a singularity at the lower limit of integration which causes the integral to be undefined at $A_i=0$. Therefore, it can be evaluated only when $A_i>0$. Any value chosen for the initial area fraction of decohesion, A_i , less than 0.001 (0.1%) yields a value for the integral of

approximately 0.026 (if evaluated correctly). The value chosen for the initial area fraction of decohesion in the unfractured, metal ($t=0$) is not very critical. The fraction of area occupied by cavities in the uncrept material should be minimal, even with a small assumed initial cavity spacing, and thus a very small value for A_i is reasonable (much less than 0.1%). Thus, when evaluated correctly,

$$\int_{A_i}^{A_f} \frac{dA}{f(A)} = 0.026 \quad (\text{Eq. 6 evaluated correctly})$$

This value is not close to the value of 0.15 used by PNNL. In order for the integral on the left hand side of Equation 6 to equal 0.15, one would have to integrate to a maximum area fraction of decohesion limit, A_f , of more than 200%, which, of course, is physically impossible. A group at Brookhaven National Laboratory (BNL) also noted this error in the PNNL report [45].

Considering the magnitude of the PNNL error in Equation 8, one would not expect the PNNL and LLNL results to be as consistent as they are reported to be by PNNL [4] (see Figure 2 below). However, it appears that the error discussed above was an internal inconsistency within the PNNL report. That is, PNNL [4] reports the LLNL equation incorrectly as shown in Equation 8 above, but it appears that they applied the equation correctly (as reported in Equation 6 above) when they developed the plots* shown in Figures D.2 through D.5 of the PNNL report.

Figure 2 below is a reproduction of Figure D.4 from the PNNL report [4] that shows two predictions for the 40 year failure (temperature) limit. One is based on the PNNL CSFM generic temperature limit. The second was evaluated by PNNL using the LLNL model and associated constants. Both models were evaluated using the temperature decay profile shown in Figure 3 (this is discussed in Section 2.4.1.1). Although the captions referring to the LLNL model in Figures D.2 through D.5 in the

* These figures plot the initial dry storage temperature as a function of initial cladding stress for 40 years in dry storage.

PNNL report [4] (from which Figure 2 is made) are wrong, as was the PNNL text, the lines showing the LLNL prediction on the figures are actually correct. We verified this by integrating the LLNL equation with the LLNL recommended constants* using the continuous power temperature decay function reported by PNNL [4]. The LLNL 40 year failure line we calculated is essentially identical to what PNNL calculated (see Figure 2 below and Figure D.4 of the PNNL report [4]). Thus, apparently, PNNL evaluated the integral correctly as shown above in Equation 6, and just reported the equation incorrectly as shown in Equation 8.

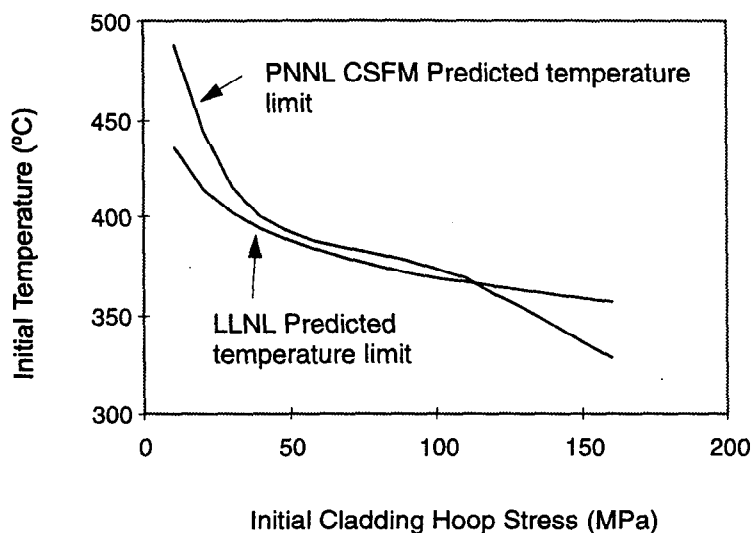


Figure 2 Comparison of PNNL and LLNL “40 year” initial temperature limits for 5 year old fuel (based on Figure D.4 in the PNNL report [4])

Thus, it appears that the LLNL (Raj and Ashby) DCCG failure model and the PNNL model yield fairly similar results between about 40 and 110 MPa initial cladding hoop stress, as shown in Figure 2. This figure, although evaluated using the correct LLNL equation, is still misleading for the following reasons. The near coincidence of the model predictions (between 40 and 110 MPa) results from a fortuitous combination of differing assumptions by LLNL and PNNL. The failure line predicted in Figure 2 is

* Except for the atomic volume where PNNL [4] reported a different value than LLNL [3] and was thus chosen when examining the PNNL evaluation of the LLNL equations.

also misleading as a result of the assumed temperature decay profile. Because of the extreme sensitivity of the models when used with the PNNL suggested power temperature decay profile, initial temperatures which are thought to predict failure in 40 years actually predict failure in 5 years. These issues are discussed as follows and in Appendix B.

2.3.2 Assumed fracture mechanism

Upon examining the PNNL study, we determined that the DCCG fracture mechanism controls fracture up to the CSFM temperature limit curve inflection point in Figure 2 at approximately 110 MPa. For initial stresses above 110 MPa, PNNL predicts that power law creep will control failure. As noted above, PNNL assumes that all failure mechanisms act independently. This is contrary to PNNL's explanation in other reports [28,32,33] about how DCCG should be coupled with a power law creep controlled mechanism. The LLNL study assumes DCCG is operational over the entire stress regime relevant to dry storage. This is not a debilitating assumption, because the stresses in dry storage typically fall in the region where the PNNL failure line and the LLNL failure lines have a consistent shape (<110 MPa where both models predict failure occurs by DCCG).

Since both failure models are based, for the most part, on the DCCG model developed by Raj and Ashby [36], one may wonder why even slightly inconsistent failure times are predicted (as shown in Figure 2 above). The inconsistency between the PNNL and LLNL models arises as a result of different assumptions and different choices for values for the material constants used in the Raj and Ashby DCCG failure equation (that is used to determine the initial dry storage temperature limit). These differences are discussed subsequently.

2.3.3 Recovery factor

The cause of the increasing divergence of the two models at low stresses (<40MPa), where both models predict failure will occur by DCCG, is the increased effect of a "recovery factor" used by PNNL (which was not used by LLNL). In

calculating the initial maximum dry storage temperature limits, PNNL modified the DCCG fracture equation (and other fracture equations) by including a “recovery factor” in its analysis. This is explained in references 28 and 32, but not mentioned in the principal PNNL report [4]. This “recovery factor” is used to account for the reduction in ductility of zirconium and zirconium alloys as a result of irradiation damage. The “recovery factor” was based on studies that showed that irradiated Zircaloy had between 200% to 1000% less ductility than non-irradiated Zircaloy [46-48] (typical fracture strains from 5-12% compared to 25-50%) [28]. Chin states the following [28]: “Irradiation was assumed to reduce the ductility of the cladding by a factor of 10 in the stress temperature region of interest for dry storage” because “... the primary effect of irradiation is a reduction in ductility which leads to a reduction in the fracture time by some constant factor”.

Chin reported that in dry storage some or all of this ductility will be recovered as a result of damage recovery in Zircaloy, especially above 350°C [28]. Chin developed a function to calculate this “recovery factor” as a function of time and temperature. Basically, the result is that the predicted failure time used for the *initial* time increment ratio for the life fraction rule is multiplied by 0.10, thus assuming that the failure time is proportional to ductility or strain to fracture. This “recovery factor” increases (to a maximum of 1) with time at higher temperatures due to an estimated recovery of ductility. Although the “recovery factor” changes with time at a given temperature, these changes have very little effect on the resulting fracture time below an initial temperature of approximately 400°C (initial stresses above approximately 40 MPa) for dry storage conditions as very little recovery of ductility is predicted to occur. This is higher than the 350°C stated by Chin because under dry storage conditions, there is a continuously decreasing temperature profile. With initial temperatures up to nearly 400°C, the fuel does not spend enough time at temperatures above 350°C for significant ductility recovery to occur. The predicted

* See Appendix C under the PNNL model or reference 28 for a description of this function.

fracture time is reduced by a factor of approximately 10 if all other factors are held constant (constant temperature).

It is this “recovery factor” that causes the difference in *shape* between the PNNL curve and the LLNL curve in Figure 2 at low stresses (below about 40 MPa). This factor was not considered by LLNL.

The fact that LLNL did not use this recovery factor warrants some discussion. If one examines the DCCG model and assumptions, one immediately notes that the model is *not* a function of strain. That is to say that the predicted failure time does not depend on the amount of strain that the metal experiences but rather only on grain boundary diffusion. Because it is independent of strain, a reduced ductility would not directly affect the fracture time. It would seem, then, that PNNL has included an unwarranted conservatism in this case.

2.3.4 Material condition assumed to correspond to failure

Another difference between the PNNL and LLNL models is the area fraction of decohesion assumed to correspond to failure. As discussed above, LLNL chose a value of 0.15 based on estimated post-dry-storage handling of the fuel rods [44]. The PNNL model, however, incorporated the original form (without apparent modification besides the recovery factor described above) of the Raj and Ashby [36] failure equation. In the development of this equation, Raj and Ashby assumed that failure occurs when the area fraction of decohesion reaches 50% or 0.50. This is much less conservative than the value of 0.15 chosen by LLNL. PNNL suggests integrating the LLNL model to an area fraction of decohesion of 0.20 in order to bring the 40 year failure lines of the PNNL and LLNL model more into coincidence, however the two models would still be applying different failure criteria (PNNL uses 0.5, not 0.15 or 0.2).

2.3.5 Inconsistency in assumed inputs

Part of the inconsistency between the two models arises because PNNL and LLNL chose different values for the material constants used in the DCCG failure equation (that is used to determine the initial dry storage temperature limit). These differences occur in the following terms:

- i. Atomic volume, Ω*
- ii. Grain boundary thickness, δ*
- iii. Average cavity spacing, λ*
- iv. Grain boundary diffusion coefficient (constant, D_o^{gb} , and activation energy, Q_{gb})*
- v. Other unspecified constants*

All of these terms are either proportional or inversely proportional to the fracture time except the activation energy, which appears inside an exponential term, and the cavity spacing, which is a cubed term. Potentially, then, the most substantial source of inconsistency between LLNL and PNNL is the value assigned to the activation energy for grain boundary diffusion. A detailed description of these differences appears in subsequent sections and in Appendix B.

2.4 Critical factors to be input by proposed dry storage licensee

2.4.1 Temperature

Both models are very sensitive to changes in the temperature decay profile. A calculated initial temperature thought to cause failure in 40 years essentially predicts failure in 5 years for the *same* initial temperature when using a temperature profile such as Equation 10 below, which PNNL suggests is reasonable. This sensitivity is now discussed.

2.4.1.1 PNNL suggested temperature decay profile

The application of the LLNL failure equation which results in the 40 year failure line (initial temperature limit) shown in Figure 2 is misleading as a result of the nature of the assumed temperature decay profile. The temperature profile used by PNNL when evaluating the LLNL equation is

$$T(K)=2.09 \times 10^3 (t)^{-0.282} \quad \text{Eq. (10)}$$

where t is the time in months. The pre-factor 2.09 can be adjusted to modify the initial temperature of the SNF. This equation calculates the temperature under dry storage conditions as a function of time after removal from reactor (the initial time being the time of removal from reactor). Because this is a power decaying temperature function, the temperature initially decreases rapidly, and decreases more slowly with time, as illustrated in Figure 3.

The temperature near the origin (approaching $t=0$) in Figure 3 is very high. This is much higher than is ever experienced by the fuel rods in wet storage. The profile actually predicts the temperature behavior of the rod if it were to be inserted into dry storage immediately following removal from the reactor (which is defined as $t=0$). In fact, the rods generally spend 5 years or more in low temperature ($<100^\circ\text{C}$) wet storage (storage in water pools) before insertion into dry storage. Thus, the above temperature prediction (Equation 10) is only used after insertion into dry storage, which we assume to be 5 years (60 months) for the current discussion. Older fuel rods (which have spent longer times in wet storage) will be discussed in a subsequent section of this report. Briefly, for older fuel rods, the same temperature equation may be utilized, but the starting point (time when removal from dry storage occurs) is simply moved to the right on the abscissa to the appropriate time [4].

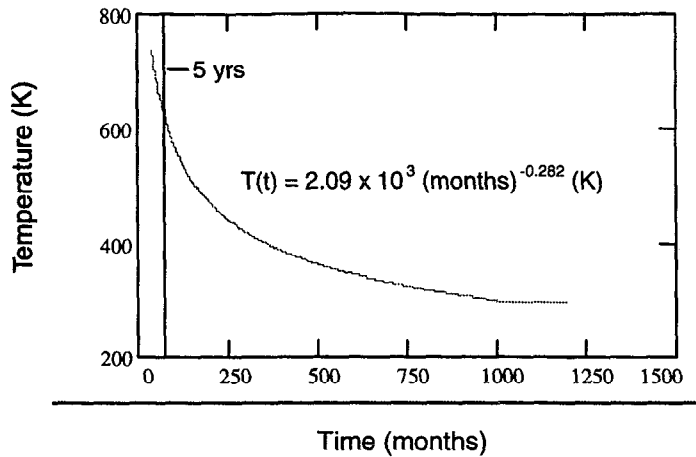
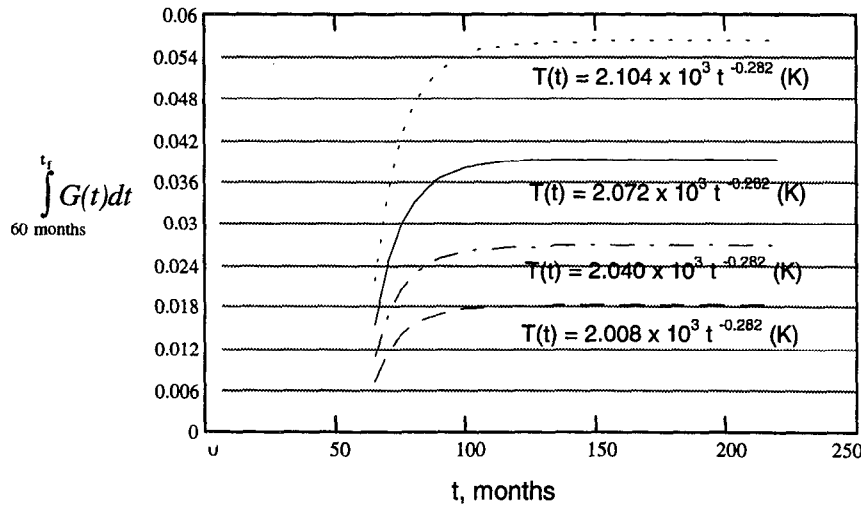


Figure 3 Plot of power temperature decay function (T in °C and t in months) used by PNNL [4]

The behavior of the power temperature decay function (initially decreasing very rapidly) has a dramatic effect when substituted into a function such as G(t), which has multiple temperature dependent terms including the diffusion coefficient and the stress. Because of the substantial temperature dependence of the DCCG fracture equation, when it is evaluated using Equation 10 as the temperature profile nearly all of the predicted damage occurs within the first 5 years. This is illustrated in Figure 4, which shows the integral of G(t) as a function of the upper integration limit, t_i , for 60 month old fuel. Changes in the initial temperature for the power decay functions shown in Figure 4 were achieved by slightly adjusting the value of the coefficient (as was the procedure used by PNNL [4]). The values used for input into the G(t) equation for Figure 4 are listed below Figure 4 and can be found in more detail in the List of Symbols and Appendix B. Again, the 60 month limit is the time that the fuel rods are removed from wet storage and inserted into dry storage.

The time at which the radionuclide gasses inside the fuel rod start to decay, then, is 5 years before insertion into dry storage. All temperature decay profile determinations (models) made by PNNL [4] were based on the time decay of the fission gas products (upon discharge from reactor, the fission gasses mainly consist

of H, He, Kr, Xe and a small fraction of Rn [49]). This decay starts at time zero (removal from reactor) and continues during wet and dry storage. Because the PNNL report first discussed 5 year old fuel, data on the figures below start at a time on the abscissa of 60 months, or 5 years.



Parameter values used for $G(t)$: $f_B = \pi \sin^2 \alpha$, $f_V = 2/3 \pi (2 - 3 \cos \alpha + \cos^3 \alpha)$, $\Omega = 3.37 \times 10^{-29}$ $m^3/atom$, $\delta = 9.69 \times 10^{-10}$ m , $\lambda = 10 \times 10^{-6}$ m , $D_{gb} = 5.9 \times 10^{-6} \exp[(-131 \text{ kJ/mole})/RT]$ m^2/sec , $\alpha = 50^\circ$, $\sigma(t) = 100 T(t)/T(60)$ MPa

Figure 4 The value of the integral of $G(t)$ as a function of the upper integration limit, t_i for 5 year old fuel rods

These results were calculated using the definition for $G(t)$ reported above as Equation 7 except using the correct value of $\pi^{1/2}$ in the denominator rather than π . The integral of $G(t)$ reaches 99% of the maximum value at approximately 60 months after insertion into dry storage (120 months after removal from the reactor). After the first 5 years in dry storage, then, no further significant damage is predicted. Four temperature profiles were compared in Figure 4 to show that the amount of time for nearly all of the damage to accumulate is relatively insensitive to changes in the initial temperature of the SNF for this type of power decay profile. If a power type temperature profile such as Equation 10 is the best choice for fuel rod temperature prediction in dry storage (this will be discussed later), then using the LLNL and PNNL DCCG models predict that *all* damage will occur within the first 5 years in dry

storage. In other words, if failures are predicted to occur, they will occur in the first 5 years of dry storage*. Predictions of short-term failures could be checked using a relatively short-term creep test that simulates the predicted power temperature decay behavior. Because of the temperature sensitivity, care must be exercised when evaluating the integral of $G(t)$ to a large upper integration limit. This temperature sensitivity is what makes the predicted maximum allowable temperatures somewhat misleading. This is now discussed.

2.4.1.2 Effect of changing the upper integration limit, t_f

If one integrates a function such as $G(t)$ using the suggested power decay function, the maximum value of this function will be reached in a relatively short time (with an upper limit on the order of 5 years as was shown in the previous section). If the same function is, instead, integrated to a time, t_f , of 40 years, the same integrated value is obtained (to 2 significant digits). For example, the integral of $G(t)$ from $t_i = 60$ months (5 year old fuel at the time of removal from wet storage) to $t_f = 110$ months with a hoop stress at 60 months of 100 MPa and a temperature at 60 months of 369 °C, is equal to 0.026**. When integrated to an upper limit of 540 months (40 years after placement in dry storage), the resulting value is still 0.026. If one assumes that failure occurs when first reaching a limit of 0.026 for the integral as suggested by LLNL, then failure is predicted after only 50 months in dry storage. If however, one were to integrate to an upper integration limit of 40 years without noting the behavior of the value of the integrated function, then the resulting value might give the impression that failure just occurred upon reaching the upper integration limit of 40 years. As a result, the 40 year LLNL failure line appearing in Figure 2 above is actually the same as a 5 year failure line. This is shown more clearly in Figure 5, below, which shows the 40 year failure line predicted by the LLNL model that appeared in Figure 2, above, compared to failure lines which show the conditions necessary for failure after 5 years and for failure after 1 year.

* A failure, according to the LLNL criteria discussed above, implies that the material has experienced a reduced cross sectional area, not necessarily a rupture.

** Initial values of 100 MPa and 369°C are arbitrary, but reasonable and realistic, choices.

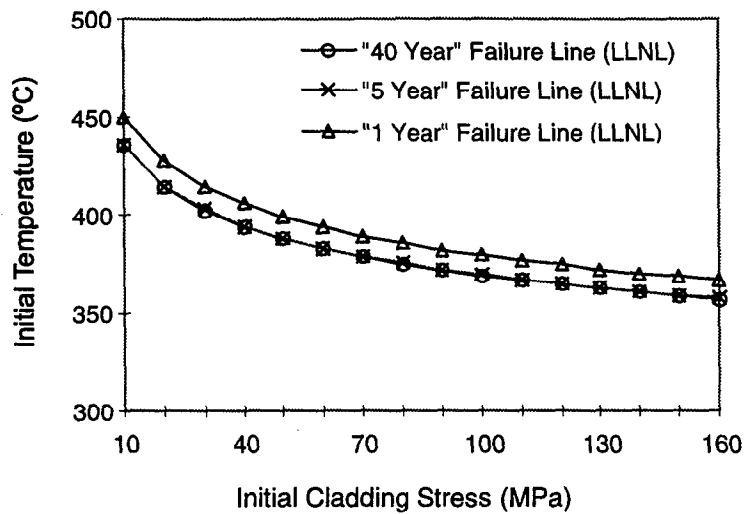


Figure 5 Comparison of a 40 year, a 5 year and a 1 year failure line predicted using the LLNL criteria (assuming the atomic volume approximation reported by PNNL, b^3 , is equal to 3.37×10^{-29} $m^3/atom$ [4])

It is difficult to distinguish between the 40 year and the 5 year LLNL failure lines as they are practically coincident. The 40 year failure line shown by PNNL for the LLNL failure prediction then, is, in reality, a 5 year failure line. It may be noted in Figure 5 that the line showing failure after only 1 year is also very close to the 40 year line predicted by LLNL. When assuming a temperature profile similar to Equation 10, very small changes in the initial temperature result in large differences in the predicted failure time. Alternatively, large changes in the specified failure times result in insignificant changes in the maximum allowable initial temperature (e.g., failure times ranging from 5 years to infinity). Therefore an applicant who determines a maximum temperature for a predicted failure of, say, 300 years has, at the same time, predicted failure after 5 years which is less than the licensed period of the storage facility. A group at Brookhaven National Laboratory (BNL) made similar conclusions about the temperature sensitivity of the LLNL model [41,45].

This same argument of sensitivity to temperature can also be made about the PNNL analysis. That is that the 40 year failure line calculated using the PNNL model is

coincident with the calculated 5 year failure line (within a fraction of a degree). This is shown in Figure 6 below. This figure was developed using Mathcad (mathematics software) to evaluate the PNNL model. The initial temperature limit curve corresponding to a 40 year failure prediction in Figure 6 varies from about two degrees (at higher stresses) to a maximum of about 20 degrees (at stresses below about 40 MPa) higher than the same curve reported by PNNL. The cause of this difference is not known, but presumably it has to do with how we evaluated the PNNL model. The details of the PNNL model are in reference 28, (by Chin, one of the authors of the PNNL report [4]) which also includes code for a program that calculates the maximum allowable temperature limits for given fuel conditions (age, stress). The fact that both models are so sensitive to the temperature profile has important implications for interim dry storage licensees using either model to certify a safe maximum allowable temperature limit. Because of this extreme sensitivity, we suggest using a conservative temperature profile.

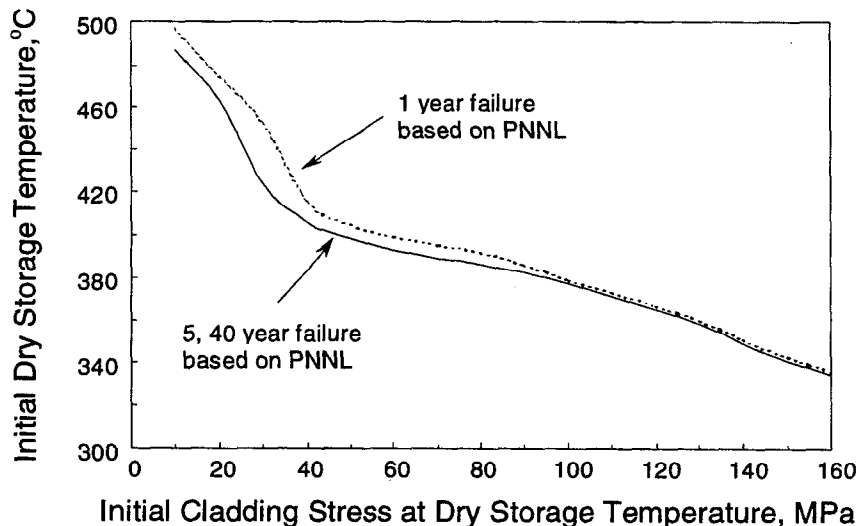


Figure 6 Comparison of 1 year, 5 year and 40 year failure lines (temperature limits) as predicted by the PNNL model [4] (PNNL model reproduced using Mathcad – see Appendix C)

2.4.1.3 Choosing a temperature decay profile

As suggested earlier, the temperature decay profile is *the most critical factor that the dry storage facility must supply* to predict the initial fuel rod temperature limit when

applying the LLNL model. Temperature is substituted into an exponential term in the DCCG fracture equation. Thus, small changes in temperature can have a significant effect on the resulting predicted fracture time and, therefore, the initial temperature limit. Choosing a single reasonable temperature decay profile to substitute into the failure equations is not straightforward as it is a function of fuel age, burnup level (amount of nuclear-reactor fuel consumption) and storage conditions.

2.4.1.3.1 Method suggested by LLNL [3]

LLNL does not suggest a temperature profile, but rather leaves this to the discretion of the individual storage facility based on the facility's TSAR (Topical Safety Analysis Report). This may leave the storage facility with insufficient guidance to apply a temperature decay model that is conservative under their specific storage conditions. The temperature decay profile given in a TSAR may not be conservative, as will be discussed below.

2.4.1.3.2 Method suggested by PNNL [4]

PNNL suggested a general temperature decay profile as a function of fuel age based on heat transfer analysis of two typical configurations and states that this should be modified to accommodate changes in the storage configuration [4]. These analyses were performed on the TN-24P and REA-2023 storage casks (two types of storage casks that are currently used to store SNF) with computer codes capable of predicting cladding temperatures to within $\pm 30^{\circ}\text{C}$ of measured temperatures [33]. The calculations were based on 1 year old fuel (fuel that had spent one year in wet storage) with a burnup level of 30 MWd/kgM. Because the TN-24P was determined to have the slower cooling rate of the two analyzed casks, this profile was chosen by PNNL to develop the generic temperature limits. PNNL [4] states that using this profile is very conservative for two reasons. First, it is based on the TN-24P cask configuration that was determined to have a slower cooling rate than the REA-2023 casks. Second, temperature profiles for older fuel (which decay more slowly) are developed by simply extrapolating the 1 year old temperature decay curve to the appropriate time and increasing the initial temperature. PNNL [4] states that using this method to develop older fuel temperature profiles predicts a slower temperature

decay rate than would be predicted if heat transfer models were used to predict the actual temperature decay of older fuel. They also state that this temperature profile is conservative enough that it always over predicts the rod temperature, even when considering rod consolidation that tends to increase rod temperatures and decrease heat transfer rates. It is not clear whether PNNL used the conservative (high) end of the $\pm 30^{\circ}\text{C}$ uncertainty of the computer generated temperature decay profile. It is important that the conservative end of this range be chosen, as a 60°C temperature swing would have a dramatic effect on the predicted failure time.

The PNNL analysis treated the temperature decay as a function of the SNF age (time in wet storage) and the storage conditions [storage atmosphere, rod configuration (rod spacing, number of rods, rod orientation), and burnup level]. The result of the PNNL analysis suggests using a power function with a negative exponent to approximate the temperature decay. This means the temperature decays rapidly at first and more slowly with time. The physical reason that the initial temperature decay rate is predicted to be more rapid is because the short-lived fission products disappear relatively quickly, after which time the decay is governed by the long-lived fission products [4]. Accordingly, fuel rods that spend more time in wet storage have less short-lived fission products and the temperature decays at a slower rate when inserted into dry storage. This suggested method for determining a temperature decay profile should also, however, be regarded with caution due to the extreme sensitivity of failure time to storage temperature.

Assuming that the PNNL calculated profile or the profile obtained from the TSAR is correct under the given storage conditions, there are likely to be variations that have not been accounted for in the profile. For example, the rod temperature during the short-term exposure to a vacuum upon removal from wet storage prior to the start of dry storage is not clear. During this time, heat transfer rates are diminished substantially as the rods are put under a vacuum to remove all moisture. McKinnon and Gilbert report an example of the temperature behavior under a vacuum drying

process [50]. They report that temperatures in the vacuum process exceeded initial storage temperatures by as much as 83°C (see Table 1 below) “during vacuum runs that typically had a duration of less than one week.” Although these peak temperatures are fairly high, it has been reported elsewhere [51] that vacuum drying can remove water trapped in the fuel rods* at temperatures “less than 200°C”. Later McKinnon and Deloach [52] reported that “temperatures during double pump-down increased by <20°C for less than 2 hours but it is anticipated that evacuating and backfilling the cask after loading in a water basin will require a longer period and result in higher temperature increases.” It was reported by Cunningham et al. that a common method of cask drying is a vacuum process that requires several hours (2 to 5) [33] and cite data from experience in Germany that showed that “excursions above 380°C are unlikely” [33]. We were not, however, able to find any standard or regulation regarding this process. Presumably an analysis of the effect of temperature excursions during vacuum drying on cladding integrity would be included in the safety analysis report. Table 1 below shows temperatures measured during a vacuum drying process on SNF. In Table 1, the highest temperature reached under vacuum as reported by McKinnon and Gilbert (Table 4.1) [50] appears as the “peak vacuum” temperature, while the normal dry initial storage temperature is denoted as the “initial helium” temperature.

Because the failure time is so sensitive to the storage temperature, any anomalies in the rod temperature could cause significant progression of DCCG. For example, fuel rods stored at 424°C under a hoop stress of 100 MPa for one week are predicted by LLNL to experience approximately 2.7% area fraction of decohesion**. In contrast, PNNL suggested that limited exposure to these temperature levels could actually be beneficial to the fuel rods [33], as some irradiation damage recovery would occur, increasing the ductility of the Zircaloy rods. It is not clear, however, what, if any,

* Water is trapped in the exterior scale or corrosion products on the fuel rods during wet storage.

** Determined by setting the upper integration limit of the integral of $G(t)dt$ equal to 0.25 months and solving for the area fraction of decohesion.

effect this recovery would have on the DCCG damage progression (e.g. effect on the number of cavities and cavity nucleation).

Table 1 Peak (while under vacuum) temperatures and normal dry (helium gas) initial storage temperatures for rods under surveillance [50]

Cask	Fuel	Temperatures, °C Peak Vacuum (t < 168 h) / Initial Helium (storage time)
Castor V21	21 PWR Assemblies	424 / 350 (t = 9.1 y)
TN-24P	48 PWR Assemblies (24 Canister)	290 / 221 (t = 1.4 y)
TN-24P (Consolidated)	48 PWR Assemblies	293 / 211 (t = 0.4 y)
MC-10	24 PWR Assemblies	217 / 139 (t = 1.4 y)
MC-10 (Consolidated)	34 PWR Assemblies (17 Canister)	397 / 321 (t = 9.2 y)
REA	52 PWR Assemblies	227 / 144 (t = 0.4 y)

PNNL [4] also stated that with more extended burnup of fuel (length of time rods are used in the nuclear reactor before the start of wet storage) planned for the future, more long-lived fission products would be produced causing peak temperatures to increase and temperature decay rates to decrease. Another uncertainty in rod temperature results from the lack of uniformity in the airflow within the dry storage cask. McKinnon and Deloach [52] reported that convection within a given cask may be increased or decreased throughout the cask to the point where in certain locations, according to their measurements, there is an “absence of convection” [52]. In view of these considerations, a more conservative temperature profile than a typical measured or calculated profile may be warranted.

2.4.1.3.3 A more conservative approach: 5 year old SNF

Brookhaven National Laboratory (BNL) [45], suggested that a linear temperature decay profile is reasonable for 10 year old fuel. Using a linear temperature decay decreases the predicted failure time and decreases the sensitivity of the failure time to the initial temperature or fuel age. The sensitivity is reduced as a result of the

difference in behavior between a linear decay function and a power decay function. The equations suggested by BNL for 10 year old fuel are not, however, directly relevant to the current discussion of 5 year old fuel. In order to illustrate the decreased sensitivity to the initial temperature resulting from more conservative temperature profiles, we developed a set of new profiles. These profiles, illustrated in Figure 7 below, range between the power temperature decay profile suggested by PNNL [4] and a linear profile based on a linear simulation of the PNNL profile.

$T_1(t)$ in Figure 7 is the temperature profile suggested by PNNL. Profiles 2 through 5 are decreasingly concave power decay functions generated by decreasing the magnitude of the negative exponent in the PNNL function and adjusting the coefficient to make the temperature at 60 months equal to that of the PNNL function (659 K or 386°C). The reason for choosing decreasingly concave functions was that these offer gradually more and more conservative temperature decay profiles before reaching the most conservative linear profile. Profile $T_6(t)$ was interpolated from the

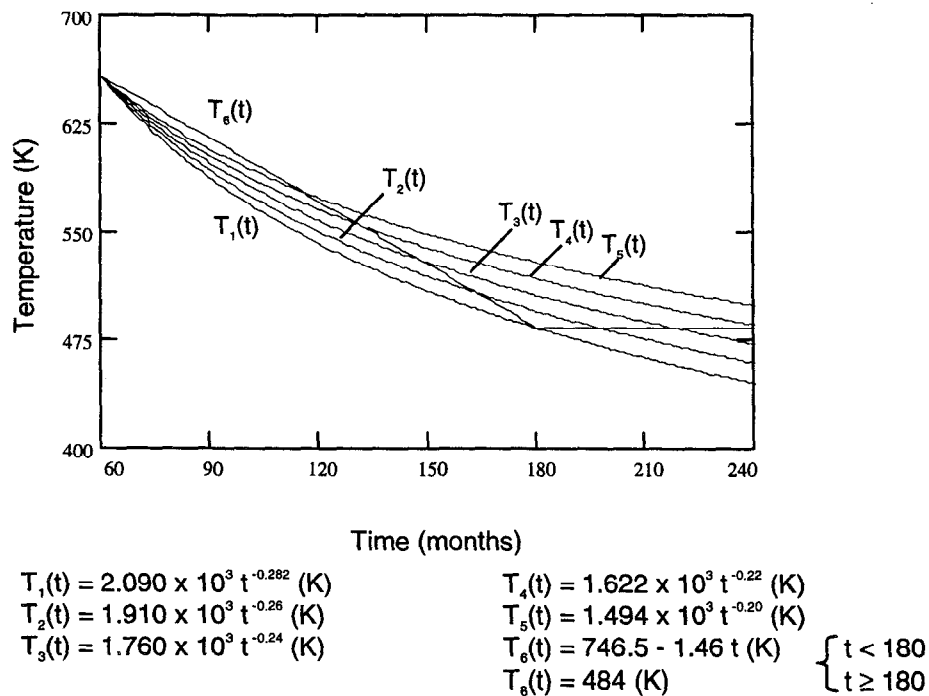
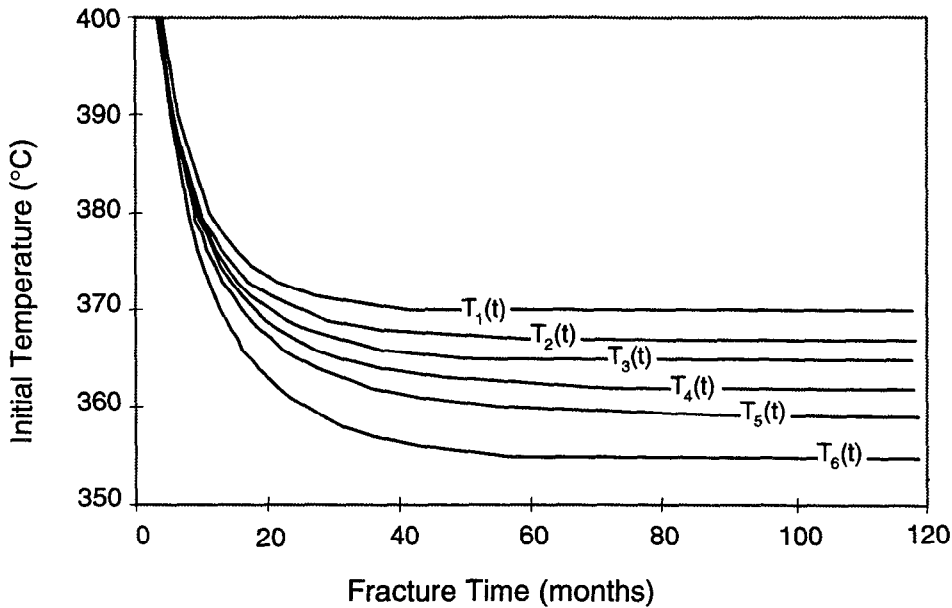


Figure 7 Comparison of power and linear temperature decrease profiles for 5 year old fuel rods

PNNL function by making the temperature equal to that of the PNNL function at both 60 and 180 months (insertion into dry storage and 10 years after insertion). After 10 years the temperature was assumed to be constant so that the linear function never became less conservative than the PNNL power decay function. Although the temperature should continue to decrease at some rate after 10 years as well, the behavior after 10 years is not of great importance as nearly all of the predicted damage occurs before 10 years (see discussion above).

Figures 8 and 9 below illustrate how more conservative temperature decay profiles affect the predicted failure times based on the LLNL model. Figure 8 shows the fracture time predicted by the LLNL model as a function of the initial storage temperature for the linear and power temperature decay functions. Figure 9 compares the value of the integral of $G(t)$ (from LLNL) as a function of the upper integration limit for power and linear temperature decay functions. Changes in the initial temperature for the power decay functions in Figures 8 and 9 were achieved by slightly adjusting the values of the pre-exponential terms (same procedure used by PNNL [4]). An initial stress of 100 MPa was chosen for reasons that will be discussed in the next section. Briefly, 100 MPa was chosen because it slightly overestimates the maximum stress according to experimentally measured stresses, and thereby (at least partially) allows for non-ideal conditions (such as stress concentrations, etc.) and rods that have experienced higher burnup levels. The stress is assumed to change with temperature according to the ideal gas law.

In Figure 8, the linear temperature decay profile was a function of the power decay profile (see definition below Figure 8) so that as the shape of the power decay profile changed with the initial fuel temperature, the linear profile changed accordingly. The constants (denoted by C) were adjusted to change the initial temperature of the fuel rods. It should be noted that the asymptotes which each of the temperature profiles approach in Figures 8 and 11 are approximately equal to the temperature limit predicted by the LLNL model for that particular temperature profile.

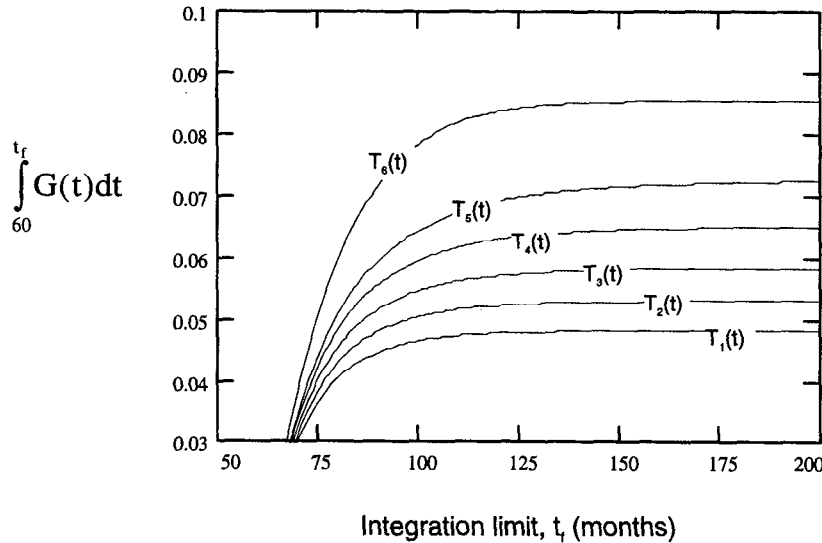


$$\begin{aligned}
 T_1(t) &= C_1 \times 10^3 t^{-0.282} \text{ (K)} & T_4(t) &= C_4 \times 10^3 t^{-0.22} \text{ (K)} \\
 T_2(t) &= C_2 \times 10^3 t^{-0.26} \text{ (K)} & T_5(t) &= C_5 \times 10^3 t^{-0.20} \text{ (K)} \\
 T_3(t) &= C_3 \times 10^3 t^{-0.24} \text{ (K)} \\
 T_6(t) &= T_1(60) + [T_1(180) - T_1(60)]/2 - [T_1(180) - T_1(60)]/120 t \text{ (K)} & & \begin{cases} t < 180 \\ t \geq 180 \end{cases} \\
 &= T_1(180) \text{ (K)} & &
 \end{aligned}$$

Figure 8 Fracture time as a function of initial storage temperature for linear and power temperature decay functions for 5 year old fuel rods with an initial cladding hoop stress of 100 MPa

Figure 8 illustrates that changes in the initial temperature have little effect on the fracture time above approximately 370°C when using the power temperature decay function suggested by PNNL ($T_1(t)$), while any temperature below 370°C results in a prediction that failure will never occur. This sensitivity is reduced with each of the successively less concave temperature decay profiles ($T_2(t)$ - $T_5(t)$). The time over which 99% of the damage occurs similarly increases with decreasing concavity (from 5 years with profile 1 to 9 years with profile 5), as illustrated in Figure 9. This is true because each successively less concave profile predicts more time at higher temperatures resulting more predicted damage of the material. The linear profile is the most conservative of all the profiles. It predicts that more damage occurs (shorter predicted fracture time) than any of the power decay profiles. It also

decreases the sensitivity of the failure time to the initial temperature of the SNF compared to the power temperature decay profile suggested by PNNL.



$$\begin{array}{ll}
 T_1(t) = 2.090 \times 10^3 t^{-0.282} \text{ (K)} & T_4(t) = 1.622 \times 10^3 t^{-0.22} \text{ (K)} \\
 T_2(t) = 1.910 \times 10^3 t^{-0.26} \text{ (K)} & T_5(t) = 1.494 \times 10^3 t^{-0.20} \text{ (K)} \\
 T_3(t) = 1.760 \times 10^3 t^{-0.24} \text{ (K)} & T_6(t) = 746.5 - 1.46 t \text{ (K)} \quad \left. \begin{array}{l} \int t < 180 \\ \int t \geq 180 \end{array} \right\} \\
 & T_6(t) = 484 \text{ (K)}
 \end{array}$$

Figure 9 Comparison of the value of the integral of $\int_0^{t_f} G(t) dt$ (from LLNL) as a function of the upper integration limit, t_f , for power and linear temperature decay functions for 5 year old fuel rods with an initial cladding hoop stress of 100 MPa

2.4.1.3.4 A more conservative approach: older SNF

The age of the fuel rods refers to the age of the fuel at the time of removal from wet storage and insertion into dry storage. Thus far we have discussed only 5 year old fuel. Table 2 below is a table reported by PNNL [4] illustrating the distribution of fuel according to fuel age. It is apparent from this table that the bulk of the reported fuel has been in wet storage for 5 years or more and, therefore, older fuel is very common and must also be considered.

Table 2 Cumulative LWR (light water reactor) spent fuel inventory of all operating reactors in year 1986 [4]

Age range of Assemblies, yr	Number of Assemblies in age range		Total
	PWR (pressure water reactor)	BWR (boiling water reactor)	
1 – 5	5,761	7,728	13,489
5 – 6	1,815	2,670	4,485
6 – 7	1,475	2,859	4,334
7 – 8	1,742	2,440	4,182
8 – 9	1,927	2,568	4,495
9 – 10	1,240	2,325	3,565
10 – 11	790	1,987	2,777
11 – 12	816	1,511	2,327
12 – 13	541	1,555	2,096
13 – 14	229	487	716
14 – 15	129	120	249
15 – 16	51	59	110
16 – 17	95	0	95
17 – 18	40	0	40

No assemblies older than 18 years

Brookhaven National Laboratory (BNL) [45], suggested that a linear temperature decay profile is reasonable for 10 year old fuel. As was discussed above, using a linear temperature decay decreases the predicted failure time and decreases the sensitivity of the failure time to the initial temperature or fuel age. Two linear temperature decay profiles suggested by BNL [45] are defined below by Equations 11 and 12 and shown in Figure 10 along with the power temperature profile (defined, above, by Equation 10) proposed by PNNL. The two “realistic but slightly offset temperature histories” [45] suggested by BNL are defined by

$$T(t)_{(BNL\ Upper)} = 350^{\circ}C - (3.5\ t)^{\circ}C/yr \quad \text{Eq. (11)}$$

$$T(t)_{(BNL\ Lower)} = 335^{\circ}C - (3.5\ t)^{\circ}C/yr \quad \text{Eq. (12)}$$

In order to compare these temperature profiles to the power temperature profile, they were adjusted slightly. For these equations the time $t = 0$ corresponds to insertion into dry storage while $t = 0$ in the power decay equation corresponds to

removal from the nuclear reactor. For 10 year old fuel, $t = 10$ years (120 months) corresponds to insertion into dry storage for the power decay functions. Adjusting the linear equations (11 and 12) is a simple matter of increasing (by 35°C) the initial temperature of the BNL equations so that the temperature at 10 years is equal to the initial temperature defined by Equations 11 and 12. Equations 11 and 12 become

$$T(t)_{(\text{BNL Upper})} = 385^{\circ}\text{C} - (3.5 t)^{\circ}\text{C}/\text{yr} \quad \text{Eq. (13)}$$

$$T(t)_{(\text{BNL Lower})} = 370^{\circ}\text{C} - (3.5 t)^{\circ}\text{C}/\text{yr} \quad \text{Eq. (14)}$$

In Figure 10, as in Figure 3 above, a vertical line indicates the point at which the temperature profile becomes relevant (point of removal from wet storage and insertion into dry storage—in this case 10 years).

The power temperature decay function utilized for Figure 10 was based on the equation reported by PNNL ($T = 2.09 \times 10^3 (\text{months})^{-0.282} \text{ K}$) and the coefficient was adjusted to match the initial fuel temperatures suggested by BNL [45] (resulting in $T = 2.0404 \times 10^3 (\text{months})^{-0.282} \text{ K}$). This method of adjusting the initial temperature was the same as that used by PNNL [4]. Figure 11 below compares the fracture time as a function of initial temperature for 10 year old fuel for both the PNNL suggested temperature decay profile and a linear temperature decay profile with a slope equal to that suggested by BNL.

It is clear from Figure 11 that the fracture time for the PNNL temperature profile is much more sensitive to small changes in the initial temperature than the BNL linear temperature profile. This is especially true for temperatures just below 370°C where, as before, the PNNL temperature profile results in a prediction that failure will never occur. This degree of sensitivity is not, however, observed in the BNL linear temperature decay profile. Temperature sensitivity of the PNNL and LLNL models for 10 year old fuel was also addressed by BNL [45] using the linear temperature

profiles given above and similar conclusions were made (that the current models are very sensitive to changes in the chosen temperature profile).

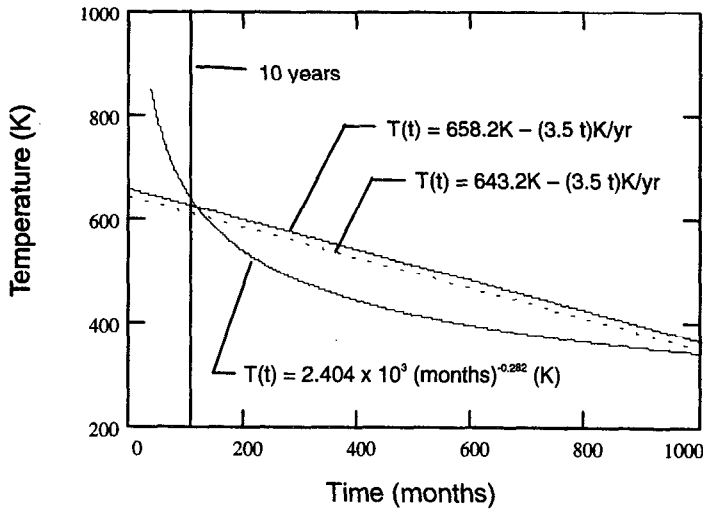


Figure 10 Comparison of power and linear temperature decrease profiles for 10 year old fuel rods suggested by PNNL [4] and BNL [45], respectively

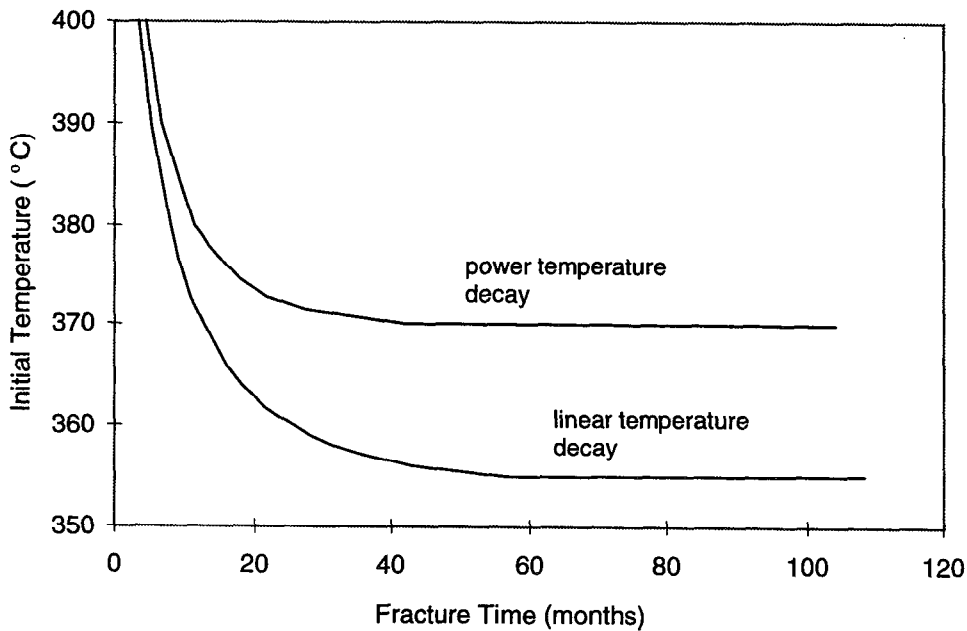


Figure 11 Fracture time as a function of initial storage temperature for a linear and power temperature decay function for 10 year old fuel rods with an initial stress of 100 MPa

Figure 12 below shows a plot of the value of the integral of $G(t)$ as a function of the upper integration limit for 5, 10 and 15 year old fuel rods. Figure 12 illustrates how the time necessary for 99% of all predicted damage to occur varies with initial fuel age (age upon insertion into dry storage) when assuming a power temperature decay function. The amount of time to reach 99% of the total predicted damage increases linearly with fuel age. As stated above, for 5 year old fuel, 99% of the total predicted damage is reached after approximately 5 years. For 10 and 15 year old fuel rods, 99% is reached after 10 and 15 years in dry storage, respectively. This is due to the nature of the power temperature decay function. The half-life of the short lived fission products has been surpassed in older fuel and long-lived fission products (slower temperature decay) govern the temperature decay. Hence, packing older fuel more closely in storage casks to achieve the same initial stress and temperature as that of newer fuel would result in the older fuel accumulating a greater amount of cladding damage with time due to its slower rate of temperature decay.

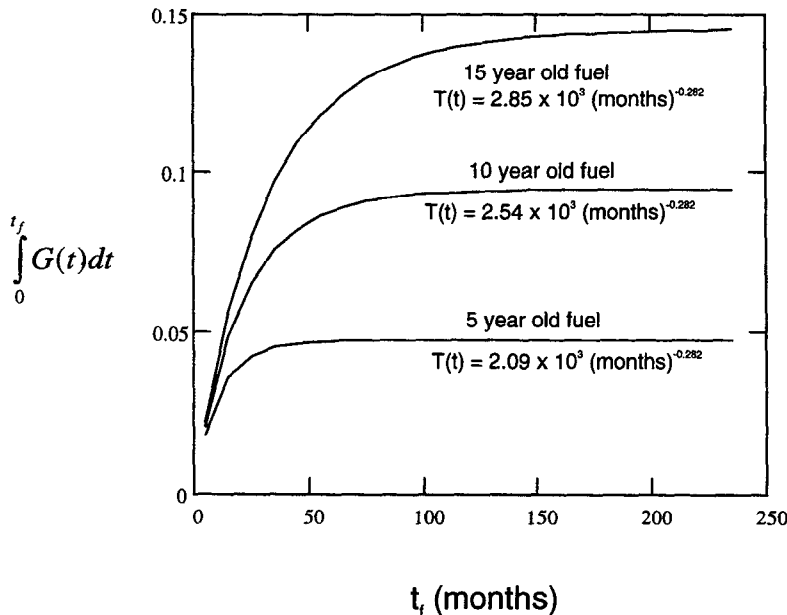


Figure 12 The value of the integral of $G(t)$ as a function of the upper integration limit, t_f for 5, 10 and 15 year old fuel rods (normalized so that the time 0 on the abscissa corresponds to the time of insertion into dry storage) using an initial (start of dry storage) stress of 100 MPa and an initial (start of dry storage) temperature of 385°C

2.4.2 Cladding stress

The stress that each fuel rod experiences in dry storage is not well defined. PNNL states that the helium fill pressure (internal rod pressure) in the rods is proprietary, but is generally more than 20 atmospheres (2.03 MPa, 294 psi) but less than 40 atmospheres (4.05 MPa, 588 psi) at standard temperature and pressure (STP) [45] for pressure water reactors (PWR) (highest pressure rods). The PWR operating pressure (internal pressure) for the fuel rods in-reactor is approximately 153 atmospheres (15.5 MPa). The amount that the internal rod pressure is allowed to exceed this pressure under off-normal conditions is proprietary [4]. Upper bound internal rod pressures are reported by PNNL for various rod types (reactor types).

Assuming that PNNL's determination is a conservative estimate, one can use the reported upper limit of 2416 psi as the maximum internal rod pressure upon insertion into dry storage (the pressure will, of course, change with temperature) for PWR rods at a burnup level of 45 MWd/kgM. This results in a cladding hoop stress of approximately 70 MPa. We chose a slightly higher initial cladding stress of 100 MPa for this analysis to consider deviations such as from stress concentrations, etc., that may arise in the cladding. This also helps account for the fact that the fuel rods may have higher burnup levels than the burnup levels assumed by PNNL to calculate the upper bound pressure*. Higher burnup levels mean that rods have spent more time in service so that more nuclear fission products (primarily H, He, Kr, Xe and a small fraction of Rn [49]) would have been produced, increasing the internal pressure. This could have a large effect on the rod pressure as the fission gasses account for up to approximately 50% of the gasses in the fuel rods after removal from reactor [52] (the other 50% is helium-fill gas).

The cladding stress is assumed to decay only with temperature as a function of the ideal gas law because the strain effects (increase in volume due to strain) were

* The trends at the time of the PNNL report were toward more extended burnup levels [4].

assumed to be minor. It has been argued that over the long periods of time relevant to dry storage and permanent disposal, the cumulative strain can significantly affect the internal pressure [53]. This effect, however, is not necessarily easy to incorporate into the calculation, as the creep of irradiated fuel rods is not well defined and may be small [28] (e.g., less than 12% strain to failure). Ignoring the increasing internal volume due to increasing strain is conservative, as the actual stress is slightly overestimated.

It should be noted that the stress-state of relevance for fuel rods in dry storage is biaxial. The current models and many past experiments have simplified this by assuming a uniaxial tensile stress. This may not be conservative as multi-axial stresses may increase void nucleation [54] and thereby decrease failure times. This will be discussed again below.

2.5 Critical material parameters

2.5.1 Grain boundary diffusion coefficient

2.5.1.1 General discussion of diffusion in zirconium

Self-diffusion coefficients reported in the literature for zirconium (Zircaloy unavailable) vary by more than four orders of magnitude [55-66]. A detailed explanation of this variation has recently been proposed by Hood and co-workers [67-70]. Hood proposed, as have others [63,71-73], that the self-diffusion studies performed in the past have all, to some extent, measured extrinsic diffusion effects rather than the intrinsic self-diffusion coefficient of zirconium. Hood suggests that these extrinsic effects may be the result of elemental impurities, such as Fe, which can alter, sometimes dramatically, the self-diffusion coefficient. This view is supported by several other authors [74-78]. Iron, for example, is a fast diffuser that is thought to interact strongly with vacancies [69] and, possibly, form pairs with monovacancies [74,75,79].

The diffusion coefficient of iron in zirconium has been reported to be approximately eight orders of magnitude higher than the zirconium self-diffusion coefficient over a range of temperatures [79,80]. The presence of iron increases the effective zirconium self-diffusion coefficient by “pulling” monovacancies along as it diffuses through the lattice. This relationship with iron has been used to explain the fact that the activation energy for self-diffusion in α -zirconium is consistently reported to increase with decreasing temperature. The solubility of Fe in zirconium is very limited and decreases with decreasing temperature. At low temperatures, much of the iron precipitates out of the lattice and the iron remaining in solid solution may be locked to dislocations. The activation energy at these temperatures, therefore, is approximately equal to that for intrinsic self-diffusion [66], or about 305 kJ/mole (3.17 eV). As the temperature increases, the Fe dissolves into solid solution and begins to diffuse very rapidly through the lattice, thereby decreasing the apparent activation energy. It has also been proposed that zirconium is very susceptible to short circuit diffusion [63,71-73] such as diffusion along dislocations. Thus, the condition (e.g. cold work) of the sample used to measure the diffusion coefficient is critical.

2.5.1.2 Diffusion coefficient value chosen by PNNL [4]

Initially Chin [37] (one of the authors of the PNNL report) suggested an activation energy for grain boundary diffusion of 112 kJ/mol and a value for D_0^{gb} of 6×10^{-10} m²/sec. In later reports [28,81,82] Chin suggested an activation energy of 175 kJ/mol and a value for D_0^{gb} of 3.89×10^{-6} m²/sec.

We were unable to evaluate Chin’s justification for which activation energy to use because a discussion of the initial value chosen for the activation energy [83] could not be located (the earlier report was not retained by Chin [84]). A justification for changing the activation energy in later reports [28,81,82] was not provided. In the “Final Report” [28], Chin states the following regarding the activation energies chosen in the fracture and deformation mapping methodology: “Experimental data from references [36,181,182,184,85-172] were analyzed and the value of the stress

exponent 'n' calculated (from least square linear fits of $\ln \dot{\epsilon}$ vs. $\ln \sigma$ plots); the activation energy 'Q' was also categorized according to n and Q values.

1 < n < 3, Q_{gb} Grain Boundary Sliding (boundary diffusion)

1 < n < 3, Q_l Grain Boundary Sliding (lattice diffusion)

3 < n < 7, Q_1 High Temperature Climb

7 < n < 9, Q_c Low Temperature Climb”

From this, one can only speculate as to how Chin has calculated the activation energies for grain boundary diffusion. Apparently, Chin may have calculated the activation energy for grain boundary diffusion based on creep data from some $\dot{\epsilon}$, T regime. The results should be viewed with caution if, in fact, this is the approach that Chin utilized, because of the anomalous creep behavior of zirconium and zirconium alloys [85-104,172,181,182,184]. There does not appear to be a consensus about which creep mechanism is rate controlling for conditions relevant to dry storage.

2.5.1.3 Diffusion coefficient value chosen by LLNL

LLNL suggested using the activation energy of 131 kJ/mol and D_{gb} of 5.9×10^{-6} m²/sec reported by Garde et al. [172]. This yields a grain boundary diffusion coefficient that is 1 to 3 orders of magnitude faster (more conservative) than Chin's earliest suggested D_{gb} [37] and 3 to 5 orders of magnitude faster than Chin's later suggested D_{gb} [28,81,82] at 400°C and 200°C, respectively. Taking a more conservative approach seems advisable as the diffusion coefficient of zirconium has been shown have a large variability in reported values [55-66]. Garde et al. [172] (source of D_{gb} suggested by LLNL) merely used the approximation that the activation energy for grain boundary diffusion is 60% of the activation energy for bulk diffusion [173]. Although the estimate by Garde et al. was more conservative than the value suggested by Chin, this estimate should still be viewed with caution, as the 0.6 ratio is empirical and hence inexact. Reported bulk self-diffusion activation energies range from 92 to approximately 305 kJ/mol [55-66]. Garde et al. [172] chose the

activation energy for bulk self-diffusion reported by Lyashenko [59] of 220 kJ/mol. Although this is somewhat of a mean value of reported self-diffusion activation energies for zirconium, it was apparently an arbitrary choice from the reported values in references 55-66 and may not be the most conservative approach.

2.5.1.4 Discussion of the diffusion coefficient values chosen by LLNL and PNNL

At the time that the current models (LLNL and PNNL) were developed, values for the self-diffusion coefficient activation energy had been reported from 92 kJ/mol to 305 kJ/mol with corresponding pre-exponential terms (D_0^{sd}) of 3.4×10^{-7} to $0.9 \text{ cm}^2/\text{sec}$. Converting to grain boundary activation energies (assumed to be approximately 60% of the lattice diffusion activation energy [173]), which would be relevant to SNF rods in dry storage, gives 55.2 to 183 kJ/mol. At 400°C, these activation energies would result in diffusion coefficients ranging from 1.77×10^{-11} to $5.63 \times 10^{-15} \text{ cm}^2/\text{sec}$, respectively (assuming $D_0^{gb} = D_0^{sd}$). It is apparent, then, that the measured diffusion coefficient in zirconium varies by several orders of magnitude depending on the conditions and composition of the samples tested.

Thus, at the time that the current models were developed, it was not straightforward how to choose an appropriate diffusion coefficient for the Zircaloy-clad SNF under dry storage conditions. LLNL selected one value from the literature while PNNL chose another. These values were based on bulk self-diffusion experiments as no grain boundary diffusion studies had been reported for zirconium or Zircaloy. The grain boundary diffusion estimations chosen by LLNL and, presumably, by PNNL were based on the above *approximate* relationship between the self-diffusion and grain boundary diffusion activation energies, $Q_{gb} \approx 0.6Q_{sd}$ [173]. This is one serious limitation with these models as the more than four order of magnitude variation in the reported values for the diffusion coefficient translates linearly to the predicted failure time (see Appendix B). Since the time of that these models were developed, however, grain boundary diffusion data have been reported.

2.5.1.5 Current grain boundary diffusion data

Vieregge and Herzig [174] measured the grain boundary diffusion coefficient of zirconium directly rather than calculate it using an approximate relationship with the bulk self-diffusion coefficient. This is the only data for true grain boundary diffusion that we were able to locate. This study gives D_{gb} as

$$D_{gb} = \frac{4.2_{-2.5}^{+5.9} \times 10^{-13} \exp\left(\frac{-167 \pm 7 \text{ kJ/mole}}{RT}\right)}{\delta} \frac{\text{m}^2}{\text{s}} \quad \text{Eq. (15)}$$

where δ is the high speed diffusion zone surrounding the grain boundary (also called the grain boundary width). This factor appears in the diffusion equation because when measuring grain boundary diffusion, you really measure a flux of atoms and then *assume* a certain diffusion zone (or grain boundary width) in order to calculate the diffusion coefficient. When evaluating the DCCG fracture equation (Equation 2), you must also assume a grain boundary diffusion zone, which is then multiplied by the diffusion coefficient resulting in a flux of diffusing atoms. It is apparent that by using the grain boundary diffusion estimation reported by Veiregge and Herzig [174], the δ term is eliminated from the DCCG fracture equation (Equation 2). Using this value, then, eliminates δ from the fracture equation and thereby reduces the uncertainty of the fracture model. The effect varying the diffusion coefficient has on the predicted failure time is discussed in Appendix B. The predictions of Equation 15 are close to the grain boundary diffusion coefficient suggested by LLNL for any reasonable grain boundary width. The error indicated in Equation 15, however, translates to a variation of more than 100°C in the maximum initial temperature when using Equation 10 for the temperature profile (see Appendix B for this analysis).

2.5.1.6 Irradiation effects

It is not clear what effect irradiation may have on the grain boundary diffusion coefficient of zirconium or zirconium alloys. Irradiation damage results in a higher

concentration of vacancy type dislocation loops near grain boundaries [175-177] and also causes “dispersion of Fe [178]” which could substantially increase the diffusion rate (see diffusion discussion above). It is also known that irradiation can cause precipitation of impurities in zirconium alloys [175,179,180], which may affect the diffusion coefficient. A detailed study of the self-diffusion of irradiated Zircaloy has not been completed to date. In view of this, the conservative end of the experimental range reported by Vieregge and Herzig [174] should be chosen ($D_{gb} = 1.0 \times 10^{-12} / \delta \text{ m}^2/\text{sec}$, $Q_{gb} = 160 \text{ kJ/mole}$).

2.5.1.7 Differences between zirconium and zirconium alloys

The effect that alloying zirconium has on grain boundary diffusion under conditions relevant to dry storage has not been established. It has been shown that Zircaloys have lower creep rates than zirconium [181,182] when compared directly. Some have suggested that this may be due to a lower grain boundary diffusion rate (lower grain boundary diffusion activation energy) [181-183] based on the premise that creep of zirconium and zirconium alloys is diffusion controlled. From the evidence reported, this appears to be a reasonable assumption *under the conditions used in those experiments*. However, the temperatures used in those experiments were much higher than are relevant to dry storage.

There is much uncertainty in the reported values for diffusion activation energies for zirconium (see above) and creep data (discussed later). In a study by Fidleris [184], which examined creep properties over a range of conditions similar to dry storage, the creep activation energy varied by more than a factor of 2. Also, the diffusion coefficient of zirconium is sensitive to impurities. It was reported that alloying zirconium with tin (one of the main components of Zircaloy) decreases the self-diffusion coefficient of zirconium, at least at high temperatures [59]. Kidson [61] suggested, however, that this variation in activation energy was within the experimental error. Zircaloys are typically very high in iron (approximately 0.1-0.2 wt% Fe), which has been shown to increase, sometimes dramatically, the self-diffusion coefficient of zirconium (refer to previous section for a discussion of the

effects of iron). For these reasons, it may be reasonable to use a grain boundary diffusion coefficient for Zircaloy that is lower (or higher) than what we have suggested based on studies of commercially pure zirconium. However, because of the apparent lack of grain boundary diffusion data (or bulk diffusion data) comparing zirconium and Zircaloy under conditions relevant to dry storage, we recommend using the grain boundary diffusion coefficient for zirconium to predict the behavior of Zircaloy. This recommendation may need to be modified when data is obtained from future diffusion and creep studies on zirconium and zirconium alloys.

2.5.2 Cavity spacing

As discussed by BNL [41], the current models based on DCCG are very sensitive to changes in the assumed cavity spacing. The fracture time according to DCCG is inversely proportional to the cube of the cavity spacing. A change of one order of magnitude in the cavity spacing results in a three order of magnitude change in the fracture time. The cavity spacing, then, is a very important parameter that should be accurately determined.

BNL [41,45] suggests that cavities do not play an important role in dry storage of SNF as they claim that cavities are only nucleated after significant strain (see discussion below). It has been shown, however, that cavities are nucleated during *all* levels of creep strain [54,185-190]. It has also been argued that classical nucleation theory fails to explain cavity nucleation in Zircaloy under dry storage conditions [191]. But, as stated by Nix [22], this same discrepancy applies to most creep conditions (because the stress necessary to nucleate cavities is so high), yet cavities still nucleate and grow. Nix explains that this is likely the result of high stress concentrations at grain boundary junctions, precipitates, etc., or due to grain boundary sliding, which can easily give rise to stresses about an order of magnitude larger than the applied stress [22]. The following rough calculation illustrates the plausibility of cavity nucleation at stress concentrations.

When assuming stresses under dry storage conditions on the order of 100 MPa, stresses at stress concentrations could reach nearly 1 GPa (a factor of 10 larger stress due to stress concentrations). According to Argon et al. [192], stresses on the order of $\sigma_{TH}/10$ are necessary for cavity nucleation, where σ_{TH} is the theoretical cohesive stress. If $\sigma_{TH} = E/10$, where E is Young's modulus, the critical stress for cavity nucleation is about E/100. E for Zircaloy at 350°C (temperature chosen by ref. 191) is about 80 GPa [193,194] so E/100 is about 800 MPa. It is reasonable to assume that stresses at stress concentrations may approach this level under dry storage conditions. Therefore cavity nucleation under dry storage conditions cannot be ignored unless and until direct experimental evidence shows otherwise.

PNNL assumes a cavity spacing of 2.6 μm (source was not reported) and LLNL assumes a spacing of 10 μm based on the work of Keusseyan and coworkers [54,185]. This results in a factor of 57 difference in predicted failure times if evaluated at a constant temperature. With a decreasing temperature profile, the effect becomes more pronounced, though still less so than the effect of changing the grain boundary diffusion coefficient or temperature profile as discussed above. The effect may not seem so great when only examining the variation in the two suggested cavity spacing values (those of LLNL and PNNL), however, these two suggested values may not be conservative.

PNNL's choice of a value for the cavity spacing is more conservative than the choice made by LLNL (2.6 μm compared to 10 μm). The assumption made by LLNL that the cavity spacing reaches a saturation value at about 10 μm may not be conservative (see Appendix B). Using the value suggested by PNNL, however, still may not be conservative. There is evidence that irradiation under conditions similar to in-reactor conditions may cause void formation [175-177,179,195,196] (see Appendix B). Voids observed in these experiments appeared near grain boundaries with cavity spacings on the order of 0.1-0.2 μm [176-177]. It may be reasonable,

therefore, to assume a much smaller cavity spacing than those assumed in the current models, possibly on the order of 0.1-0.2 μm .

2.6 Conclusions about current models

Assuming DCCG is the operative fracture mechanism, LLNL is the more conservative of these two models (see Appendix B) and more adaptable to specific dry storage conditions (e.g. easily allows for modifications in the input values and temperature profile by proposed dry storage licensees). Because there is a large uncertainty in Zircaloy diffusion data, very little long term creep data, and virtually no relevant creep fracture data, a conservative failure model is justified. However, values suggested by LLNL for input into the Raj and Ashby failure equation may be non-conservative and should also be viewed with caution. Although LLNL claims to use a conservative estimate in every numerical value, we have shown (see above and in Appendix B) that this does not always appear to be the case. LLNL justified using their selected values based on the supposition that they chose conservative values. The LLNL suggested values should be modified before calculations of the predicted failure times can be argued to be conservative.

3 Rod Surveillance Testing

It has been argued [197] that unconsolidated fuel rods stored under current dry storage conditions appear to be safe over extended periods of time based on rod surveillance testing. Under normal dry storage conditions, failures were seldom observed [197], much less than the allowed 1% pinhole leaks or hairline cracks specified by the NRC [1]. Rod consolidation has increased the number of failures [197] (12 failed rods out of a total of 9800). These failures, however, are still within the 1% limit and are not considered to be “gross ruptures” by NRC standards [1] as long as uranium is not allowed to escape from the fuel rods. Other groups in the US [198-201] and abroad [24,26,201-206] have reported similar results, though some were at lower temperatures [204]. Post-dry-storage processing (e.g., handling of rods for consolidation or transfer from the storage cask into a waste disposal package), however, has not (to our knowledge) been evaluated after long term

storage under conditions relevant to dry storage in the United States. Post-storage processing fuel integrity is also a requirement of dry storage [1].

Although extended and continuing surveillance of PWR assemblies in dry storage is helpful to determine the safety of those specific storage conditions, the results of these tests cannot be directly quantified in terms of stresses and temperatures. The stresses and temperatures of the fuel rods under surveillance are not accurately known, nor can they be measured. Therefore, the fact that failure may or may not have occurred in the observed set of fuel rods simply illustrates the probable safety or lack of safety for the fuel rod conditions and environment existing for that particular surveillance test. Furthermore, the microstructure of these fuel rods was not examined after dry storage. It is not known whether the condition of the fuel rods is still safe according to the current safety standards. The established 15% area fraction of decohesion limit may have been surpassed *without* rupture occurring in dry storage, but the rods may be unsuitable for post dry storage handling [43,44].

4 Discussion of Brookhaven National Laboratory 1989 [41] and 1994 [45] Reports

A group at Brookhaven National Laboratory (BNL) reported that current standards for calculating the maximum allowable temperature for SNF in interim dry storage are far too conservative and unrealistic. The basis for the BNL argument is that current methods ([3,4]) are based on creep and creep-fracture theory rather than experimental data. These authors state that DCCG (used by both LLNL and PNNL) “is based on creep-theoretical consideration applicable only to the tertiary stage of creep” [45]. They also state that “there is little evidence that cavities play a major role in the creep degradation of both irradiated and unirradiated Zircaloy” [45]. Although Keusseyan [54,185] was able to observe the presence of cavities in Zircaloy after short term creep tests under near dry storage conditions, BNL cites other researchers who did not observe cavity formation [207-209] and states that the formation and growth of cavities is extremely unlikely. One should be careful not

to throw out this experimental data so quickly. Furtado and Le May [210] have demonstrated that even when cavities exist, investigators very often fail to detect them. Also, as has been discussed above and in detail in Appendix B, in-reactor irradiation may result in cavity formation, contrary to the suggestions made by BNL [41,45]. These cavities may continue to grow and/or multiply in dry storage.

4.1 The BNL strain-based approach

Instead of a theoretical approach, BNL suggests using a creep-strain limit approach where creep-strain is not allowed to progress beyond 1% which is prior to “tertiary” creep. It appears that the NRC is now accepting this approach and feels that it should be used in place of the LLNL DCCG model (though they still feel that the DCCG based PNNL model is acceptable). The strain-based approach has been advocated by Peehs and coworkers in Germany for some time [see, for example, 25,26,211,212] and is also supported by Mayazumi et al. [213]. The 1% creep-strain limit was chosen based on the proposition that cavities are not nucleated until large levels of strain and that at strains below 1% fracture cannot occur. It has been shown [54,185-190], however, that cavities can nucleate and grow in various metals at *all* levels of strain. Furthermore, fracture by DCCG is *independent of strain* (Equation 2 is not a function of strain) as damage occurs as a result of local diffusion along grain boundaries without large far field strains and therefore may result in “a sudden non-ductile type of failure” without “external evidence of damage” [3]. BNL has argued that fracture by DCCG does not fit the definition of “creep” (time dependent strain at elevated temperatures) and cannot, therefore, be “utilized for creep engineering purposes”. As DCCG is currently assumed to be the operative fracture mechanism and can predict failure in the absence of strain, an engineering creep-strain limit approach does not seem applicable for the case of Zircaloy cladding under dry storage conditions.

Using creep data as BNL has done may be reasonable if there were reliable long-term creep data. Unfortunately, creep tests on irradiated or unirradiated Zircaloy have not been crept to fracture under conditions relevant to dry storage. Thus creep

limit determinations must either be extrapolated from short-term creep data or based on data measured at higher stresses and/or temperatures where rupture data is available. Extrapolation may be unreliable because creep behavior of zirconium and zirconium alloys is anomalous [181,182,184,85-104,172]. These investigators have found that Zircaloy never reaches a true secondary creep stage as the creep rate continually changes with time at a given true stress. Using data measured under non-dry storage conditions is also unreliable as the creep mechanism and/or fracture mechanism may change with stress and temperature. Also, recovery in zirconium has been shown to occur at very low temperatures [214] in relatively short periods of time. It was also shown that increasing temperature by 100°C can change the rate of defect recovery by orders of magnitude [214]. Failure strains may be increased dramatically at higher temperatures. Thus, citing data where creep tests were performed to strains of 10% or more at higher temperatures and stresses than are relevant for dry storage, is not necessarily a conservative approach.

Also, as was mentioned above, the Zircaloy-clad fuel rods are in a state of biaxial loading (stress). The addition of multiaxial stresses tends to decrease the strain to failure and may increase void nucleation [54]. Thus, data from experiments performed in uniaxial tension should be viewed with caution when applying the results to the Zircaloy-clad fuel rod case.

4.2 Errors committed by BNL

The authors at BNL made some important points about the sensitivity of the currently applied models (by PNNL and LLNL). We have referenced these points in the appropriate places in this report. In questioning the applicability of current theories, however, we noted that BNL made a few fundamental errors that suggested the current models appear more inconsistent than they are.

When comparing the LLNL model with the PNNL model, BNL [45] noted the apparent error as discussed above. That is, they noticed that PNNL had apparently set the integral of the $dA/f(A)$ function equal to 0.15 rather than setting the upper

integration limit to 0.15 (see Section 2.3.1 for more details). BNL did not realize, however, that PNNL actually evaluated the LLNL model *correctly* when developing the failure curves to compare to the PNNL CSFM model. BNL uses this point as part of their discussion to show that the PNNL and LLNL models are fundamentally inconsistent.

The second error made by BNL in comparing the PNNL and LLNL models occurred when BNL tried to show the difference in the failure predictions of the PNNL and LLNL models for a given set of conditions. The calculations were made for 10 year old fuel with an initial temperature of 350°C and a corresponding initial stress of 54 MPa. BNL states (page 72, reference 45) that the LLNL model predicts failure after 4 years in dry storage while the PNNL model predicts that under the same conditions that fuel could be stored safely for at least 40 years. The error BNL made was that they used a linear profile to evaluate the LLNL model and compared the result to the 10 year old fuel fracture curve in the PNNL report which was based on a power temperature decay profile (Equation 10 above). If this same power temperature decay profile were used to evaluate the LLNL model, it also would have predicted that fuel could be stored safely for more than 40 years.

The third error that we noted occurred on pages 25 and 36 of the 1989 BNL report [41]. BNL states that the PNNL equation for DCCG appears to be based on Raj and Ashby [36], and that “the important observation, however, is that Chin’s expression for t'_{CD} does not display a dependence on the area of decohesion.” BNL also states that “the failure criterion used by Chin* is 100% decohesion.” In contrast with BNL’s assertion, the PNNL failure criterion does have a dependence on the area fraction of decohesion. When using the Raj and Ashby failure equation as PNNL has done, the area function has already been evaluated and integrated between some small initial value and a final value of 0.5, or 50% area fraction of decohesion (not 1.0 as

* Note that Chin is a co-author of the PNNL report, and that BNL’s references to “Chin” refer to modeling features reported in 1983 [37], 1986 [32], 1987 [4] and 1989 [81].

suggested by BNL). By using this equation, then, the PNNL equation has an inherent dependence on the area fraction of decohesion.

One further error that we noted appears on page 36 of the 1989 BNL report [41]. BNL states that PNNL used a slightly different temperature decay profile when evaluating the LLNL model than when they evaluated their CSFM model. PNNL states on page D.1, however, that they used a single temperature decay profile to evaluate both the LLNL and CSFM models.

4.3 Conclusions about the BNL work

It does not appear DCCG has been firmly supported with experimental creep fracture data in zirconium or zirconium alloys, but with a lack of a better or more current failure theory for Zircaloy, DCCG remains the currently accepted failure theory. Using a creep-strain limit approach, as suggested by BNL, does not appear to be a useful alternative for the case of Zircaloy where failure, according to current theories, does not appear to be strain dependent. It is, however, possible that some other fracture mechanism may be operating under most dry storage conditions that has not yet been considered.

5 Discussion of April 1999 LLNL report

In April 1999 G.R. Thomas of LLNL published a report [215] in an attempt to 'substantially update' the LLNL model discussed above. Thomas suggests that the DCCG model can be improved by using 'thermal-physical' modeling to determine the cavity spacing. Thomas relates the critical cavity size to the vacancy concentration in the material by assuming that the void spacing is simply a function of the number of vacancies. Thomas calculates the void spacing by assuming that all of the vacancies in a given volume condense into a critical-sized void nucleus, stating that "the initial total volume of the cavity nuclei is, in practice, necessarily limited primarily by the vacancy concentration near the grain boundary." Thomas then develops a relationship between the initial cavity spacing and the thermal equilibrium vacancy concentration. This method does not appear to be

fundamentally sound because once one cavity is formed, the material surrounding the cavity would immediately return to its equilibrium vacancy concentration. According to this method, there would be enough vacancies in that volume to nucleate another set of cavities. This process would continue unabated until fracture occurs. Such nucleation based on the equilibrium vacancy concentration, then, does not seem likely. It is not clear that cavity nucleation is even related to vacancy condensation. As discussed above, classical nucleation theory fails to explain cavity nucleation under most conditions, yet cavities still nucleate and grow. Instead, cavities may nucleate at discrete sites in the material, such as at grain boundary junctions, precipitates, inclusions, dislocation pileups, etc., or nucleate as a result of grain boundary sliding.

If nucleation were actually to occur by vacancy condensation, it seems it would only occur as a result of a dramatic excess of vacancies above the equilibrium concentration. In fact, Thomas suggests that there would be an excess of vacancies (above the thermal equilibrium) due to various sources. The sources he suggests include alloying, fabrication processes, irradiation history, irradiation damage and added stress effects. In order to modify his analysis based on thermally induced vacancies, Thomas 'normalizes' the updated model to correspond to the results of the *original* LLNL model. Thomas suggests multiplying the calculated vacancy concentration from his analysis based on thermal vacancies by a factor of 10^9 . Thomas rationalizes this factor by suggesting that the difference between his calculations based on only thermally induced vacancies and the results of the original model is due solely to the existence of other sources of vacancies that would increase void nucleation. Thomas considers a factor of 10^9 reasonable considering all of the sources of excess vacancies. Of the sources he considers, however, irradiation appears to be the only significant source of excess vacancies*.

* Alloying does not significantly affect the thermal equilibrium vacancy concentration. Excess vacancies from fabrication would most likely be annealed out during the service life of the fuel rods. Stresses present in the fuel rods are much too small to significantly affect the vacancy concentration.

It is not clear whether irradiation would increase the vacancy concentration by a factor of 10^9 , nor whether these excess vacancies would condense to form a cavity.

Even if it is assumed that the Thomas methodology is sound, it still is not clear how the LLNL model is improved. Normalizing the updated model to the *original* LLNL model (by multiplying by a factor of 10^9) immediately precludes the possibility of improving the model because any uncertainty in the original model is thereby included in the new model. Any further uncertainties introduced in Thomas' analysis are then combined with the former uncertainties, increasing the total uncertainty. Thomas, in fact, concludes that "the updated DCCG model cannot be used as a replacement for the original DCCG model" and suggests that "the original DCCG model be retained."

Finally, Thomas states that "the specific evidence for possible DCCG behavior has come into question regarding applicability to dry storage conditions. The work performed for the present report to update the DCCG model was initiated before these concerns came to light." He then suggests using a strain-based model as suggested by BNL in 1994 (see above) in place of the LLNL model.

6 Conclusions

DCCG is the fracture mechanism assumed to control failure under dry storage conditions by both PNNL and LLNL. As discussed by BNL, this may not necessarily be the case, but available experimental evidence and theory place this as the most "reasonably established mechanism." Although based on the same fundamental fracture theory (DCCG), the two currently accepted models (by PNNL and LLNL) include many inconsistent assumptions, including the assumed failure condition and choice of values for constants in the DCCG failure equation. Many of the inconsistent assumptions arise because both models include variables that have not been accurately measured for irradiated Zircaloy (e.g., grain boundary diffusion coefficient and cavity spacing). Using the limited data available for zirconium is tenuous, as the effects of alloying on the grain boundary diffusion coefficient of

zirconium and the effects of irradiation on the diffusion coefficient and the cavity spacing have not been established. These factors combined with extreme sensitivity to temperature leave the current models with marginal value. It should not be assumed that these models yield conservative temperature limits until experimental data is obtained for cavity spacing and grain boundary diffusion coefficient of irradiated Zircaloy and until post dry storage SNF integrity is evaluated.

A strain-based model is not applicable as long as DCCG is the assumed fracture mechanism. Rod surveillance testing does not give conclusive evidence that current dry storage conditions are safe. The tested SNF may have surpassed the 15% area fraction of decohesion limit without failure, but may fail when handled after completion of dry storage. Creep tests performed on irradiated [23] and unirradiated Zircaloy fuel cladding [212] to times beyond predicted failure times according to the current LLNL failure model did not include post-creep microstructural examination, nor did they address post-dry-storage (post-creep) loading issues. It is not clear, therefore, whether the 15% area fraction of decohesion limit specified by LLNL was passed or if void nucleation and growth occurred.

7 Recommendations

7.1 *Recommended model*

Because the LLNL model is easily modified to accommodate additional experimental data (e.g. cavity spacing and grain boundary diffusion coefficient), we recommend using this model. The LLNL suggested values should be modified before calculations of the predicted failure times (or the initial temperature limit) can be argued to be conservative.

Irradiation commonly induces void formation with void spacings more than an order of magnitude lower than the spacing suggested by either LLNL or PNNL. We recommend using a spacing of $\lambda = 0.1 \mu\text{m}$ based on irradiation data unless and until further experimentation suggests otherwise. Until detailed studies of the grain

boundary diffusion coefficient in irradiated Zircaloy have been completed, the grain boundary diffusion coefficient suggested by Vieregge and Herzig [174] should be used in place of the values chosen by LLNL [3]. The most conservative end of the experimental range ($D_{\text{gb}} = 1.0 \times 10^{-12} / \delta \text{ m}^2/\text{sec}$, $Q_{\text{gb}} = 160 \text{ kJ/mole}$) reported by Vieregge and Herzig should be used because it is the only reported data of its kind and because the effects of irradiation and alloying zirconium on diffusion are not established.

7.2 Recommended SNF temperature decay profile

A conservative temperature profile should be chosen by each potential licensee based on: a) an accurate profile measured under the proposed storage configuration, or b) a linear profile that conservatively approximates the behavior of fuel rods based on measured temperature profiles from rods stored under similar conditions. Special attention should also be paid to the temperatures the rods experience after removal from reactor until insertion into dry storage (especially during the vacuum drying process). If these temperatures are significant (above 300 °C), a damage calculation should be made and the result (value of the integral of $G(t)$) should be included in the dry storage damage calculations.

7.3 Recommended experiments

Creep testing under typical dry storage conditions (temperatures ranging from 300-400°C and stresses from 50-100 MPa) should be started immediately. The predicted failure times can be quite low under dry storage conditions, and these tests could verify if short predicted failure times such as these are possible. Long term creep testing (> 5 years) would allow observation of failure in Zircaloy under conditions similar to dry storage which could help determine whether or not the existing failure models are conservative enough or over-conservative and whether voids nucleate and grow in zirconium under dry storage conditions. The existence of (or lack of) cavities due to creep may more easily be determined using modern techniques, such as ion etching and high resolution scanning electron microscopy. This is very

important because, as shown by BNL [45], significant increases in the initial temperature could be allowed if DCCG is not the correct failure model.

The grain boundary diffusion coefficient of zirconium, Zircaloy and irradiated Zircaloy should be measured. Values reported for self-diffusion in zirconium vary by orders of magnitude from study to study. This variance translates linearly to the predicted fracture time of the current models. Knowing the grain boundary diffusion coefficient accurately, then, eliminates much of the uncertainty implicit in the current failure models.

8 Acknowledgements

This work was performed under the auspices of the U.S. Department of Energy (DOE) by Lawrence Livermore National Laboratory (LLNL) under Contract W-7405-ENG-48, and a subcontract from LLNL to the University of California, San Diego under Contract B345708. The financial support from the DOE National Spent Nuclear Fuel Program and Office of Spent Fuel Management is greatly appreciated. We gratefully acknowledge the helpful discussions and comments made by Professor T. Kennedy of Oregon State University.

9 List of Symbols [3,36]

A	a fractional measure of the grain boundary area occupied by voids (area fraction of grain boundary decohesion)	Q_{gb}	grain boundary self-diffusion activation energy
A_f	final area fraction of decohesion	r	cavity radius in the plane normal to the plane of the grain boundary *
A_i	initial area fraction of decohesion	r_B	cavity radius in the plane of the grain boundary *
A_{min}	minimum area fraction of decohesion (initial)	r_c	critical radius for void nucleation
A_{max}	maximum area fraction of decohesion (final)	R	ideal gas constant
A.W.	atomic weight	t	time
b	burgers vector	t_{DCCG}	fracture time predicted by DCCG model used by Chin and PNNL [4]
D_{gb}	grain boundary self-diffusion coefficient $= D_o^{gb} \exp\left[\frac{-Q}{RT}\right]$	t_{PLC}	fracture time predicted by power law creep model used by Chin and PNNL [4]
D_o^{gb}	grain boundary self-diffusion coefficient constant	t_f	time to fracture
f_B	a function of energy angles used to calculate the area of grain boundary that the void occupies* $= \pi \sin^2 \alpha$	T	temperature
f_v	a function of energy angles used to calculate the void volume * $= \frac{2\pi}{3}(2 - 3\cos\alpha + \cos^3 \alpha)$	T_n	traction stress normal to the grain boundary which cause void growth
k	Boltzmann's constant	V	total volume of the void
l	average cavity (void) half spacing	α	energy angle (of void) *
		β	net number of atoms leaving per unit volume of the grain boundary during the steady state growth of voids
		δ	grain boundary thickness

$\Delta\mu$ excess chemical potential of the atoms in the boundary relative to the stress free state

γ surface free energy per unit area of the matrix material

λ average cavity or void spacing

ρ void density or the number of voids per unit area of grain boundary (defined for square periodic array)

σ_{∞} applied stress (hoop stress)

σ_e equivalent (Von Mises) stress

$$= \left[\frac{1}{2} \left[(\sigma_1 - \sigma_2)^2 + (\sigma_1 - \sigma_3)^2 + (\sigma_2 - \sigma_3)^2 \right] \right]^{\frac{1}{2}}$$

where σ_1 , σ_2 and σ_3 are the principal stresses

σ_{TH} theoretical cohesive stress

σ_{zz} axial stress

Ω atomic volume

* See Raj and Ashby [36] for a detailed definition

10 References

- [1] U.S. Nuclear Regulatory Commission, "Standard Review Plan for Dry Cask Storage Systems: Final Report," NUREG-1536, January 1997
- [2] *U.S. Code of Federal Regulations*, Part 72, "Licensing Requirements for the Independent Storage of Spent Nuclear Fuel and High-Level Radioactive Waste," Title 10, "Energy"
- [3] M.W. Schwartz and M.C. Witte, "Spent Fuel Cladding Integrity During Dry Storage," Lawrence Livermore National Laboratory, UCID-21181, September 1987
- [4] I.S. Levy, B.A. Chin, E.P. Simonen, C.E. Beyer, E.R. Gilbert, and A.B. Johnson, Jr., "Recommended Temperature Limits for Dry Storage of Spent Light Water Reactor Zircaloy-Clad Fuel Rods in Inert Gas," Pacific Northwest Laboratory, PNL-6189, May 1987
- [5] G.H. Edward and M.F. Ashby, "Intergranular Fracture During Power-Law Creep," *Acta Met.*, V27, pp. 1505-1518, 1979
- [6] A.C.F. Cocks and M.F. Ashby, "On Creep Fracture by Void Growth," *Prog. Mater. Sci.*, V27, pp. 189-244, 1982
- [7] A.C.F. Cocks and M.F. Ashby, "Intergranular Fracture During Power-Law Creep under Multiaxial Stresses," *Met. Sci.*, V14, pp. 395-402 1980
- [8] A.C.F. Cocks and M.F. Ashby, "Creep Fracture by Coupled Power-Law Creep and Diffusion under Multiaxial Stress," *Met. Sci.*, V16, pp. 465-474, 1982
- [9] I.W. Chen and A.S. Argon, "Diffusive Growth of Grain Boundary Cavities," *Acta Met.*, V29, pp. 1759-1768, 1981
- [10] W. Beere and M.V. Speight, "Creep Cavitation by Vacancy Diffusion in Plastically Deforming Solid," *Met. Sci.*, V12, pp. 172-176, 1978
- [11] P.M. Anderson and J.R. Rice, "Constrained Creep Cavitation of Grain Boundary Facets," *Acta Met.*, V33, No. 3, pp. 409-422, 1985

-
- [12] D.S. Wilkinson, "The Effect of Time-Dependent Void Density on Grain Boundary Creep Fracture-I. Continuous Void Coalescence," *Acta Met.*, V35, pp. 1251-1259, 1987
- [13] D.S. Wilkinson, "The Effect of Time-Dependent Void Density on Grain Boundary Creep Fracture-II. Continuous Nucleation," *Acta Met.*, V35, pp. 2791-2799, 1987
- [14] A.H. Chokshi, "Analysis of Constrained Cavity Growth During High Temperature Creep Deformation," *Mater. Sci and Tech.*, V3, pp. 656-664, 1987
- [15] J. Svoboda and J. Cadek, "Modeling Intergranular Cavity Growth with Special Reference to the Mechanism of Coupled Diffusion and Power-Law Creep," *Mater. Sci. and Eng.*, V93, pp. 135-149, 1987
- [16] J.S. Wang, L. Martinez and W.D. Nix, "A Study of Intergranular Cavity Growth Controlled by the Coupling of Diffusion and Power Law Creep," *Acta Met.*, V31, pp. 873-881, 1983
- [17] H.M. Lu and T.J. Delph, "Models for Coupled Diffusive/Strain Controlled Growth of Creep Cavities," *Scripta Met.*, V29, pp. 281-285, 1993
- [18] L. Martinez and W.D. Nix, "Effects of Capillarity on Intergranular Cavity Growth Controlled by Diffusion and Plasticity," *Scripta Met.*, V15, pp. 757-761, 1981
- [19] A. Needleman and J.R. Rice, "Plastic Creep Flow Effects in the Diffusive Cavitation of Grain Boundaries," *Acta Met.*, V28, pp. 1315-1332, 1980
- [20] J.H. Schneibel and L. Martinez, "The Limitations of the Chen and Argon and Martinez and Nix Models for Intergranular Cavity Growth," *Scripta Met.*, V21, pp. 495-500, 1987
- [21] W.D. Nix, "Mechanisms and Controlling Factors in Creep Fracture," *Mech. Behavior of Mater.-V*, V2, pp. 1383-1398, 1988
- [22] W.D. Nix, "Mechanisms and Controlling Factors in Creep Fracture," *Mater. Sci. and Eng.*, V A103, pp. 103-110, 1988
- [23] G. Kaspar, M. Peehs, E. Steinberg and H. Schonfeld, "Experimental Investigations of Post-Pile Creep on Zircaloy Cladding Tubes," in Trans. 8th Intl. SMiRT Conf., North Holland, Amsterdam, paper C1/8, 1985

-
- [24] M. Peehs, R. Bokelmann and J. Fleisch, "Spent Fuel Dry Storage Performance in Inert Atmosphere," in Proc. 3rd Intl. Spent Fuel Storage Technology Symp./ Workshop, CONF-860417, V1, pp. S-215 to S-230, 1986
- [25] M. Peehs, G. Kaspar and E. Steinberg, "Experimentally Based Spent Fuel Dry Storage Performance Criteria," in Proc. 3rd Intl. Spent Fuel Storage Technology Symp./ Workshop, CONF-860417, V1, pp. S-316 to S-331, 1986
- [26] M. Peehs and J. Fleisch, "LWR Spent Fuel Storage Behaviour," *J. Nuc. Mater.*, V137, pp. 190-202, 1986
- [27] G. Porsch, J. Fleisch and B. Heits, "Accelerated High-Temperature Tests with Spent PWR and BWR Fuel Rods under Dry Storage Conditions," *Nuc. Tech.*, V74, pp. 287-298, 1986
- [28] B.A. Chin, "Final Report, Deformation and Fracture Map Methodology for Predicting Cladding Behavior During Dry Storage," 872BC1PNLF, September 15, 1987
- [29] R. Roehnelt, M.E. Kassner, T.C. Kennedy, and R.S. Rosen, "Elastic Incompatibility Stresses Across Planar and Nonplanar Grain Boundaries in Silver, Aluminum, and Zirconium Applied to Ductile Fracture Criteria under High Triaxial Stress," Lawrence Livermore National Laboratory, UCRL-ID-124394, July 1996
- [30] R. Roehnelt, M.E. Kassner, T.C. Kennedy, and R.S. Rosen, "Elastic Incompatibility Stresses Across Planar and Non-Planar Grain Boundaries Applied to Ductile Fracture Criteria under High Triaxial Stress," *Scripta Mater.*, V36, pp. 605-610, 1997
- [31] M.E. Kassner, T.C. Kennedy and K.K. Schrems, "The Mechanisms of Ductile Fracture in Constrained Thin Silver Films," *Acta Mater.*, V46, pp. 6445-6457, 1998
- [32] B.A. Chin, M.A. Khan, J.C.L. Tarn and E.R. Gilbert, "Deformation and Fracture Map Methodology for Predicting Cladding Behavior During Dry Storage," Pacific Northwest Laboratory, PNL-5998, 1986
- [33] M.E. Cunningham, E.P. Simonen, R.T. Allemann, I.S. Levy, R.F. Hazelton and E.R. Gilbert, "Control of Degradation of Spent LWR Fuel During Dry Storage in an Inert Atmosphere," Pacific Northwest Laboratory, PNL-6364, October 1987
- [34] U.S. Nuclear Regulatory Commission, Spent Fuel Project Office Interim Staff Guidance – 11, May 13, 1999

-
- [35] K. Gruss, NMSS, private communication, December 1999
- [36] R. Raj and M.F. Ashby, "Intergranular Fracture at Elevated Temperature," *Acta Met.*, V23, pp. 653-666, 1975
- [37] B.A. Chin, N.H. Madsen and M.A. Khan, "Application of Zircaloy Deformation and Fracture Maps to Predicting Dry Spent Fuel Storage Conditions," Auburn University, under DOE Contract number DOE-ACOG-76RLO-1830, CONF8308975 at Pacific Northwest Laboratory, 1983
- [38] D. Hull and D.E. Rimmer, "The Growth of Grain-boundary Voids under Stress," *Philos. Mag.*, V4, pp. 673-687, 1959
- [39] M.V. Speight and J.E. Harris, "The Kinetics of Stress-Induced Growth of Grain-Boundary Voids," *Met. Sci.*, V1, pp. 83-85, 1967
- [40] M.V. Speight and W. Beere, "Vacancy Potential and Void Growth on Grain Boundaries" *Met. Sci.*, V9, pp. 190-191, 1975
- [41] C. Pescatore, M.G. Cowgill and T.M. Sullivan, "Zircaloy Cladding Performance under Spent Fuel Disposal Conditions – Progress Report," Brookhaven National Laboratory, BNL-52235 (Nuclear Waste Management-DOE/OSTI-4500-R75), October 1989
- [42] U.S. Nuclear Regulatory Commission (NRC), "Safety Evaluation Report Related to the Topical Safety Analysis Report for CASTOR V/21 Dry Spent Fuel Storage Cask – Appendix A: Analysis of Diffusion Controlled Cavity Growth (DCCG) Damage to Fuel Cladding in Dry Storage," September 1985
- [43] R. Chun, M. Witte, and M. Schwartz, "Dynamic Impact Effect on Spent Fuel Assemblies," Lawrence Livermore National Laboratory, UCID-21246, October 20, 1987
- [44] R. Chun, M. Witte, and M. Schwartz, "Dynamic Impact Effect on Spent Fuel Assemblies," in Proc. 9th Intl. Symp. on the Packaging and Transportation of Radioactive Materials, PATRAM '89, Washington DC, pp. 186-194, June 11-16, 1989
- [45] C. Pescatore and M.G. Cowgill, "Temperature Limit Determination for the Inert Dry Storage of Spent Nuclear Fuel – Final Report," Brookhaven National Laboratory, EPRI TR-103949, May 1994
- [46] F.L. Yaggee, R.F. Mattas and L.A. Neimark, "Characterization of Irradiated Zircaloys: Susceptibility to Stress-Corrosion Cracking – An Interim Report," Argonne National Laboratory, NP-1155, September 1979

-
- [47] J. Novak, I.J. Hastings, E. Mizzan and R.J. Chenier "Post-Irradiation Behavior of UO₂ Fuel I: Elements at 220-250°C in Air," *Nuc. Tech.*, V63, pp. 254-266, 1983
- [48] M. Peehs, H. Stehle and E. Steinberg, "Out-of-Pile Testing of Iodine Stress Corrosion Cracking in Zircaloy Tubing in Relation to Pellet Cladding Interaction Phenomenon," in Zirconium in the Nuclear Industry, ASTM STP 681, ASTM, pp. 244-260, 1979
- [49] J. Planell, M. Mason, and G. Guerra, "Extended Fuel Burnup Demonstration Program Topical Report," Transnuclear, Inc., DOE/ET/34014—11, 1983
- [50] M.A. McKinnon and E.R. Gilbert, "Dry Storage Surveillance Plan," Prepared for the Electric Power Research Institute under Contract Number RP 2813-27, Pacific Northwest Laboratory, Richland, Washington 99352, Informal Letter, November 1993
- [51] International Atomic Energy Agency, "Survey of Experience with Dry Storage of Spent Nuclear Fuel and Update of Wet Storage Experience," Technical Reports Series No. 290, IAEA, Vienna, 1988
- [52] M.A. McKinnon and V.A. Deloach, "Spent Nuclear Fuel Storage - Performance Tests and Demonstrations," Pacific Northwest Laboratory, PNL-8451, UC-510, April 1993
- [53] R.S. Rosen and W.J. O'Connell, "Creep Strains Predicted from Constitutive Equations for Zircaloy-Clad Spent Fuel Rods," in Proc. 6th Ann. Intl. Conf. on High-Level Radioactive Waste Management, Las Vegas, NV, ASCE and ANS, pp. 621-624, 1995
- [54] R.L. Keusseyan, "Grain Boundary Sliding and Related Phenomena," Ph.D. Dissertation, Cornell University, June 1985
- [55] P.L. Gruzin, V.S. Yemel'yanov, G.C. Ryabova, and G.B. Federov, "Study of the Diffusion and Distribution of the Elements in Zirconium and Titanium Base Alloys by the Radioactive Isotope Method," in Proc. 2nd UN International Conference on the Peaceful Uses of Atomic Energy; Volume 19, The Use of Isotopes: Industrial Use, Geneva, pp. 187-192, 1958
- [56] G.B. Fedorov, and F.I. Zhomov, "Diffusion of Zr and Sn in Sn Alloys of α -Zr," *Metall. Metall. Metall.*, No. 1, pp. 161-169, 1959
- [57] F. Dymant, and C.M. Libanati, "Self-Diffusion of Ti, Zr, and Hf in their HCP Phases, and Diffusion of Nb⁹⁵ in HCP Zr," *J. Mater. Sci.*, V3, pp. 349-359, 1968

-
- [58] P. Flubacher, "Selbst-Diffusionsversuche in α -Zirkon," EIR-Bericht Nr., V49, 1963
- [59] V.S. Lyashenko, V.N. Bykov, and L.V. Pavlinov, "A Study of Self-Diffusion in Zirconium and Its Alloys With Tin," *Phys. of Metall. and Metallog.*, V8, No. 3, pp. 40-46, 1959
- [60] G.M. Hood, "Diffusion and Vacancy Properties of α -Zr," *J. Nuc. Mater.*, V139, pp. 179-184, 1986
- [61] G.V. Kidson, "A Review of Diffusion Processes in Zirconium and Its Alloys," *Electrochem. Tech.*, V4, pp. 193-205, 1966
- [62] E.V. Borisov, Yu.G. Godin, P.L. Gruzin, A.J. Evstyukhin and V.S. Emel'yanov, "Study of Diffusion in Zirconium and in Certain Zirconium Based Alloys," in All-Union Conf. Use of Isotopes and Radiation, Moscow, *Metall. and Metallog.*, pp. 291-298, 1957 (Pub. 1958)
- [63] J. Horvath, F. Dymont, and H. Mehrer, "Anomalous Self-Diffusion in a Single Crystal of α -Zirconium," *J. Nuc. Mater.*, V126, pp. 206-214, 1984
- [64] F. Povolo and G.H. Rubiolo, "Influence of Strain-Aging on the Load-Relaxation of α -Zirconium," *Philos. Mag.*, V56, pp. 209-229, 1987
- [65] E.A. Smirnov, K.E. Smirnov, I.L. Krylov and Yu.A. Shevchuk, "The Regularities of the Diffusion Processes in the Close Packed Phases of the Anomalous Metals," *Def. and Diff. Forum*, V66-69, pp. 359-364, 1989
- [66] N. Matsuura, G.M. Hood and H. Zou, "The Correspondence Between Self-diffusion Properties and Melting Temperatures for α -Zr and α -Ti," *J. Nuc. Mater.*, V238, pp. 260-263, 1996
- [67] G.M. Hood, "The Anomalous Self-diffusion in α -Zr," *J. Nuc. Mater.*, V135, pp. 292-295, 1985
- [68] G.M. Hood, "Point Defect Diffusion in α -Zirconium," *J. Nuc. Mater.*, V159, pp. 149-175, 1988
- [69] M. Lubbehusen, K. Vieregge, G.M. Hood, H. Mehrer and Chr. Herzig, "Self-diffusion in α -Zr Single Crystals," *J. Nuc. Mater.*, V182, pp. 164-169, 1991
- [70] G.M. Hood, H. Zou, R.J. Schultz, E.H. Bromley and J.A. Jackman, "Diffusion of Ti in α -Zr Single Crystals," *J. Nuc. Mater.*, V217, pp. 229-232, 1994

-
- [71] M.C. Naik, R.P. Agarwala, "Self and Impurity Diffusion in Alpha-Zirconium," *Acta Met.*, V15, pp. 1521-1525, 1967
- [72] N.L. Peterson, "Diffusion in Anomalous BCC Metals," *Comments Solid State Phys.*, V8, pp. 93-106, 1978
- [73] G.M. Hood, "Tracer Diffusion in α -Zr," *Acta Met.*, V22, pp. 459-464, 1974
- [74] W. Frank, "The Mechanism of Self-diffusion in alpha-Zirconium," *Defect and Diff. Forum*, V66-69, pp. 387-394, 1989
- [75] E. Forlerer de Svarch and C. Rodriguez, "On the Influence of Iron on the Zr- α (hcp) Self-diffusion," *J. Nuc. Mater.*, V185, pp. 167-173, 1991
- [76] C. Rodriguez and E. Forlerer de Svarch, "The Influence of Iron Impurities on Grain Boundary Self-diffusion in Zirconium below 1138 K," *J. Nuc. Mater.*, V187, pp. 97-98, 1992
- [77] R.A. Perez, F. Dymant, Hj. Matzke, G. Linker and H. Dhers, "Zr Diffusion in α -Ti Measured by RBS and HIRBS," *J. Nuc. Mater.*, V217, pp. 48-53, 1994
- [78] F. Dymant, M. Behar, H. Dhers, P.L. Grande, E. Savino and F.C. Zawislak, "Diffusion of Hf in α -Zr," *Appl. Phys. A*, V51, pp. 29-33, 1990
- [79] G.M. Hood, "Diffusion in α -Zr, HCP and Open Metals," *Def. and Diff. Forum*, V95-98, pp. 755-774, 1993
- [80] H. Nakajima, G.M. Hood and R.J. Schultz, "Diffusion of ^{59}Fe in Single-Crystal α -Zr," *Philos. Mag. B*, V58, pp. 319-337, 1988
- [81] B.A. Chin and E.R. Gilbert, "Prediction of Maximum Allowable Temperatures for Dry Storage of Zircaloy-Clad Spent Fuel in Inert Atmosphere," *Nuc. Tech.*, V85, pp. 57-65, 1989
- [82] L. Santanam, S. Raghavan, and B.A. Chin, "Zircaloy Cladding Rupture During Repository Storage," *Nuc. Tech.*, V97, pp. 316-322, 1992
- [83] B.A. Chin, N.H. Madsen, and E.R. Gilbert, "Deformation and Fracture Maps for Predicting the Failure Behavior of Zircaloy Clad Spent Fuel -- First Report," Battelle Pacific Northwest Laboratory, September 1982
- [84] B.A. Chin, private communication, October 1997

-
- [85] V. Fidleris, "Summary of Experimental Results on In-Reactor Creep and Irradiation Growth of Zirconium Alloys," *At. Energy Rev.*, V13, pp. 51-80, 1975
- [86] R.B. Jones, "Diffusion-Creep in Zirconium Alloys," *J. Nuc. Mater.*, V19, pp. 204-207, 1966
- [87] D.S. Wood and B. Watkins, "A Creep Limit Approach to the Design of Zircaloy-2 Reactor Pressure Tubes at 275°C," *J. Nuc. Mater.*, V41, pp. 327-340, 1971
- [88] M. Pahutova, K. Kucharova and J. Cadek, "Some Basic Creep Characteristics of Zr-Sn-Mo and Zr-Sn-Mo-Nb Alloys, Part I. Steady State Creep," *Mater. Sci. and Eng.*, V27, pp. 239-248, 1977
- [89] M. Pahutova, K. Kucharova and J. Cadek, "Some Basic Creep Characteristics of Zr-Sn-Mo and Zr-Sn-Mo-Nb Alloys, Part II. Fracture in Creep," *Mater. Sci. and Eng.*, V27, pp. 249-255, 1977
- [90] O.D. Sherby and P.M. Burke, "Mechanical Behavior of Crystalline Solids at Elevated Temperature," *Prog. in Mater. Sci.*, V13, pp. 325-390, 1967
- [91] A.J. Ardell and O.D. Sherby, "The Steady-State Creep of Polycrystalline Alpha Zirconium at Elevated Temperatures," *Trans. Met. Soc. of AIME*, V239, pp. 1547-1556, 1967
- [92] E.R. Gilbert, "In-Reactor Creep of Zr-2.5 at% Nb," *J. Nuc. Mater.*, V26, pp. 105-111, 1968
- [93] C.E. Coleman, A.R. Causey and V. Fidleris, "In-Reactor Creep of Zirconium-2.5 wt% Niobium at 570K," *J. Nuc. Mater.* V60, pp. 185-194, 1976
- [94] Y. Matsuo, "Thermal Creep of Zircaloy-4 Cladding under Internal Pressure," *J. Nuc. Sci. and Tech.*, V24[2], pp. 111-119, 1987
- [95] J. Novotny, J. Fiala and J. Cadek, "Harper-Dorn Creep in Alpha-Zirconium," *Acta Met.*, V33, pp. 905-911, 1985
- [96] F. Povolo and A.J. Marzocca, "Creep of Cold-Worked Zry-4 at 673K," *J. Nuc. Mater.*, V97, pp. 323-332, 1981
- [97] J. Fiala and J. Cadek, "Creep in Zirconium at Low Stresses and Temperatures from 748 to 973K," *Mater. Sci. and Eng.*, V75, pp. 117-126, 1985

-
- [98] R.C. Ecob and A.T. Donaldson, "A Microstructural Investigation of Steady State Creep of Zircaloy-4 at 973K," *J. Nuc. Mater.*, V132, pp. 110-125, 1985
- [99] M. Pahutova and J. Cadek, "Steady State Creep of Zr-Nb Alloys in a Temperature Interval 350 to 550°C," *J. Nuc. Mater.*, V61, pp. 285-296, 1976
- [100] K.L. Murty and S.T. Mahmood, "Effects of Recrystallization and Neutron Irradiation on Creep Anisotropy of Zircaloy Cladding," in Zirconium in the Nuclear Industry, ASTM STP 1132, ASTM, pp. 198-217, 1991
- [101] M. Stephan, E. Adam and L. Wetzel, "Activation Energies for Thermal Creep of the Zr 1%Nb Alloy in the α -Zr and β -Zr Phase Regions," *Kerntechnik*, V57, pp. 129-132, 1992
- [102] H. Maki and T. Hara, "Out-of-Reactor Study on External-Pressure Creep of Zircaloy-2 Fuel Cladding Tubes," *J. Nuc. Sci. and Tech.*, V12[1], pp. 43-52, 1975
- [103] H. Siethoff and K. Ahlborn, "Steady-State Deformation of α -Zr and α -Ti at Intermediate Temperatures," *Scripta Met.*, V21, pp. 1439-1444, 1987
- [104] J.J. Holmes, "The Activation Energies for Creep of Zircaloy-2," *J. Nuc. Mater.*, V13, pp. 137-141, 1964
- [105] H.E. Rosinger, P.C. Bera, and W.R. Clendening, "Steady-State Creep of Zircaloy 4 Fuel Cladding from 940 to 1873°K," *J. Nuc. Mater.*, V82, pp. 286-297, 1979
- [106] E.H. Toscano, M. Bocek, and C. Petersen, "The Prediction of Failure Strain for Zircaloy 4 Subjected to Non-Stationary Loading Conditions," *J. Nuc. Mater.*, V91, pp. 151-155, 1980
- [107] G.S. Clevinger, "Ex-Reactor Biaxial Creep of Zircaloy 4 Cladding," *ANS Trans.*, V19, pp. 143-150, 1974
- [108] U.M. Corso and R.A. Queeney, "Sustained Load Crack Growth in Zircaloy-4 at Elevated Temperatures," *Met. Trans. A*, V12A, pp. 357-359, 1981
- [109] R.C. Aungst, "Stress Rupture Tests of Zircaloy 2 Pressure Tubes," BNWL-8, January 1965
- [110] J.A. VanEcho and S.W. Porembka, "Long-Term Creep Rupture of Sintered Aluminum Powder and Zircaloy 2 Alloys," BMI-X-10113, January 25, 1965

-
- [111] T.C. Monkman and N.H. Grant, "An Empirical Relationship Between Rupture Life and Minimum Creep Rate in Creep-Rupture Tests," *Proc. ASTM*, V56, pp. 593-605, 1956
- [112] W.D. Nix, D.K. Matlock and R.J. DiMelfi, "A Model for Creep Fracture Based on the Plastic Growth of Cavities at the Tips of Grain Boundary Wedge Cracks," *Acta Met.*, V25, pp. 495-503, 1977
- [113] R. Raj, "Intergranular Fracture in Bicrystals," *Acta Met.*, V26, pp. 341-349, 1978
- [114] M. Bocek and P. Hoffman, "Creep Rupture at Superimposed Non-Stationary Stress and Temperature Loading," *J. Nuc. Mater.*, V89, pp. 62-70, 1980
- [115] M. Bocek, "Creep Rupture at Monotonous Stress and Temperature Ramp Loading II. Application to Zircaloy," *J. Nuc. Mater.*, V82, pp. 339-346, 1979
- [116] L.I. Ivanov and V.A. Yanushkevich, "High Temperature Mechanism of Steady-State Creep in BCC Metals, Creep of Zirconium," *Phys. Met. and Metall.*, V17, No. 1, pp. 102-106, 1964
- [117] E.F. Ibrahim, "Creep Ductility of Cold Worked Zr-2.5 wt% Nb and Zircaloy 2 Tubes In-Reactor," *J. Nuc. Mater.*, V96, pp. 297-304, 1981
- [118] B. Lustman and J.G. Goodwin, "Zirconium and Its Alloys," in C.R. Tipton, ed., Reactor Handbook-Second Edition, Vol. 1 Materials, Interscience, New York, pp. 708-738, 1960
- [119] J.E. Harbottle, "Anisotropic Irradiation Creep of Zircaloy 2," *Philos. Mag. A*, V38, pp. 49-60, 1978
- [120] B. Watkins and D.S. Wood, "The Significance of Irradiation-Induced Creep on Reactor Performance of a Zircaloy-2 Pressure Tube," in Applications-Related Phenomena for Zirconium and Its Alloys ASTM STP 458, ASTM, pp. 226-240, 1969
- [121] J. Ahlf, A. Reymann, O. Eichhorn, and M. Gartner, "Design of an Irradiation Device for the Determination of the In-Pile Creep Behavior of Zircaloy Cladding Tubes under Internal and External Overpressure, in FRG-2," *J. Nuc. Mater.*, V65, pp. 302-306, 1977
- [122] E. Tenckhoff, "Operable Deformation Systems and Mechanical Behavior of Textured Zircaloy Tubing," in Zirconium in Nuclear Applications, ASTM STP 551, ASTM, pp. 179-180, 1974

-
- [123] M. Bocek, "On the Comparison Between Stationary and Non-Stationary High Temperature Tensile Creep," *J. Nuc. Mater.*, V102, pp. 47-53, 1981
- [124] M. Bocek and A. Armas, "Comparison Between Tensile Static and Cyclic Creep at High Temperature," *Res. Mechanica Letters*, V1, pp. 383-386, 1981
- [125] C.R. Woods, ed. "Properties of Zircaloy 4 Tubing," WAPD-TM-585, 235 pp., December 1966
- [126] D.G. Franklin and H.D. Fisher, "Requirements for In-Reactor Zircaloy Creep Measurements for Application in the Design of PWR Fuel," *J. Nuc. Mater.*, V65, pp. 192-199, 1976
- [127] F. Dobes and K. Milicka, "The Relation Between Minimum Creep Rate and Time to Fracture," *Met. Sci.*, V10, pp. 382-384, 1976
- [128] E.H. Toscano and M. Bocek, "Relationship Between Strain Rate, Strain to Failure and Life Time," *J. Nuc. Mater.*, V96, pp. 29-36, 1981
- [129] M.A. Eisenberg, C.S. Hartley, J.C. Lee, and C.F. Yen, "Influence of Texture on the Analysis of Thermoelastic/Plastic Anisotropy and the Initial Yielding of Zircaloy Tubes," *J. Nuc. Mater.*, V88, pp. 138-152, 1980
- [130] D.O. Pickman, "Properties of Zircaloy Cladding," *Nuc. Eng. and Design*, V21, pp. 212-236, 1972
- [131] D.A. Woodford, "Creep Analysis of Zircaloy 4 and Its Application in the Prediction of Residual Stress Relaxation," *J. Nuc. Mater.*, V79, pp. 345-353, 1979
- [132] P.J. Pankaskie, "Irradiation Effects on the Mechanical Properties of Zirconium and Dilute Zirconium Alloys: A Review," Battelle Pacific Northwest Laboratories, BN-SA-618, July 1976
- [133] V. Ramachandran, A.T. Santhanam and R.E. Reed-Hill, "Dislocation-Solute Interactions and Mechanical Behavior of Zirconium and Titanium," *Indian J. of Tech.*, V11, pp. 485-492, 1973
- [134] G.P. Sabol, and S.G. McDonald, "Strain Rate Dependent Mechanical Response of Zircaloy 4," *J. Nuc. Mater.*, V64, pp. 223-227, 1977
- [135] D.G. Hardy, "The Effect of Neutron Irradiation on the Mechanical Properties of Zirconium Alloy Fuel Cladding in Uniaxial and Biaxial Test," in Irradiation Effects on Structural Alloys for Nuclear Reactor Applications, ASTM STP 484, ASTM, pp. 215-257, 1970

-
- [136] P.J. Pankaskie, "Creep Properties of Zircaloy 2 for Design Application," U.S. Atomic Energy Commission Report, HW-75267, 25pp., 1962
- [137] K.M. Rose and E.D. Hindle, "Diameter Increases in Steam Generating Heavy Water Reactor Zircaloy Cans under Loss-of-Coolant Accident Conditions," in Zirconium in the Nuclear Industry, ASTM STP 633, ASTM, pp. 24-35, 1977
- [138] C.E.L. Hunt, and D.E. Foote, "High Temperature Strain Behavior of Zircaloy-4 and Zr-2.5 Nb Fuel Sheaths," in Zirconium in the Nuclear Industry, ASTM STP 633, ASTM, pp. 50-56, 1977
- [139] M. Bocek, P. Hofmann, and C. Petersen, "Superplasticity of Zircaloy-4," in Zirconium in the Nuclear Industry, ASTM STP 633, ASTM, pp. 66-81, 1977
- [140] E. Kohn, "In-Reactor Creep of Zr-2.5 Nb Fuel Cladding," in Zirconium in the Nuclear Industry, ASTM STP 633, ASTM, pp. 402-417, 1977
- [141] A.K. Miller, "Progress in Modeling of Zircaloy Nonelastic Deformation using a Unified Phenomenological Model," in Zirconium in the Nuclear Industry, ASTM STP 633, ASTM, pp. 523-540, 1977
- [142] C.C. Dollins and F.A. Nichols, "Mechanisms of Irradiation Creep in Zirconium-Base Alloys," in Zirconium in Nuclear Applications, ASTM STP 551, ASTM, pp. 229-248, 1974
- [143] D.L. Douglas, The Metallurgy of Zirconium, *At. Energy Rev.*, Supplement, V9, 1971
- [144] E.R. Gilbert, S.A. Duran, and A.L. Bement, "Creep of Zirconium from 50 to 850C," in Applications-Related Phenomena for Zirconium and Its Alloys, ASTM STP 458, ASTM, p. 210-225, 1968
- [145] M.J. Luton and J.J. Jonas, "Solute Strengthening at High Temperatures in Zirconium-Tin Alloys," *Canadian Metall. Quarterly*, V11, pp. 79-90, 1972
- [146] B.D. Clay and R. Stride, "Creep Rupture Properties of Zircaloy-2 Tubes from 1000 to 1200°C," Central Electricity Generating Board, Berkeley Nuclear Laboratories Report, CEGB-RD/B/N 3782, Berkeley, England, 1976
- [147] W.R. Clendening, "Primary and Secondary Creep Properties for Zircaloy Cladding at Elevated Temperatures of Interest in Accident Analysis," in Proc. 2nd SMIRT Conf., paper C2/6, London, 1975

-
- [148] T. Healey, H.E. Evans, and R.B. Duffey, "Deformation and Rupture of Pressurized and Transiently Heated Zircaloy Tube," *J. British Nuc. Energy Soc.*, V15, pp. 247-251, 1976
- [149] B.D. Clay and R. Stride, "The Primary and Secondary Creep Properties of Beta Phase Zircaloy-2 in the Region 1200 to 1500°C" Central Electricity Generating Board, Berkeley Nuclear Laboratories Report, CEGB-RD/B/N 3950, Berkeley, England, 1977
- [150] H.E. Evans and G. Knowles, "A Model of Creep in Pure Metals," *Acta Met.*, V25, pp. 963-975, 1977
- [151] H.E. Evans and G. Knowles, "Dislocation Creep in Non-Metallic Materials," *Acta Met.*, V26, pp. 141-145, 1978
- [152] K.L. Murty, G.S. Clevinger and T.P. Papazaglow, "Thermal Creep of Zircaloy-4 Cladding," in Trans. 4th SMiRT Conf., paper C3/4, August 1977
- [153] F. Povolo, "The Determination of Creep Constants from Stress Relaxation Measurements in Bending and Torsion," *J. Nuc. Mater.*, V68, pp. 308-314, 1977
- [154] J.J. Kearns, J.E. McCauley and F.A. Nichols, "Effect of Alpha/Beta Phase Constitution on Superplasticity and Strength of Zircaloy 4," *J. Nuc. Mater.*, V61, pp. 169-184, 1976
- [155] K.M. Rose and E.D. Hindle, "The Deformation of Zircaloy 2 Fuel Cladding under Loss-of-Coolant Accident Transients," BNES International Conference on Liquid Alkali Metals, Nottingham, UK, paper 83, April 4-6, 1973
- [156] M.J. Luton, "High Temperature Deformation of Zirconium and Zirconium-Tin Alloys," Ph.D. Thesis, McGill University, Montreal, Quebec, Canada, 1971
- [157] D.G. Hardy, "High Temperature Expansion and Rupture Behavior of Zircaloy Tubing," National Topical Meeting on Water Reactor Safety, Salt Lake City, UT, NTIC-CONF-730304, pp. 254-273, March 26-28, 1973
- [158] P.A. Ross-Ross and M.J. Pettigrew, "The Creep Deflection of Pressure Tubes in Horizontal Reactors," in Proc. 1st SMiRT Conf., Berlin, West Germany, p. 1, 1971
- [159] P.A. Ross-Ross, V. Fidleris and D.E. Fraser, "Anisotropic Creep Behaviour of Zirconium Alloys in a Fast Neutron Flux," *Can. Metall. Q.*, V11, No. 2, pp. 101-111, 1972

-
- [160] J. Schroeder and M.J. Holicky, "On Secondary Creep of Anisotropic Nuclear Materials," *J. Nuc. Mater.*, V33, pp. 53-63, 1969
- [161] P.A. Ross-Ross and C.E.L. Hunt, "The In-Reactor Creep of C.W. Zircaloy-2 and Zr-2.5% Nb Pressure Tubes," *J. Nuc. Mater.*, V26, pp. 2-17, 1968
- [162] V. Fidleris, "The Effect of Texture and Strain Aging on Creep of Zircaloy-2," in Applications-Related Phenomena in Zirconium and Its Alloys, ASTM STP 458, ASTM, pp. 1-17, 1969
- [163] E. Tenckhoff, "Operation of Dislocations with (c+a) Type Burgers Vector during the Deformation of Zirconium Single Crystals," *Zeitschrift Fuer Metallkunde*, V63, pp. 192-197, 1972
- [164] J.A. Jensen and W.A. Backofen, "Deformation and Fracture of Alpha Zirconium Alloys," *Can. Metall. Q.*, V11, No. 1, pp. 39-51, 1972
- [165] C.C. Busby and K.B. Marsh, "High Temperature Time-Dependent Deformation in Internally Pressurized Zircaloy-4 Tubing (LBWR Development Program)," Westinghouse Electric Corporation, Bettis Atomic Power Laboratory Report, WAPD-TM-1043, 1974
- [166] H.E. Sills and R.A. Holt, "Predicting High-Temperature Transient Deformation from Microstructural Models," in Zirconium in the Nuclear Industry, ASTM STP 681, ASTM, pp. 325-341, 1978
- [167] R.A. Holt and H.E. Sills, "A Mathematical Model for Transient Deformation of α -Zirconium-Tin Alloys," *ANS Trans.*, V27, pp. 295-296, 1977
- [168] E.D. Hindle, "Creep and Mechanical Properties of Zircaloy Fuel Element Cladding in Steam," Proceedings Water Reactor Information Meeting, Washington, D.C., September 1975
- [169] B.D. Clay and G.B. Redding, "Creep Rupture Properties of Alpha-Phase Zircaloy Cladding Relevant to the Loss-of-Coolant Accident," CEGB Report RD/B/N 3187, 1975
- [170] T. Healey, H.E. Evans and R.B. Duffey, "Deformation and Rupture of Pressurized and Transiently Heated Zircaloy Tube," CEGB Report RD/B/N 3248, 1976
- [171] M.J. Luton and J.J. Jonas, "Solute and Sub-Structure Strengthening at High Temperatures in Zr-Sn Alloys," in Proc. 4th Conf. on Materials Technology, Caracas, pp. 1-7, 1975

-
- [172] A.M. Garde, H.M. Chung and T.F. Kassner, "Micrograin Superplasticity in Zircaloy at 850°C," *Acta Met.*, V26, pp. 153-165, 1978
- [173] D.W. James and G.M. Leak, "Grain Boundary Diffusion of Iron, Cobalt and Nickel in Alpha-iron and Iron in Gamma-iron," *Philos. Mag.*, V12, pp. 491-503, 1965
- [174] K. Vieregge and Chr. Herzig, "Grain Boundary Diffusion in α -Zirconium Part I: Self-Diffusion," *J. Nuc. Mater.*, V173, pp. 118-129, 1990
- [175] M. Griffiths, "A Review of Microstructure Evolution in Zirconium Alloys," *J. Nuc. Mater.*, V159, pp. 190-218, 1988
- [176] M. Griffiths, R.W. Gilbert and C.E. Coleman, "Grain Boundary Sinks in Neutron-Irradiated Zr and Zr-Alloys," *J. Nuc. Mater.*, V159, pp. 405-416, 1988
- [177] M. Griffiths, R.C. Styles, C.H. Woo, F. Phillipp and W. Frank, "Study of Point Defect Mobilities in Zirconium During Electron Irradiation in a High-Voltage Electron Microscope," *J. Nuc. Mater.*, V208, pp. 324-334, 1994
- [178] M. Griffiths, R.W. Gilbert and G.J.C. Carpenter, "Phase Instability, Decomposition and Redistribution of Intermetallic Precipitates in Zircaloy-2 and -4 During Neutron Irradiation," *J. Nuc. Mater.*, V150, pp. 53-66, 1987
- [179] D. Gilbon and C. Simonot, "Effect of Irradiation on the Microstructure of Zircaloy-4," in Zirconium in the Nuclear Industry, ASTM STP 1245, ASTM, pp. 521-548, 1994
- [180] G.J.C. Carpenter and J.F. Watters, "Irradiation Damage Recovery in Some Zirconium Alloys," in Zirconium in Nuclear Applications, ASTM STP 551, ASTM, pp. 400-415, 1974
- [181] I.M. Bernstein, "Diffusion Creep in Zirconium and Certain Zirconium Alloys," *Trans. Met. Soc. of AIME*, V239, pp. 1518-1522, 1967
- [182] N. Prasad, G. Malakondaiah and P. Rama Rao, "Low Stress Creep Behaviour of Zircaloy-2 Vis-A-Vis Zirconium," *Scripta Met.*, V26, pp. 541-543, 1992
- [183] D.B. Knorr and M.R. Notis, "Deformation Mechanism Mapping of α -Zr and Zircaloy-2," *J. Nuc. Mater.*, V56, pp. 18-24, 1975
- [184] V. Fidleris, "Uniaxial In-Reactor Creep of Zirconium Alloys," *J. Nuc. Mater.*, V26, pp. 51-76, 1968

-
- [185] R. Wu and R. Sandstrom, "Creep Cavity Nucleation and Growth in 12Cr-Mo-V Steel," *Mater. Sci. and Eng.*, V11, pp. 579-588, 1995
- [186] R.L. Keusseyan, C.P. Hu and C.Y. Li, "Creep Damage in Zircaloy-4 at LWR Temperatures," *J. Nucl. Mater.*, V80, pp. 390-392, 1979
- [187] B.J. Cane and G.W. Greenwood, "Nucleation and Growth of Cavities in Iron During Deformation at Elevated Temperatures," *Met. Sci.*, V9, pp. 55-60, 1975
- [188] D.M.R. Taplin and L.J. Barker, "A Study of the Mechanism of Intergranular Creep Cavitation by Shadowgraphic Electron Microscopy," *Acta Met.*, V14, pp. 1527-1531, 1966
- [189] R.C. Boettner and W.D. Robertson, "A Study of the Growth of Voids in Copper During the Creep Process by Measurement of the Accompanying Change in Density," *Trans. AIME*, V221, pp. 613-622, 1961
- [190] R.T. Ratcliffe and G.W. Greenwood, "The Mechanism of Cavitation in Magnesium During Creep," *Philos. Mag.*, V12, pp. 59-69, 1965
- [191] J.K. McCoy and T.W. Doering, "Prediction of Cladding Life in Waste Package Environments," *High Level Radioactive Waste Management: Proceedings of the 5th Annual International Conference, Volume 2, Las Vegas, pp. 565-572, May 22-26, 1994*
- [192] A.S. Argon, I.-W. Chen and C.W. Lau, "Intergranular Cavitation in Creep: Theory and Experiments," in R.M. Pelloux and N.S. Stoloff, eds., Creep-Fatigue-Environment Interactions, TMS/AIME, New York, pp. 46-83, 1980
- [193] G.B. Fedorov, "Some Aspects of Physical and Mechanical Properties of Zirconium and Its Alloys," in V.S. Yemel'yanov and A.I. Yevstyukhin, eds., Metallurgy and Metallography of Pure Metals, New York, pp. 106-112, 1962
- [194] A.I. Dashkovskiy and Ye.M. Savitskiy, "Temperature Function of Internal Friction, Youngs Modulus and Shear Modulus of Zirconium, Niobium and Zirconium-Niobium Alloys," in V.S. Yemel'yanov and A.I. Yevstyukhin, eds., Metallurgy and Metallography of Pure Metals, New York, pp. 218-227, 1962
- [195] M. Griffiths, D. Gilbon, C. Regnard and C. Lemaignan, "HVEM Study of the Effects of Alloying Elements and Impurities on Radiation Damage in Zr-Alloys," *J. Nuc. Mater.*, V205, pp. 273-283, 1993

-
- [196] A. Jostsons, P.M. Kelly, R.G. Blake and K. Farrell, "Neutron Irradiation-Induced Defect Structures in Zirconium," in Effects of Radiation on Structural Materials, ASTM STP 683, ASTM, pp. 46-61, 1979
- [197] M.A. McKinnon and A.L. Doherty, "Spent Nuclear Fuel Storage - Performance Tests and Demonstrations," Pacific Northwest National Laboratory, PNNL-11576, June 1997
- [198] N.Z. Godlewski, "Spent-Fuel Storage – An Update," *Nuc. News*, V30, pp. 47-52, 1987
- [199] J.P. Roberts and F.C. Sturz, "Progress in Dry Spent Fuel Storage Licensing and Rulemaking," in Proc. 3rd Intl. Spent Fuel Storage Technology Symp./ Workshop, CONF-860417, V1, pp. S-204 to S-212, 1986
- [200] A.B. Christensen, K.D. Fielding, L.W. Madsen and D.R. Teuscher, "Lessons Learned During Start-Up of a Facility for Storing Spent LWBR in Dry Wells at the Idaho Chemical Processing Plant," in Proc. 3rd Intl. Spent Fuel Storage Technology Symp./ Workshop, CONF-860417, V1, pp. S-156 to S-174, 1986
- [201] International Atomic Energy Agency, "Further analysis of extended storage of spent fuel," Final Report of a Co-ordinated Research Programme on the Behaviour of Spent Fuel Assemblies during Extended Storage (BEFAST III) 1991-1996, IAEA-TECDOC-944, May 1997
- [202] J. Fleisch and M. Peehs, "Analysis of Spent Fuel Behavior in Dry Storage Cask Demonstrations in the FRG," in Proc. 3rd Intl. Spent Fuel Storage Technology Symp./ Workshop, CONF-860417, V1, pp. S-253 to S-262, 1986
- [203] D.W. Patterson and D.S. Hoyer, "Canadian Experience Storing Irradiated CANDU Fuel in Concrete Canisters," in Proc. 3rd Intl. Spent Fuel Storage Technology Symp./ Workshop, CONF-860417, V1, pp. S-136 to S-155, 1986
- [204] B.R. Cundill, D.J. Wheeler and R.O. Barrett, "The Addition of Air-Cooled Dry Vault Storage Facilities to Operating Nuclear Plants," in Proc. 3rd Intl. Spent Fuel Storage Technology Symp./ Workshop, CONF-860417, V1, pp. P-16 to S-26, 1986
- [205] K.M. Wasywich, J. Freire-Canosa, S.J. Naqvi, "Canadian spent fuel storage experience," in Proc. IAEA Symp. on Safety and Engineering Aspects of Spent Fuel Storage, IAEA, Vienna, Austria, pp. 41-55, Oct. 10-14, 1994

-
- [206] M. Peehs, F. Takats, E. Vitkainen, K.M Wasywich, "The IAEA Co-ordinated research programme on the behaviour of spent fuel and storage facility components During Long Term Storage (BEFAST)", in Proc. IAEA Symp. on Safety and Engineering Aspects of Spent Fuel Storage, IAEA, Vienna, Austria, pp. 157-166, Oct 10-14, 1994
- [207] C.E. Coleman, "Tertiary Creep in Cold-Worked Zircaloy-2," *J. Nuc. Mater.*, V42, pp. 180-190, 1972
- [208] V. Fidleris and C.D. Williams, "Influence of Neutron-Irradiation on the Creep of Zircaloy-2 at 300°C," *Electrochem. Tech.*, V4, pp. 258-267, 1966
- [209] F. Povolo and A.J. Marzocca, "Creep of Cold-Worked Zry-4 at 673K," *J. Nuc. Mater.*, V97, pp. 323-332, 1981
- [210] H.C. Furtado, and I. Le May, "Modelling of Creep Damage to Estimate Remaining Life," *Mater. Sci. and Eng. A*, V A234-236, pp. 87-90, 1997
- [211] G. Kaspar, M. Peehs, J. Fleisch, and H. Unger, "Dry Storage Instrumented Bundle Experiments," in Proc. Specialist Workshop on Techniques for the Dry Storage of Spent Fuel Elements, Madrid, pp. 114-123, 1982
- [212] H. Spilker, M. Peehs, H-P. Dyck, G. Kaspar and K. Nissen, "Spent LWR Fuel Dry Storage in Large Transport and Storage Casks After Extended Burnup," *J. Nuc. Mater.*, V250, pp. 63-74, 1997
- [213] M. Mayuzumi and T. Onchi, "The Applicability of the Strain-Hardening Rule to Creep Deformation of Zircaloy Fuel Cladding Tube under Dry Storage Condition," *J. Nuc. Mater.*, V178, pp. 73-79, 1991
- [214] T.A. Hayes, M.E. Kassner, R.S. Rosen and D.A. Amick, "Thermal Stability of Surfaced Deformed Zirconium," *J. Nuc. Mater.*, V246, pp. 60-69, 1997
- [215] G.R. Thomas, "Updated Model for Predicting Spent Fuel Cladding Integrity During Dry Storage," Lawrence Livermore National Laboratory, UCID-134217, April 1999
- [216] C. Herring, "Diffusional Viscosity of a Polycrystalline Solid," *J. Appl. Phys.*, V21, pp. 437-445, 1950
- [217] A.J. Ardell, "On the Calculation of Melting Temperatures for Low-Temperature Phases of Polymorphic Metals," *Acta Met.*, V11, pp. 591-594, 1963

-
- [218] M.W. Schwartz and M.C. Witte, "Zircaloy Fuel Cladding Integrity During Dry Storage," in Proc. 9th Intl. Symp. on the Packaging and Transportation of Radioactive Materials, PATRAM '89, Washington DC, pp. 1523-1531, June 11-16, 1989
- [219] P.G. Shewmon, Diffusion in Solids, J. Williams Book Company, Jenks, OK, 1983
- [220] A. Wolfenden and K. Farrell, "On the Questions of Void Formation in Neutron Irradiated Zirconium," *Scripta Met.*, V6, pp. 127-130, 1972
- [221] G.J.C. Carpenter, "Void Formation in Zirconium under the High-Voltage Electron Microscope," *Radiation Effects*, V19, pp. 189-190, 1973
- [222] D. Lee, E.F. Kock, R.B. Adamson and W.L. Bell, "Use of Ion Bombardment to Study Irradiation Damage in Zr Alloys," Zirconium in Nuclear Applications, ASTM STP 551, ASTM, pp. 215-228, 1974
- [223] A. Riley and P.J. Grundy "Study by Electron Microscopy of Neutron Damage in Zirconium and Zircaloy-2," *Physica Status Solidi A*, V14, pp. 239-247, 1972
- [224] M. Yoo, "Suppression of Void Formation in Zirconium," Zirconium in Nuclear Applications, ASTM STP 551, ASTM, pp. 292-307, 1974
- [225] D.O. Northwood, "Irradiation Damage in Zirconium and Its Alloys," *At. Energy Rev.*, V15, pp. 547-610, 1977
- [226] M. Hadji-Mirzai and K.C. Russell, "Prediction of Void Formation Susceptibility in Irradiated Metals," *J. Nuc. Mater.*, V92, pp. 229-236, 1980

A Appendix A: Discussion of LLNL [3] Report

The DCCG models in the reports by LLNL [3] and, presumably, PNNL [4] (see discussion above) are based on the work of Raj and Ashby [36]. The work of Raj and Ashby is discussed below.

A1.1 Raj and Ashby [36]

The fracture time equation as it appears in Raj and Ashby for failure by diffusion controlled cavity growth, assuming a constant void density (no void nucleation) is

$$t_r = \frac{3\sqrt{\pi}}{32} \frac{kT}{\Omega D_{gb} \delta} \frac{1}{\sigma_{\infty} \rho^{\frac{3}{2}}} \frac{f_v(\alpha)}{f_B^{\frac{3}{2}}(\alpha)} \int_{A_{min}}^{A_{max}} \frac{dA}{f(A)} \quad (A-1)$$

where $f(A)$ is defined as

$$f(A) = \frac{\left[1 - \left(\frac{A_i}{A}\right)^{1/2}\right] (1-A)}{A^{1/2} \left[\frac{1}{2} \ln\left(\frac{1}{A}\right) - \frac{3}{4} + A\left(1 - \frac{A}{4}\right)\right]} \quad (A-2)$$

This definition of $f(A)$ is slightly different than the definition used by LLNL as will be discussed later. Raj and Ashby obtained the failure time in Equation A-1, t_r , by integrating the rate of area fraction of decohesion

$$\frac{dA}{dt} = \frac{32}{3\sqrt{\pi}} \frac{\Omega D_{gb} \delta}{kT} \sigma_{\infty} \rho^{\frac{3}{2}} \frac{f_B^{\frac{3}{2}}(\alpha)}{f_v(\alpha)} f(A) \quad (A-3)$$

or,

$$\int_{A_{min}}^{A_{max}} \frac{dA}{f(A)} = \frac{32}{3\sqrt{\pi}} \frac{\Omega D_{gb} \delta}{kT} \sigma_{\infty} \rho^{\frac{3}{2}} \frac{f_B^{\frac{3}{2}}(\alpha)}{f_v(\alpha)} \int_0^{t_f} dt \quad (A-4)$$

For the case of Zircaloy-clad spent nuclear fuel (SNF) rods in dry storage, some of the terms assumed constant by Raj and Ashby are not constant. Specifically, all temperature related terms are now functions of time, as the spent nuclear fuel rods experience temperature decay with time. The following constants in the Raj and Ashby equation can be considered nearly time independent:

Ω = atomic volume

δ = grain boundary thickness

ρ^{**} = void density, or voids per unit area of grain boundary (GB) for this analysis. The analysis of Raj and Ashby utilized by LLNL is only valid for the case where the void density remains constant (no nucleation).

k = Boltzmann's constant

$f_b(\alpha), f_v(\alpha)$ = functions of the void geometry. Assuming that the void shape remains constant, these functions are not functions of time.

** It should be noted that although it has been shown that there may be continuous nucleation of voids [54], the void density has been assumed to be constant by LLNL (this is discussed below).

The following variables are functions of temperature (and hence time):

D_{gb} = grain boundary diffusion coefficient

σ_{∞} = applied (hoop) stress. The hoop stress varies with pressure, which depends on the temperature according to the ideal gas law

T = temperature

Incorporating the appropriate time (temperature) functions into Equation A-4,

$$\int_{A_{min}}^{A_{max}} \frac{dA}{f(A)} = \frac{32}{3\sqrt{\pi}} \frac{\Omega\delta}{k} \rho^{\frac{3}{2}} \frac{f_B^{\frac{3}{2}}(\alpha)}{f_V(\alpha)} \int_0^{t_f} \frac{\sigma_{\infty}(t) D_{gb}(t)}{T(t)} dt \quad (A-5)$$

A1.2 LLNL [3]

Equation A-5 above results directly from Raj and Ashby when taking into account the time dependent terms in Equation A-4. LLNL reports the following equation for the fracture time

$$\int_{A_i}^{A_t} \frac{dA}{f(A)} = \int_0^{t_f} \frac{32}{3\sqrt{\pi}} \frac{f_B^{3/2}(\alpha)}{f_V(\alpha)} \frac{\Omega\delta\sigma_{\infty}}{k\lambda^3} \frac{D_{gb}(t)}{T(t)} dt \quad (A-6)$$

Equations A-5 and A-6 are, basically, equivalent. The void density, ρ , raised to the 3/2 and the inverse if the void spacing, λ , cubed are equivalent as Raj and Ashby define the void density as voids per unit area for a square, periodic, array of voids.

Raj and Ashby state that failure, as predicted by the integral of Equation A-5, approximately corresponds to an area fraction of decohesion, A , of 0.5. LLNL adopted a more limited area fraction of decohesion of 0.15 (15% area fraction of decohesion) as the failure criterion. This limit was developed based on the requirement that the fuel rods must be handled after dry storage and therefore must be able to withstand certain estimated loads and accelerations. Estimated loading calculations by Chun et al. [43,44] led to the 0.15 decohesion limit.

Upon examining the other terms in the equation for consistency, one notes that Raj and Ashby have used A_{min} and A_{max} whereas, LLNL have used A_i and A_t . According to the definitions of the terms given by the respective authors, the only difference between these terms is that A_{max} is the area fraction of decohesion upon creep rupture while A_t is the area fraction of decohesion after a time t . The terms $F_V(\alpha)$, $F_B(\alpha)$, σ_{∞} , δ , D_{gb} , T and Ω are all defined consistently by LLNL and Raj and Ashby.

As mentioned in the main body of this report, one inconsistency between Raj and Ashby and LLNL appears in the definition of $f(A)$. LLNL states that “in accordance with Raj and Ashby...” and then report the following equation when defining $f(A)$:

$$f(A) = \frac{\left[1 - \left(\frac{A_i}{A}\right)^{1/2}\right](1-A)}{A^{1/2} \left[\frac{1}{2} \ln\left(\frac{1}{A}\right) - \frac{3}{4} + A\left(1 - \frac{A}{4}\right) \right]} \quad (\text{A-7})$$

Equation A-7 was defined above as Equation 7. This differs in form from Raj and Ashby who define $f(A)$ according to Equation A-2.

$$f(A) = (1-A) \frac{\left[1 - \left(\frac{r_c}{r}\right)(1-A)\right]}{A^{1/2} \left[\frac{1}{2} \ln\left(\frac{1}{A}\right) - \frac{3}{4} + A\left(1 - \frac{A}{4}\right) \right]} \quad (\text{A-2})$$

The term $(A_i/A)^{1/2}$ in the LLNL Equation A-7 is equivalent to the term r_c/r appearing in the Raj and Ashby Equation A-2. These terms can be shown to be equivalent in two steps. First,

$$(A_i/A)^{1/2} = (r_c/r)$$

since r , the radius of the cavity in the plane of the grain boundary, is the basis for calculating A (the area fraction of decohesion) and r_i , the initial cavity radius, is the basis for calculating A_i (the initial area fraction of decohesion). For an initial value of the cavity radius r_i (and hence the initial area fraction of decohesion, A_i), one should look at the initial condition of the material. Initially, the material could be assumed to contain no cavities, so one might assume a value for r_i of zero. To be conservative, however, LLNL suggests that at the time that the fuel rods are inserted into dry storage, that a certain number of cavities exist and the growth of the cavities starts

at the time of insertion into dry storage. This assumption is conservative as long as the maximum void density (minimum void spacing) value is chosen, such as the void spacing at fracture (continuous nucleation may occur, possibly decreasing the void spacing with time – this is discussed below). LLNL and Raj and Ashby assume that radius of these cavities would be equal to the critical radius necessary for the formation of a stable cavity, defined as r_c . If

$$r_i = r_c$$

then

$$(A_i/A)^{1/2} = r_c/r$$

Equation A-7 as reported by LLNL is, however, different from the Raj and Ashby equation (Equation A-2) by a factor of $(1-A)$. This difference is due to different assumptions made by LLNL compared to Raj and Ashby when defining the mechanical equilibrium equation for forces acting across the grain boundary. LLNL includes a cavity surface tension force whereas Raj and Ashby ignore this term. This is shown in detail in the next section. The resulting difference between the equation reported by LLNL (A-7) and the equation reported by Raj and Ashby (A-2) in the

integral of $\int_{A_i}^{A_f} \frac{dA}{f(A)}$ is very minor (about 0.02%).

A1.3 Derivation of Raj and Ashby $f(A)$ equation

The equation reported by Raj and Ashby for the volumetric cavity growth rate is different than that reported by LLNL. An internal inconsistency was discovered in the Raj and Ashby analysis, which was probably due to a typographical error. The following mathematical exercise verifies which of the inconsistently reported Raj and Ashby equations is correct and why the LLNL equation is slightly different.

Starting with Equation A-8 for the chemical potential of atoms on the grain boundary where cavities are present, which is reported consistently by both Raj and Ashby and LLNL,

$$\Delta\mu = -\frac{\beta k T \Omega}{4D_{gb}}(R^2 - r_B^2) - \frac{\beta k T \Omega l^2}{2D_{gb}} \ln\left(\frac{r_B}{R}\right) - \frac{2\gamma\Omega}{r} \quad (\text{A-8})$$

combined with the equation for the excess chemical potential of atoms in the boundary relative to the stress free state [36,216]

$$\Delta\mu = -T_n \Omega \quad (\text{A-9})$$

and dividing by Ω gives

$$T_n = +\frac{\beta k T}{4D_{gb}}(R^2 - r_B^2) + \frac{\beta k T l^2}{2D_{gb}} \ln\left(\frac{r_B}{R}\right) + \frac{2\gamma}{r} \quad (\text{A-10})$$

Mechanical equilibrium across the grain boundary gives

$$\pi l^2 \sigma_\infty = \int_{r_B}^l T_n(R) 2\pi R dR \quad (\text{A-11})$$

In Equation A-11, the left-hand term is the applied stress (normal to the grain boundary) multiplied by the area associated with one cavity and the surrounding material (included radius of l ($\lambda/2$)), resulting in a force across the grain boundary. The right hand term is the equilibrating force that acts on the “donut” (decreased area surrounding each cavity). This force is obtained by integrating the product of the “traction”, T_n , acting on this reduced area and the differential area $2\pi R dR$. This is where the analysis by Raj and Ashby differs from that of LLNL. In the LLNL analysis, a cavity surface tension component was accounted for in the mechanical

equilibrium equation whereas Raj and Ashby only account for the increased stress on the reduced grain boundary area. This leads to the difference between the Raj and Ashby and the LLNL f(A) equations.

Substituting A-10 into A-11,

$$\pi l^2 \sigma_{\infty} = 2\pi \int_{r_B}^l \frac{\beta k T}{4D_{gb}} (R^3 - r_B^2 R) dR + 2\pi \int_{r_B}^l \frac{\beta k T l^2}{2D_{gb}} \ln\left(\frac{r_B}{R}\right) R dR + 2\pi \int_{r_B}^l \frac{2\gamma}{r} R dR \quad (\text{A-12})$$

Upon evaluation of the integrals and eliminating π ,

$$l^2 \sigma_{\infty} = \frac{\beta k T}{2D_{gb}} \left(\frac{R^4}{4} - r_B^2 \frac{R^2}{2} \right) \Big|_{r_B}^l + \frac{\beta k T l^2}{2D_{gb}} \left(\ln\left(\frac{r_B}{R}\right) R^2 + \frac{1}{2} R^2 \right) \Big|_{r_B}^l + \frac{2\gamma}{r} R^2 \Big|_{r_B}^l$$

or

$$l^2 \sigma_{\infty} = \frac{\beta k T}{2D_{gb}} \left(\frac{l^4}{4} - \frac{r_B^2 l^2}{2} + \frac{r_B^4}{4} \right) + \frac{\beta k T}{2D_{gb}} \left(\ln\left(\frac{r_B}{l}\right) l^4 + \frac{1}{2} l^4 - \frac{1}{2} r_B^2 l^2 \right) + \frac{2\gamma l^2}{r} - \frac{2\gamma r_B^2}{r}$$

Combining terms, eliminating l^2 and solving for β ,

$$\beta = \frac{\left(\sigma_{\infty} - \frac{2\gamma}{r} + \frac{2\gamma r_B^2}{l^2 r} \right) 2D_{gb}}{\left(\frac{3}{4} + \ln\left(\frac{r_B}{l}\right) - \left(\frac{r_B}{l}\right)^2 \left(1 - \left(\frac{r_B}{2l}\right)^2 \right) \right) k T l^2} \quad (\text{A-13})$$

The volumetric growth rate of the void is given by

$$\frac{dV}{dt} = -\beta \delta \pi l^2 \Omega \left(1 - \frac{r_B^2}{l^2} \right) \quad (\text{A-14})$$

This equation is reported consistently by both Raj and Ashby and LLNL. Substituting for β yields the equation for the volumetric cavity growth-rate

$$\frac{dV}{dt} = 2\pi\Omega \frac{D_{gb}\delta}{kT} \left(1 - \frac{r_B^2}{l^2}\right) \left[\frac{\sigma_\infty - \frac{2\gamma}{r} \left(1 - \frac{r_B^2}{l^2}\right)}{\ln \frac{l}{r_B} - \frac{3}{4} + \frac{r_B^2}{l^2} \left(1 - \frac{r_B^2}{4l^2}\right)} \right] \quad (\text{A-15})$$

This is different than the equation for the cavity growth rate reported by Raj and Ashby which appears as Equation 8 in Raj and Ashby [36], or

$$\frac{dV}{dt} = 2\pi\Omega \frac{D_B\delta}{kT} \left(1 - \frac{r_B^2}{l^2}\right) \left[\frac{\overbrace{\left(\sigma_\infty - \frac{2\gamma}{r}\right)}^* \left(1 - \frac{r_B^2}{l^2}\right)}{\ln \frac{l}{r_B} - \frac{3}{4} + \frac{r_B^2}{l^2} \left(1 - \frac{r_B^2}{4l^2}\right)} \right] \quad (\text{A-16})$$

Equation A-16 differs from A-15 in the placement of a set of parentheses in the term indicated by * in Equation A-16. The difference in Equation A-16 is, apparently, a typographical error made in the Raj and Ashby manuscript. This is shown as follows.

In order to express Equation A-15 in terms of the area fraction of decohesion, Raj and Ashby define the equation

$$A(t) = \frac{r_B^2}{l^2} \quad (\text{A-17})$$

where r_b is the radius of the cavity in the plane of the grain boundary and l is the half cavity spacing. This is defined by taking the ratio of cavity area on the grain

boundary (πr_B^2) to the total grain boundary area (πl^2). This is an approximation for an assumed periodic array of voids. Raj and Ashby have assumed a periodic array of voids with the configuration shown in Figure A-1

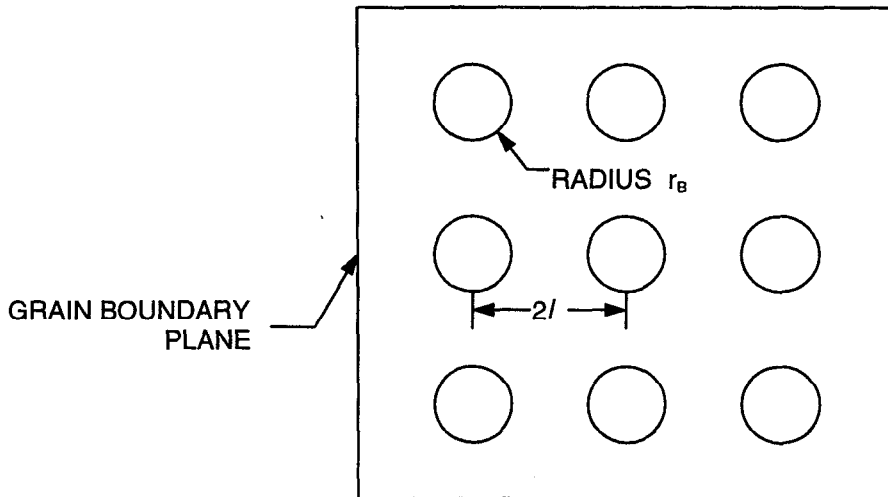


Figure A-1 Void configuration assumed by Raj and Ashby [36]

From Figure A-1, one might note that a more accurate definition of the area fraction of decohesion would be given by

$$A(t) = \frac{\pi r_B^2}{4l^2} \quad (\text{A-18})$$

Raj and Ashby instead chose to use a circular approximation for the grain boundary area, using a radius equal to half the cavity spacing. This results in an over prediction of the area fraction of decohesion $A(t)$ (under prediction of the grain boundary area) by 21.5%. Examination of Figure A-1, however, shows that the array of cavities is not the typical random array, which would be more accurately modeled by the configuration in Figure A-2.

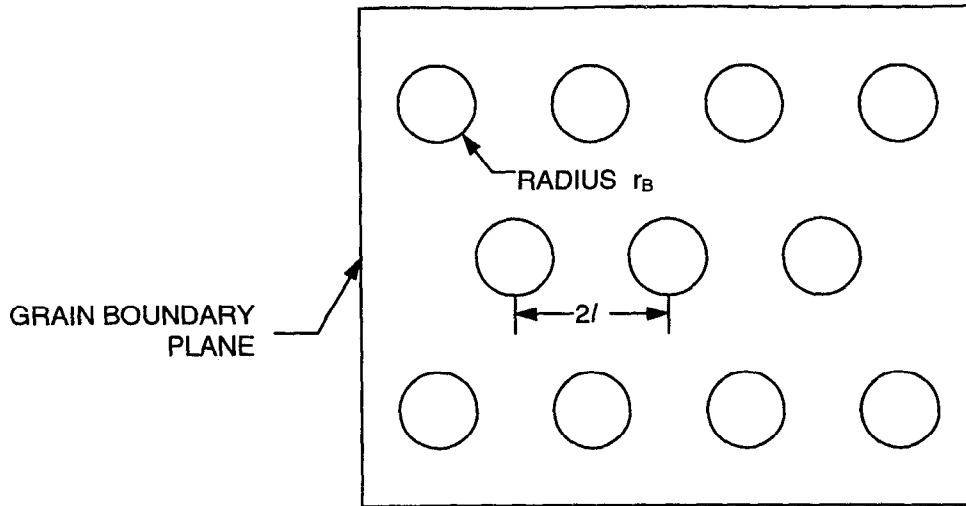


Figure A-2 A more realistic configuration for a periodic array of voids in a grain boundary

Using the periodic array model shown in Figure A-2, the exact area fraction of decohesion can be calculated by finding the area of a hexagon that surrounds each cavity, given by

$$6l^2 \tan 30 \tag{A-19}$$

The area fraction of decohesion becomes

$$A(t) = \frac{\pi r_B^2}{6l^2 \tan 30} \tag{A-20}$$

Using this model for the array of voids, the approximation made by Raj and Ashby overestimates the area fraction of decohesion by only 9.3%. Although the definition by Equation A-20 for the area fraction of decohesion may be more accurate, the definition given by Raj and Ashby (Equation A-17) is more convenient mathematically.

Substituting the Raj and Ashby definition for A (Equation A-17) into Equation A-15 yields

$$\left(\frac{dV}{dt}\right)_B = 2\pi\Omega \frac{D_{gb}\delta}{kT} (1-A) \left[\frac{\left(\sigma_\infty - \frac{2\gamma}{r}\right)(1-A)}{\ln\left(\frac{l}{r_B}\right) - \frac{3}{4} + A\left(1 - \frac{A}{4}\right)} \right] \quad (\text{A-21})$$

The $\ln\left(\frac{l}{r_B}\right)$ term can also be written in terms of the area fraction of decohesion, A ,

by

$$\frac{l}{r_B} = \frac{1}{A^{1/2}} \quad (\text{A-22})$$

$$\ln\left(\frac{l}{r_B}\right) = \ln\left(\frac{1}{A^{1/2}}\right) = \ln\left(\frac{1}{A}\right)^{1/2} = \frac{1}{2}\ln\left(\frac{1}{A}\right) \quad (\text{A-23})$$

The critical radius (the radius necessary for stable cavity growth based on surface tension), r_c , is defined by

$$r_c = \frac{2\gamma}{\sigma_\infty} \quad (\text{A-24})$$

Dividing by r ,

$$\frac{2\gamma}{r} = \frac{r_c \sigma_\infty}{r} \quad (\text{A-25})$$

Substituting Equations A-23 and A-25 into Equation A-21 yields

$$\frac{dV}{dt} = 2\pi\Omega \frac{D_{gb}\delta}{kT} (1-A) \left[\frac{\sigma_{\infty} \left(1 - \frac{r_c}{r} (1-A)\right)}{\frac{1}{2} \ln \frac{1}{A} - \frac{3}{4} + A \left(1 - \frac{A}{4}\right)} \right] \quad (\text{A-26})$$

The following relationships [36] are utilized to modify this in terms of the rate of change of the area fraction of decohesion:

$$r_B^2 = \frac{r^2}{\pi} f_B(\alpha) \quad (\text{A-27})$$

$$V = r^3 f_v(\alpha) \quad (\text{A-28})$$

Solving for r in Equation A-27 and substituting r into Equation A-28 yields

$$V = \frac{r_B^3 \pi^{\frac{3}{2}}}{f_B^{\frac{3}{2}}(\alpha)} f_v(\alpha) = \left(\frac{r_B^2}{l^2}\right)^{3/2} l^3 \frac{\pi^{3/2} f_v(\alpha)}{f_B^{3/2}(\alpha)} = \frac{A^{3/2} l^3 \pi^{3/2} f_v(\alpha)}{f_B(\alpha)} \quad (\text{A-29})$$

Differentiating with respect to t,

$$\frac{dV}{dt} = \frac{dA}{dt} \frac{3}{2} \frac{A^{1/2} l^3 \pi^{3/2} f_v(\alpha)}{f_B^{3/2}(\alpha)} \quad (\text{A-30})$$

or, solving for dA/dt,

$$\frac{dA}{dt} = \frac{2}{3} \frac{f_B^{3/2}(\alpha)}{f_v(\alpha) A^{1/2} l^3 \pi^{3/2}} \frac{dV}{dt} \quad (\text{A-31})$$

Finally, substituting dV/dt from Equation A-26 yields

$$\frac{dA}{dt} = \frac{4 \Omega D_{gb} \delta \sigma_{\infty}}{3 \pi^{1/2} kT} \frac{f_B^{\frac{3}{2}}(\alpha)}{l^3 \pi^2 f_v(\alpha)} (1-A) \left[\frac{\left(1 - \frac{r_c}{r}\right)(1-A)}{\frac{1}{2} \ln\left(\frac{1}{A}\right) - \frac{3}{4} + A\left(1 - \frac{A}{4}\right)} \right] \quad (\text{A-32})$$

Raj and Ashby use the cavity density ρ instead of the half cavity spacing, l , shown in Equation A-32. The cavity density can be expressed by

$$\rho = \frac{1}{4l^2} \quad (\text{A-33})$$

or,

$$l^3 = \frac{1}{8\rho^{\frac{3}{2}}} \quad (\text{A-34})$$

Substituting Equation A-34 into Equation A-32 results in.

$$\frac{dA}{dt} = \frac{32 \Omega D_{gb} \delta \sigma_{\infty}}{3 \pi^{\frac{1}{2}} kT} \frac{\rho^{\frac{3}{2}} f_B^{\frac{3}{2}}(\alpha)}{A^{\frac{1}{2}} f_v(\alpha)} (1-A) \left[\frac{1 - \left(\frac{r_c}{r}\right)(1-A)}{\frac{1}{2} \ln\left(\frac{1}{A}\right) - \frac{3}{4} + A\left(1 - \frac{A}{4}\right)} \right] \quad (\text{A-35})$$

This is precisely the equation reported by Raj and Ashby in Appendix II. The equation reported by Raj and Ashby for the volumetric cavity growth rate (reported above as Equation A-16 and in Raj and Ashby as Equation 8), then, must have had a typographical error. This was simply in the placement of one set of parentheses.

B Appendix B: Evaluation of and Comparison of LLNL and PNNL Suggested Constants

As was stated above, the LLNL (Raj and Ashby) DCCG failure model and the PNNL model yield fairly similar *results* as shown in Figure 2. This figure, although evaluated using the correct LLNL equation, is still misleading. The fact that the two models yield reasonably consistent dry storage temperature limits results from a combination of vastly different assumptions. This is discussed in further detail below.

B1.1 Input values suggested by PNNL

Before comparing PNNL [4] with LLNL [3], it may be helpful to first examine the values chosen by Chin (one of the authors of the PNNL report) in both earlier and later reports. This is difficult, however, because Chin appears to change the reported values in various reports without specifically stating the basis for this change. For example,

B1.1.1 Chin 1983 [37]:

$$t_{fDCCG} = \frac{6 \times 10^{-3} \lambda^3}{\delta D_o^{gb} b^2 \exp\left(\frac{-Q_{gb}}{RT}\right)} \frac{kT}{Eb} \left(\frac{\sigma}{E}\right)^{-1} \quad \text{DCCG fracture time equation}$$

$$t_{fPLC} = \frac{\left(1 - 0.78 \frac{P_0}{l_0}\right)}{1.48} \frac{1}{\dot{\epsilon}} \quad \text{power law creep fracture time equation}$$

$$Q_{gb} = 112 \frac{\text{kJ}}{\text{mole}} \quad \text{activation energy for grain boundary diffusion}$$

$$D_o^{gb} = 6 \times 10^{-10} \frac{\text{m}^2}{\text{s}} \quad \text{grain boundary diffusion constant}$$

$$Q_l = 250 \frac{\text{kJ}}{\text{mole}} \quad \text{activation energy for lattice diffusion}$$

$$D_o^l = 1 \times 10^{-4} \frac{\text{m}^2}{\text{s}} \quad \text{lattice diffusion constant}$$

$$E = \left(11.81 - 14.59 \frac{T}{T_m} \right) \times 10^4 \text{ MPa}, \frac{T_m}{T} \geq 4.06 \quad \text{modulus}$$

$$E = \left(11.09 - 11.61 \frac{T}{T_m} \right) \times 10^4 \text{ MPa}, \frac{T_m}{T} \leq 4.06$$

$$T_m = 2125 \text{ K}$$

melting temperature of Zircaloy

$$A_1 = 5 \times 10^7$$

low and high temperature climb creep strain rate coefficient

$$A_{CO} = 5 \times 10^2$$

Coble creep strain rate coefficient

$$A_{NH} = 5$$

Nabarro-Herring creep strain rate coefficient

$$A_{GBS} = 7.5 \times 10^6$$

grain boundary sliding (boundary diffusion) strain rate coefficient

$$A_{GBL} = 1 \times 10^3$$

grain boundary sliding (lattice diffusion) strain rate coefficient

B1.1.2 Chin 1986 [32]

$$t_{pCCG} = \frac{1.3462 \times 10^{-4} \lambda^3}{\delta D_o^{gb} b^2 \exp\left(\frac{-Q_{gb}}{RT}\right)} \frac{kT}{Eb} \left(\frac{\sigma}{E}\right)^{-1} \Leftarrow \text{before was } \frac{6 \times 10^{-3} \lambda^3}{\delta D_o^{gb} b^2 \exp\left(\frac{-Q_{gb}}{RT}\right)} \frac{kT}{Eb} \left(\frac{\sigma}{E}\right)^{-1}$$

$$t_{pLC} = \frac{(1 - 0.78 \frac{P_0}{l_0})}{4.87} \frac{1}{\dot{\epsilon}} \Leftarrow \text{before was } \frac{(1 - 0.78 \frac{P_0}{l_0})}{1.48} \frac{1}{\dot{\epsilon}}$$

fracture time equations

$$Q_{gb} = 175 \frac{\text{kJ}}{\text{mole}} \Leftarrow \text{was } 112 \frac{\text{kJ}}{\text{mole}}$$

activation energy for grain boundary diffusion

$$D_{o_{gb}} = 3.89 \times 10^{-6} \frac{\text{m}^2}{\text{s}} \Leftarrow \text{was } 6 \times 10^{-10} \frac{\text{m}^2}{\text{s}}$$

grain boundary diffusion constant

$$Q_l = 250 \frac{\text{kJ}}{\text{mole}}$$

activation energy for lattice diffusion

$$D_{ol} = 2 \times 10^{-4} \frac{\text{m}^2}{\text{sec}} \Leftarrow \text{was } 1 \times 10^{-4} \frac{\text{m}^2}{\text{s}}$$

lattice diffusion constant

$$E = \left(11.81 - 14.59 \frac{T}{T_m} \right) \times 10^4 \text{ MPa}, \frac{T_m}{T} \geq 4.06$$

modulus

$$E = \left(11.09 - 11.61 \frac{T}{T_m} \right) \times 10^4 \text{ MPa}, \frac{T_m}{T} \leq 4.06$$

$$T_m = 2125 \text{ K}$$

melting temperature of Zircaloy

$$A_1 = 7.4 \times 10^7 \Leftarrow \text{was } 5 \times 10^7$$

low and high temperature climb creep strain rate coefficient

Coble creep strain rate coefficient

$$A_{CO} = 5.362 \times 10^2 \Leftarrow \text{was } 5 \times 10^2$$

Nabarro-Herring creep strain rate coefficient

$$A_{NH} = 0.92 \Leftarrow \text{was } 5$$

$$A_{GBS} = 8.85 \times 10^6 \Leftarrow \text{was } 7.5 \times 10^6$$

grain boundary sliding (boundary diffusion) strain rate coefficient

$$A_{GBL} = 5 \times 10^2 \Leftarrow \text{was } 1 \times 10^3$$

grain boundary sliding (lattice diffusion) strain rate coefficient

B1.1.3 Chin 1987 (PNNL) [4]:

$$t_{pDCCG} = \frac{2.525 \times 10^{-3} \lambda^3}{\delta D_o^{gb} b^2 \exp\left(\frac{-Q_{gb}}{RT}\right)} \frac{kT \left(\frac{\sigma}{E}\right)^{-1}}{Eb \left(\frac{\sigma}{E}\right)^{-1}} \Leftarrow \text{before was } \frac{6 \times 10^{-3} \lambda^3}{\delta D_o^{gb} b^2 \exp\left(\frac{-Q_{gb}}{RT}\right)} \frac{kT \left(\frac{\sigma}{E}\right)^{-1}}{Eb \left(\frac{\sigma}{E}\right)^{-1}}$$

$$t_{pPLC} = \frac{(1 - 0.78 P_o l_o) 1}{4.87 \dot{\epsilon}} \quad \text{fracture time equations}$$

These equations were reported as “corrected” from previous reports, apparently after discovering some unspecified “typographical errors”. It appears that there was another “typo” in this report because it seems that P_o should be divided by l_o in the equation for t_{pPLC} , but instead the terms are multiplied, making the resulting term inside the parentheses non-dimensional. In later reports, Chin suggests the following equations and values for the fracture equation parameters:

B1.1.4 Chin 1987 [28] and Chin 1989 [81]:

The fracture equations in these reports are consistent with Chin 1987 (PNNL) [4], while the rest of the constants are consistent with Chin 1986 [32].

B1.1.5 Chin 1992 [82]:

The fracture equations in this paper are consistent with Chin 1987 (PNNL) [4], the diffusion constants are consistent with Chin 1986 [32], while the other constants vary as shown below.

$$E = \left(11.81 - 13.0434577 \frac{T}{T_m} \right) \times 10^4 \text{ MPa}, \frac{T_m}{T} \geq 3.63 \Leftarrow \text{before was}$$

$$E = \left(11.81 - 14.59 \frac{T}{T_m} \right) \times 10^4 \text{ MPa}, \frac{T_m}{T} \geq 4.06$$

$$E = \left(11.09 - 10.3793382 \frac{T}{T_m} \right) \times 10^4 \text{ MPa}, \frac{T_m}{T} \leq 3.63 \Leftarrow \text{before was}$$

$$E = \left(11.09 - 11.61 \frac{T}{T_m} \right) \times 10^4 \text{ MPa}, \frac{T_m}{T} \leq 4.06$$

$$T_m = 1900K \Leftarrow \text{before was } 2125K$$

$$A_l = 7.4 \times 10^3 \Leftarrow \text{before was } 7.4 \times 10^7$$

$$A_{CO} = 5.34 \times 10^8 \Leftarrow \text{before was } 5.362 \times 10^2$$

$$A_{NH} = 9.2 \times 10^5 \Leftarrow \text{before was } 9.2 \times 10^{-1}$$

$$A_{GBS} = 8.81 \times 10^{12} \Leftarrow \text{before was } 8.85 \times 10^6$$

$$A_{GBL} = 5 \times 10^2$$

The melting temperature of 1900K was a prediction of the theoretical melting temperature of alpha-phase Zircaloy based on the work of Ardell [217]. Various other constants (as can be observed above) are reported inconsistently between the various Chin reports without any explanation except, possibly, that some “typographical errors” occurred. A change in the activation energy is very substantial since it appears in an exponential term and a justification for this change should probably be provided. It is not clear which of the constants reported by Chin are correctly reported values and which ones may be “typographical errors”. Reports authored or co-authored by Chin [28, 37-82] on the subject of Zircaloy fracture maps refer to an earlier report [83] for details on the derivation of the fracture equations and the assumptions made in determining the relevant constants. Unfortunately, the earlier report [83], which appears to contain this critical information, is no longer available [84].

It is assumed here that the values reported by Chin in 1989 [81] are correct (free from any typographical errors). This assumption has been made because the values for the constants in the 1989 paper [81] were consistent with those reported by Chin in 1987 [28]. Also, when evaluating the deformation and fracture equations reported in these two reports [28, 81], the full and reduced deformation and fracture equations yield consistent results when using the constants reported in the 1989 report [81]. The two sets of equations yield inconsistent results when using the constants reported in the 1992 report [82], indicating that the values reported in 1992 [82] are most likely in error. Assuming the values for the constants reported in

1989 [81] are correct, the values suggested by Chin can then be compared with those suggested by LLNL.

B1.2 Comparison and discussion of LLNL and PNNL suggested input values

We will now discuss the effect that the differences between LLNL and PNNL have on the time-to-fracture equation according to diffusion controlled cavity growth. The general form of the fracture equation for DCCG is

$$t_f = C \frac{kT}{\Omega D_{gb} \delta \sigma} \frac{1}{\rho^{3/2}} \quad \text{Eq. (8)}$$

The values that LLNL [3] and PNNL [4] suggest for input into this equation are discussed as follows.

B1.2.1 Atomic volume, Ω :

PNNL	LLNL
$b^3 = 3.37 \times 10^{-29} \text{ m}^3/\text{atom}$	$A.W./N_p = 2.31 \times 10^{-29} \text{ m}^3/\text{atom}$

Here b is the burgers vector, A.W. is the atomic weight (gm/mole), N is Avogadro's number (atoms/mol) and ρ is the specific gravity (gm/cm³). The value chosen by LLNL agrees well with the solid sphere model value of $2.35 \times 10^{-29} \text{ m}^3/\text{atom}$ calculated using $4/3\pi r_{\text{atomic}}^3$ divided by the atomic packing factor (0.73) when using an atomic radius of 0.160 nm. This term is inversely proportional to the fracture time, so the resulting values vary by approximately 30% (PNNL is approximately 30% more conservative). The authors of the LLNL [3] report, however, later [218] change their suggestion for the atomic volume, making it consistent with the PNNL estimation.

B1.2.2 Grain boundary thickness, δ :

PNNL	LLNL
$50b = 1.6 \times 10^{-8} \text{ m}$	$3b = 9.69 \times 10^{-10} \text{ m}$

The grain boundary thickness is inversely proportional to the failure time, so PNNL has chosen a value that is more than an order of magnitude more conservative than LLNL. A value of $3b$ was “considered adequate” by LLNL. Although PNNL (reference [4] pg B.4) states that $3b$ “is more reasonable than the wide width assumed”, they chose to use $50b$ for conservatism. For diffusion in pure metals, Shewmon [219] suggests a value approximately equal to the burger’s vector, b for the width of the short-circuit diffusion zone in the vicinity of a grain boundary. The value of $3b$ chosen by LLNL was a factor of 16.7 less conservative than the value of $50b$ chosen by PNNL.

B1.2.3 Average cavity spacing, λ :

PNNL	LLNL
$2.6 \times 10^{-6} \text{ m}$	$10 \times 10^{-6} \text{ m}$

It is not clear how PNNL chose this value, but it is more conservative than the value chosen by LLNL. The value chosen by LLNL is based on cavity nucleation data reported by Keusseyan [54]. LLNL claims that “the cavity density appeared to reach a saturation level ... suggesting a limited number of nucleation sites in the material.” LLNL, for conservatism, then assumes that the cavity spacing upon insertion into dry storage is equal to this “limit”. If, indeed, the cavity level did reach some saturation limit, or the cavity density at failure were known, this would be a conservative estimate. The maximum cavity density would be assumed to be present at the start of dry storage. This assumption does not appear to be unreasonable, as Keusseyan [54] showed that voids nucleate and grow from the very early stages of creep. The assumption that the cavity density reaches a saturation limit is, however, in contradiction to the data reported by Keusseyan [54]. Keusseyan states that “It would be interesting to verify if the grain boundary surface cavities reached a saturation number similar to the grain boundary corner cavities, such that the existence of a upper limit for the number of cavities could be established. Consequently the rupture life for a material could be predicted from this creep cavity saturation number... However, because of grain boundary migration, the grain

boundary surface configuration may change and hence preventing the creep cavities from reaching a saturation number. More work on the above subject is needed." From Figure II-15 in Keusseyan, which appears below as Figure B-1, one can observe that, although corner cavities appear to reach a saturation density after about 10 days, no saturation level is evident for surface cavities. One may argue, however, that *if* continuous nucleation occurs, the effect of this nucleation on void spacing (continuous nucleation decreases void spacing) may be somewhat offset by void coalescence (which increases void spacing) during much of the creep life [12,13]. Unfortunately, it is not clear whether this would be the case with Zircaloy (there is no experimental evidence supporting this for Zircaloy).

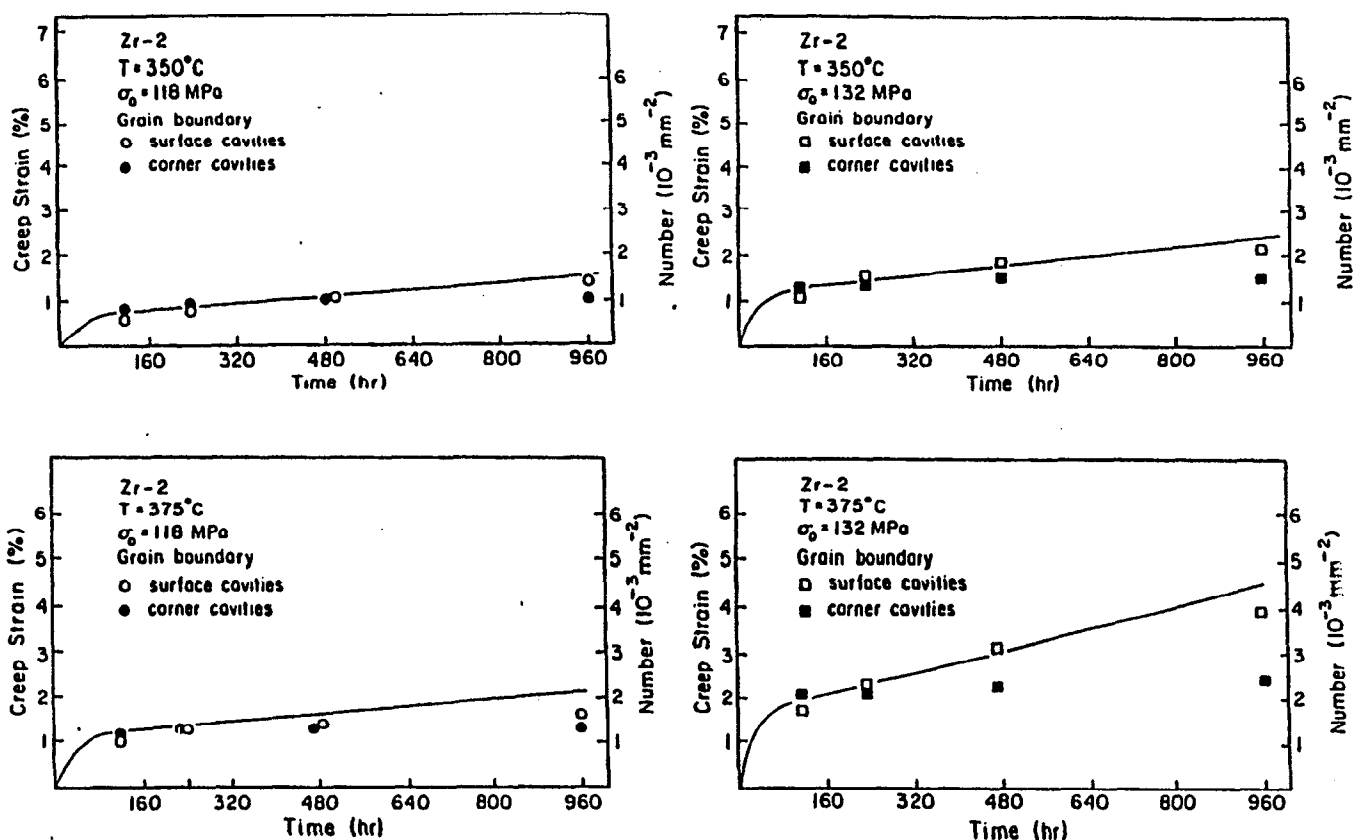


Figure B-1 Creep cavity nucleation data for Zircaloy-2 at 350°C and 375°C [54]

It is also possible that voids are nucleated while in-reactor due to irradiation damage. It has been shown that zirconium is very resistant to radiation induced void formation [e.g. 220-223], at least under the specific conditions of the respective experiments. Others have suggested theories as to why voids do not form under irradiation [see 224-226]. More, recently, however, it has been shown that cavities commonly form in zirconium and zirconium alloys under neutron irradiation [175-177,179,195,196]. The voids appear along defects such as vacancy dislocation loops that form preferentially near grain boundaries during irradiation [175-177]. The cavity size has been measured after irradiation (fluences up to 1.5×10^{26} n/m² at temperatures between 392 and 437°C) in pure zirconium [176]. Average cavity diameters were 30 and 90 nm (there was a bimodal distribution of cavity sizes) [176]. The cavity spacing was on the order of 0.1-0.2 μm [176-177]. Similar results were found in Zircaloy [176-177], though fewer cavities were formed (although the cavity spacing appeared similar according to the TEM micrographs presented by Griffiths [176]). Irradiation induced cavities have not been reported to have been found on grain boundaries to date, but they exist in the vicinity of the grain boundary (see TEM micrographs in [176]) with spacings much smaller than those suggested by either LLNL or PNNL. These cavities may form close enough to the grain boundaries to be within the fast diffusion zone around the grain boundary (some of the cavities in reference 176 even appear to fall on the grain boundary—see figure 3 of reference 176). It is also possible that after irradiation, stable void nuclei exist on or next to the grain boundaries that are too small to detect (on the order of several nm), but will grow with stress in dry storage. Assuming a void spacing such as those observed after irradiation (on the order of 0.1-0.2 μm) may be a reasonable assumption.

In summary, there is little creep cavitation data available, but there is no apparent saturation limit (minimum separation distance) according to the available data [54]. Irradiation, at least under certain conditions, commonly induces void formation with void spacing more than an order of magnitude lower than the spacing suggested by

either LLNL or PNNL. The values chosen by LLNL and PNNL could be overestimating the distance between cavities (underestimating the number of cavities). A smaller, more conservative estimate for the cavity spacing (possibly 0.1 μm as suggested from irradiation data) should be chosen when using the Raj and Ashby model that assumes no cavity nucleation.

The fracture time is proportional to the cube of the cavity spacing. From the values shown above suggested by LLNL and PNNL, PNNL is a factor of 57 more conservative than LLNL, but it is not known whether PNNL is sufficiently conservative.

B1.2.4 Grain boundary diffusion, D_{gb} :

Chin [28,81]	LLNL
$3.89 \times 10^{-6} \exp[(-175 \text{ kJ/mole})/RT] \text{ m}^2/\text{sec}$	$5.9 \times 10^{-6} \exp[(-131 \text{ kJ/mole})/RT] \text{ m}^2/\text{sec}$

The most recent equation reported by Chin [28,81] yields a slower diffusion coefficient than his previously reported equation of $6 \times 10^{-10} \exp(-112/RT) \text{ m}^2/\text{sec}$ [37] by 1 to 3 orders of magnitude at 400°C and 200°C, respectively. The difference between Chin and LLNL is fairly significant. LLNL predicts diffusion coefficients that are 3 to 5 orders of magnitude faster at 400°C and 200°C, respectively, than the most recent diffusion estimate by Chin. The fracture time is inversely proportional to the grain boundary diffusion coefficient. Thus, using the LLNL suggested value for the grain boundary diffusion coefficient yields a failure time that is more than 3 orders of magnitude shorter (more conservative) than PNNL (who use Chin's estimation). LLNL chose to use the above diffusion equation rather than that of Chin because it is a more conservative prediction. This choice may not, however, be the most accurate choice.

LLNL selected one value from the literature that they thought was conservative while PNNL chose another. These values were not based on true grain boundary diffusion experiments, but rather on bulk self-diffusion experiments. Besides the fact

that there is a wide range of self-diffusion coefficient values reported for zirconium, the method by which the grain boundary diffusion coefficient was calculated is very approximate (see discussion in main body of this report). Since the time that the PNNL and LLNL reports were written, there has been one study on grain boundary diffusion in zirconium [174]. This is the only data for true grain boundary diffusion that we were able to locate.

The grain boundary diffusion coefficient as reported by Veiregge and Herzig is

$$D_{gb} = \frac{4.2_{-2.5}^{+5.9} \times 10^{-13} \exp\left(\frac{-167 \pm 7 \text{ kJ/mole}}{RT}\right) \text{ m}^2}{\delta \text{ s}}$$

where δ is the high speed diffusion zone surrounding the grain boundary. This is the same δ that was called the grain boundary width above. This factor appears in the diffusion equation because when measuring grain boundary diffusion, you really measure a flux of atoms and then *assume* a certain diffusion zone (or grain boundary width) in order to calculate the diffusion coefficient. In Equation 2 (the DCCG fracture equation) you must also assume a grain boundary diffusion zone, which is multiplied by the diffusion coefficient resulting in a flux of diffusing atoms. Using this value, then, eliminates δ from the fracture equation and thereby reduces the uncertainty of the fracture model.

The conservative end of the experimental range ($D_o^{gb} = 1.0 \times 10^{-12} / \delta \text{ m}^2/\text{sec}$, $Q_{gb} = 160 \text{ kJ/mole}$) reported by Vieregge and Herzig should be used because it is the only study to date on grain boundary diffusion in zirconium and the effect that irradiation and alloying has on diffusion in zirconium has not been clearly established. For reference, this conservative value, combined with the grain boundary width recommended by LLNL, results in a grain boundary diffusion coefficient that is similar to the value suggested by LLNL.

The current data reported by Vieregge and Herzig supersedes the zirconium self-diffusion data used by either PNNL or LLNL and should be used in place of the current choices. This results in a more conservative diffusion coefficient than suggested by PNNL and reduces the uncertainty of both PNNL and LLNL fracture models (this will be discussed in detail below).

B1.2.5 Other constants in the fracture equation:

PNNL

LLNL

$$C = 2.525 \times 10^{-3}$$

$$C = 1.22 \times 10^{-3}$$

The source of the constant 2.525×10^{-3} given in the fracture equation by PNNL is not known as the earlier report [83] in which it may have been discussed appears to no longer exist [84]. The LLNL constant includes the evaluation of the two functions $f_v(\alpha)$ and $f_s(\alpha)$ using a cavity dihedral angle, α , of 50° . The cavity dihedral angle refers to the angle made by the cavity wall with the grain boundary surface. Raj and Ashby suggested a value of 75° as a typical value for “clean surfaces in pure metals”. LLNL chose a lower (more conservative) value of 50° to account for “non-ideal” conditions that may exist in irradiated Zircaloy. This constant also includes the

integral $\int_{A_i}^{A_f} \frac{dA}{f(A)}$ evaluated using a final area fraction of decohesion limit, A_f , of 0.15

(compared to a value of 0.5 suggested by Raj and Ashby). The “combined” constant as evaluated by LLNL is a factor of approximately two more conservative than that of PNNL.

B1.2.6 Recovery Factor

As was stated above, when PNNL applied the DCCG failure equation, they modified it by multiplying by a “recovery factor” that was developed by Chin [28]. This “recovery factor” is used to account for the reduction in ductility of zirconium and zirconium alloys as a result of irradiation damage. The “recovery factor” was based on studies that showed that post-irradiated Zircaloy had between 200% and 1000% less ductility than non-irradiated Zircaloy [46-48] (typical fracture strains from 5-12%

compared to 25-50%). Chin states "Irradiation was assumed to reduce the ductility of the cladding by a factor of 10 in the stress and temperature region of interest for dry storage" [28] because "... the primary effect of irradiation is a reduction in ductility which leads to a reduction in the fracture time by some constant factor" [28]. In dry storage, however, Chin reported that some or all of this ductility is recovered as a result of damage recovery in Zircaloy, especially above 350°C [28]. Chin developed a function to calculate this "recovery factor" as a function of time and temperature (see Appendix C under the PNNL model for a description of this function). LLNL does not account for this reduced ductility in their analysis.

The resulting predicted fracture time is increased by a factor of approximately 10 for initial stresses below 40 MPa (initial temperatures above about 400°C) in the PNNL model. Although the "recovery factor" changes with time at temperatures above approximately 350°C, these changes have very little effect on the resulting fracture time below an initial temperature of approximately 400°C when using a power temperature decay profile. It is this "recovery factor", then, that causes the difference in shape between the PNNL curve and the LLNL curve in Figure 2 at low stresses (below about 40 MPa). Again, this is because at the higher initial temperatures, some of the ductility is recovered, increasing the fracture time. Because LLNL does not consider the reduction in ductility due to irradiation, their model is a factor of about 10 less conservative (with respect to this one factor) for the stresses most relevant to dry storage (about 40-100 MPa).

The fact that LLNL did not use this recovery factor warrants some discussion. If one examines the DCCG model and assumptions, one immediately notes that the model is NOT a function of strain. That is to say that the predicted failure time does not depend on the amount of strain that the metal experiences but rather only on the grain boundary diffusion. Because it is independent of strain, a reduced ductility would not directly affect the fracture time. It would seem, then, that PNNL has included an unwarranted conservatism in this case.

B1.3 Results:

First we will examine the “pure” DCCG failure predictions (according to Equation 2), combining all of the above effects (except the recovery factor which we will consider below). Using a constant temperature of 400°C and a constant stress of 100 MPa, result in predicted fracture times of 2.4 and 0.4 years according to the PNNL and LLNL DCCG equations, respectively. These values are calculated directly from Equation 2 (NOT according to the complete PNNL CSFM model that includes the “recovery factor”). Here LLNL is a factor of six more conservative than PNNL. The difference becomes larger when evaluated with a decreasing temperature profile because the temperature is inside an exponential term. When using the temperature profile suggested by PNNL [4] of

$$T(K)=2.09 \times 10^3 (t)^{-0.282}$$

where t is in months, and an initial stress of 100 MPa for 5 year old fuel (temperature at start of dry storage equal to 386°C), LLNL predicts a failure time of 17 months while PNNL predicts that the rods would *never* fail by diffusion controlled cavity growth alone.

From the above discussion, it is apparent that although PNNL [4] claims that the two (LLNL and PNNL analyses) yield consistent results (see Figure 2 above), this consistency seems to be a coincidence resulting from a combination of many very different assumptions.

B1.4 Sensitivity of current models to the fracture equation input variables

A good discussion of the sensitivity of the current models was given by BNL [41]. In this report, we have taken a slightly different approach to illustrate the sensitivity by assessing the cumulative variability in the predicted failure time with respect to the various input variables reported in the literature.

To illustrate the sensitivity of the current models, we will show the range of failure times that are predicted when using the most conservative or least conservative reported values available in the literature for the fracture equation (Equation 2) input variables. This was performed for all variables in the fracture equation where the value was “disputed” (meaning more than one value has been reported in the literature). The “recovery factor” was also considered (this was used by PNNL, but not by LLNL). The fracture times were predicted by applying the values from tables B-1 and B-2 below to the LLNL failure model and using the temperature decay model suggested by PNNL. The initial temperature was adjusted until failure was predicted after 40 years in dry storage. This is different than the approach taken by either PNNL or LLNL who appear to have used a combination of conservative and non-conservative values for the fracture equation variables.

B1.4.1 LLNL model evaluated using the most conservative constants

To calculate a “most conservative” fracture time, the most conservative value was chosen for each of the variables where more than one value was reported in the literature. The most conservative values are reported in table B-1 along with the appropriate reference. Values of other variables (not appearing in Table B-1) that are required when using the LLNL model were used as reported by LLNL and PNNL (these values were not “disputed” in the literature).

Table B-1 Most conservative input values for the LLNL fracture time prediction

Variable	Most conservative value	Reference
Ω (atomic volume)	$3.37 \times 10^{-29} \text{ m}^3$	[4]
D_{gb} (grain boundary diffusion coefficient)*	$3.4 \times 10^{-11} \exp\left(\frac{-55.2 \text{ kJ/mol}}{RT}\right) \frac{\text{m}^2}{\text{sec}}$	[61**,62]
δ (gb width)	$1.6 \times 10^{-8} \text{ m}$	[4]
λ (cavity spacing)	$2.6 \times 10^{-6} \text{ m}$	[4]
C (constant from Eq. 8)	1.22×10^{-3}	[3]

* This estimation of the grain boundary diffusion coefficient was based on the general relationship $Q_{gb} \approx 0.6Q_{sd}$ (as was the case for the value suggested by LLNL) where the data reported in reference [62] represent Q_{sd}

** Data originally reported by [62] and estimation of the coefficient term recalculated by [61]

Using an initial stress of 100 MPa, a maximum area fraction of decohesion of 15%, and a power temperature decay profile, **a maximum initial temperature of 56°C** was calculated. If the "recovery factor" [28] (used by PNNL) is incorporated into the LLNL model, the maximum initial temperature is lowered to 22°C. These temperatures are extremely low compared to the limit of 375°C recommended by PNNL or 368°C recommended by the current LLNL model for this initial stress.

B1.4.2 LLNL model evaluated using the least conservative constants

Similar to the most conservative case, the least conservative value for each variable was chosen from the reported values. The least conservative values chosen are reported in Table B-2.

Table B-2 Least conservative input values for the LLNL fracture time prediction

Variable	Least conservative value	Reference
Ω (atomic volume)	$2.312 \times 10^{-29} \text{ m}^3$	[3]
D_{gb} (grain boundary diffusion coefficient)	$3.89 \times 10^{-6} \exp\left(\frac{-175 \text{ kJ/mol}}{RT}\right) \frac{\text{m}^2}{\text{s}}$	[4]
δ (gb width)	$9.69 \times 10^{-10} \text{ m}$	[3]
λ (cavity spacing)	$10 \times 10^{-6} \text{ m}$	[3]
C (constant from Eq. 8)	2.525×10^{-3}	[4]

Using an initial stress of 100 MPa, a maximum area fraction of decohesion of 15% and a power temperature decay profile, **a maximum initial temperature of 653°C** was calculated. The recovery factor would have essentially no effect at initial temperatures this high because the zirconium is predicted to immediately recover 100% of the pre-irradiated ductility. Thus, there is a difference of approximately 600°C between the most conservative maximum temperature estimation and the least conservative maximum temperature estimation when the most extreme literature values are used for the fracture equation (Equation 2) variables.

Although this discussion was based on calculations using the LLNL (Raj and Ashby) model, the same effect would be realized if the PNNL model were utilized, as it is based on the same general fracture equation.

B1.4.3 Discussion

The most critical parameter that can be changed in the above discussion is the grain boundary diffusion coefficient. For the most conservative case, the value chosen for the grain boundary diffusion coefficient was based on a study of self-diffusion [62] where many extrinsic effects were probably involved (e.g. short circuit diffusion or impurity enhanced diffusion). The extent to which these effects would also be involved in the case of Zircaloy is not clear. Apparently all grain boundary diffusion estimations were based on the *approximate* relationship, $Q_{gb} \approx 0.6Q_{sd}$ [173] except the study performed by Vieregge and Herzig [174].

B1.5 Model sensitivity using the grain boundary diffusion coefficient of Vieregge and Herzig [174]

It is apparent that the current models are overly sensitive to a number of variables that were not well known at the time that the PNNL and LLNL reports were written. The most important material property that needs to be input into the LLNL model is the grain boundary diffusion coefficient. LLNL selected one value from the literature while PNNL chose another. These values were not based on true grain boundary diffusion experiments but rather on bulk self-diffusion experiments. Besides the fact that there is a wide range of self-diffusion values reported for zirconium, the method by which the grain boundary diffusion coefficient was calculated is very approximate. Since the time that the PNNL and LLNL reports were written, there has been one study on grain boundary diffusion in zirconium [174]. This is the only data available (that we know of) for true grain boundary diffusion. If we assume, then, that this value for grain boundary diffusion is accurate (this should be confirmed with further experimentation), then we can re-evaluate the sensitivity (uncertainty) of the LLNL model.

B1.5.1 Combination of most and least conservative input variables

The grain boundary diffusion coefficient as reported by Veiregge and Herzig is

$$D_{gb} = \frac{4.2_{-2.5}^{+5.9} \times 10^{-13} \exp\left(\frac{-167 \pm 7 \text{ kJ/mole}}{RT}\right) \text{ m}^2}{\delta \text{ s}}$$

where δ is the high speed diffusion zone surrounding the grain boundary. This is the same δ that was called the grain boundary width above. This factor appears in the diffusion equation because when measuring grain boundary diffusion, you really measure a flux of atoms and then *assume* a certain diffusion zone (or grain boundary width) in order to calculate the diffusion coefficient. In Equation 2 (the DCCG fracture equation) you must also assume a grain boundary diffusion zone which is multiplied by the diffusion coefficient resulting in a flux of diffusing atoms. Using this value, then, eliminates δ from the fracture equation and thereby reduces the uncertainty of the fracture model.

We can use the same method as above to evaluate the sensitivity of the LLNL model to the variables in the fracture equation, assuming that this estimation is the correct value for the diffusion coefficient. The values for the most conservative case are shown in Table B-3

Table B-3 Most conservative input values for the LLNL fracture time prediction based on the grain boundary diffusion coefficient of Vierrege and Herzig [174]

Variable	Most conservative value	Reference
Ω (atomic volume)	$3.37 \times 10^{-29} \text{ m}^3$	[4]
D_{gb} (grain boundary diffusion coefficient)	$\frac{1.01 \times 10^{-12}}{\delta} \exp\left(\frac{-160 \text{ kJ/mol}}{RT}\right) \frac{\text{m}^2}{\text{sec}}$	[174]
λ (cavity spacing)	$2.6 \times 10^{-6} \text{ m}$	[4]
C (constant from Eq. 8)	1.22×10^{-3}	[3]

The diffusion coefficient in table B-3 is the fastest diffusion coefficient possible within the range of error reported by Vieregge and Herzig. This results in a **maximum initial temperature of 301°C**, which is much closer to the currently defined limits. If the "recovery factor" [28] (used by PNNL) is incorporated into the LLNL model, the maximum initial temperature is lowered to 264°C.

Table B-4 lists the values used in making a similar calculation for the least conservative case based on the Vieregge and Herzig grain boundary diffusion study. The diffusion coefficient is the slowest possible within the range of error reported by Vieregge and Herzig.

Table B-4 Least conservative input values for the LLNL fracture time prediction based on the grain boundary diffusion coefficient of Vieregge and Herzig [174]

Variable	Least conservative value	Reference
Ω (atomic volume)	$2.312 \times 10^{-29} \text{m}^3$	[3]
D_{gb} (grain boundary diffusion coefficient)*	$\frac{1.70 \times 10^{-13}}{\delta} \exp\left(\frac{-174 \text{kJ} / \text{mol}}{RT}\right) \frac{\text{m}^2}{\text{s}}$	[174]
λ (cavity spacing)	$10 \times 10^{-6} \text{m}$	[3]
C (constant from Eq. 8)	2.525×10^{-3}	[4]

This results in a **maximum initial temperature of 516°C**. The recovery factor has essentially no effect at initial temperatures this high because the zirconium is predicted to immediately recover 100% of the pre-irradiated ductility (using the recovery factor changes the initial temperature by about 1°C). Although the difference between the most and least conservative cases is still large (more than 200°C), using a known value for the grain boundary diffusion coefficient eliminates a large amount of the sensitivity of the model.

B1.5.2 Variability within range of error report by Vieregge and Herzig [174]

Calculating the most conservative and least conservative maximum allowable temperature when changing *only* the grain boundary diffusion coefficient within the

range of experimental error reported by Vieregge and Herzig [174] is useful. This can show the lowest possible uncertainty when using the Vieregge and Herzig value for the grain boundary diffusion coefficient, assuming that all other variables are accurately known.

When applying the power temperature decay profile suggested by PNNL (adjusting the coefficient to change the initial temperature) and using the input variables suggested by LLNL, the following maximum temperatures were calculated:

Most conservative [$D_{gb} = 1.0 \times 10^{-12}/\delta \exp(-160\text{kJ}/RT)$]; $T_{max} = 380^\circ\text{C}$

Least conservative [$D_{gb} = 1.7 \times 10^{-13}/\delta \exp(-174\text{kJ}/RT)$]; $T_{max} = 484^\circ\text{C}$

Though there is still a 100°C range between the most and least conservative maximum allowable temperature, this is much smaller than the variability due to the uncertainty in grain boundary diffusion coefficient in the current models of several hundred degrees.

C Appendix C: Mathcad Documents Used to Evaluate the Failure Models

Mathcad Document for Figures 3, 4, 5

$\alpha := .8727 \cdot \text{rad}$ Angle formed at junction of cavity and G.B.

$$F_b := \pi \cdot \sin(\alpha)^2 \qquad F_v := \frac{2 \cdot \pi}{3} \cdot (2 - 3 \cdot \cos(\alpha) + \cos(\alpha)^3)$$

$k := 1.38 \cdot 10^{-23} \frac{\text{joule}}{\text{K}}$ Boltzmann's Constant

$\Omega := 3.37 \cdot 10^{-29} \cdot \text{m}^3$ Atomic Volume by PNNL -- LLNL
suggested a value of $2.312 \cdot 10^{-29} \text{m}^3$

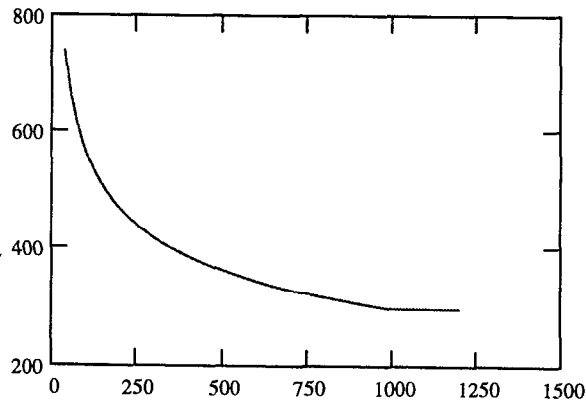
$R := 8.314 \frac{\text{joule}}{\text{K} \cdot \text{mole}}$ Gas Constant

Creep temperature

$T(t) := 2.09 \cdot 10^3 \cdot t^{-0.282} \cdot \text{K}$ PNNL temp profile

$T(t) := \text{if}(t < 1000, 2.09 \cdot 10^3 \cdot t^{-0.282} \cdot \text{K}, T(999.9))$

$t_2 := 40..1200$ plotting variable



Defining a range of temperature profiles based on PNNL profile
(changing the initial temp by changing the coefficient)

$x := 2.10355$

$T(t) := x \cdot 10^3 \cdot t^{-.282} \cdot \text{K}$ $T(60) = 663.001 \text{ K}$

$T_1(t) := 2.07182 \cdot 10^3 \cdot t^{-.282} \cdot \text{K}$ $T_1(60) = 653 \text{ K}$

$T_2(t) := 2.0401 \cdot 10^3 \cdot t^{-.282} \cdot \text{K}$ $T_2(60) = 643.003 \text{ K}$

$T_3(t) := 2.00837 \cdot 10^3 \cdot t^{-.282} \cdot \text{K}$ $T_3(60) = 633.002 \text{ K}$

$T_1(60) - 273.15 \text{K} = 379.85 \text{ K}$

temperature at 5 yrs in Celcius

Grain boundary diffusion coefficients (based on value suggested by LLNL)

$$D_{gb}(t) := 5.9 \cdot 10^{-6} \cdot e^{-\frac{131 \cdot 10^3 \frac{\text{joule}}{\text{mole}}}{R \cdot T(t)}} \cdot \frac{\text{m}^2}{\text{sec}}$$

$$D_{gb1}(t) := 5.9 \cdot 10^{-6} \cdot e^{-\frac{131 \cdot 10^3 \frac{\text{joule}}{\text{mole}}}{R \cdot T_1(t)}} \cdot \frac{\text{m}^2}{\text{sec}}$$

$$D_{gb2}(t) := 5.9 \cdot 10^{-6} \cdot e^{-\frac{131 \cdot 10^3 \frac{\text{joule}}{\text{mole}}}{R \cdot T_2(t)}} \cdot \frac{\text{m}^2}{\text{sec}}$$

$$D_{gb3}(t) := 5.9 \cdot 10^{-6} \cdot e^{-\frac{131 \cdot 10^3 \frac{\text{joule}}{\text{mole}}}{R \cdot T_3(t)}} \cdot \frac{\text{m}^2}{\text{sec}}$$

$\delta := 9.69 \cdot 10^{-10} \cdot \text{m}$ Grain Boundary Thickness (approximated by 3b)

Hoop stress in fuel cladding

$$\sigma_e(t) := 100 \cdot 10^6 \cdot \text{Pa} \cdot \frac{T(t)}{T(60)}$$

$$\sigma_{e2}(t) := 100 \cdot 10^6 \cdot \text{Pa} \cdot \frac{T_2(t)}{T_2(60)}$$

$$\sigma_{e1}(t) := 100 \cdot 10^6 \cdot \text{Pa} \cdot \frac{T_1(t)}{T_1(60)}$$

$$\sigma_{e3}(t) := 100 \cdot 10^6 \cdot \text{Pa} \cdot \frac{T_3(t)}{T_3(60)}$$

$\lambda := 10 \cdot 10^{-6} \cdot \text{m}$ Cavity spacing as suggested by LLNL

defining integration function G(t)

$$G(t) := \frac{32}{3 \cdot \pi^{0.5}} \cdot \frac{F_b^{\frac{3}{2}}}{F_v} \cdot \frac{\Omega \cdot \delta \cdot \sigma_e(t) \cdot D_{gb}(t)}{k \cdot \lambda^3 \cdot T(t)}$$

$$G_2(t) := \frac{32}{3 \cdot \pi^{0.5}} \cdot \frac{F_b^{\frac{3}{2}}}{F_v} \cdot \frac{\Omega \cdot \delta \cdot \sigma_{e2}(t) \cdot D_{gb2}(t)}{k \cdot \lambda^3 \cdot T_2(t)}$$

$$G_1(t) := \frac{32}{3 \cdot \pi^{0.5}} \cdot \frac{F_b^{\frac{3}{2}}}{F_v} \cdot \frac{\Omega \cdot \delta \cdot \sigma_{e1}(t) \cdot D_{gb1}(t)}{k \cdot \lambda^3 \cdot T_1(t)}$$

$$G_3(t) := \frac{32}{3 \cdot \pi^{0.5}} \cdot \frac{F_b^{\frac{3}{2}}}{F_v} \cdot \frac{\Omega \cdot \delta \cdot \sigma_{e3}(t) \cdot D_{gb3}(t)}{k \cdot \lambda^3 \cdot T_3(t)}$$

$b := 3.2 \cdot 10^{-10} \cdot \text{m}$ Burgers vector for zircaloy

$T_m := 2125 \cdot \text{K}$ Melting temperature for zircaloy

$E(t) := \left(11.09 - 11.61 \cdot \frac{T(t)}{T_m} \right) \cdot 10^{10} \cdot \text{Pa}$ Elastic modulus in temperature range of interest as suggested by Chin

The following exercise is only to verify that the damage level (integral of G(t)) should be 0.026 after 15% area fraction of decohesion

$$\gamma := \frac{E(60) \cdot b}{100} \quad \text{Free surface approximation}$$

$$\gamma = 0.239 \frac{\text{joule}}{\text{m}^2}$$

$$r_c(t) := \frac{2 \cdot \gamma}{\sigma_e(t)} \quad \text{Determining the critical cavity radius (initial cavity radius)}$$

$$r_c(60) = 4.779 \cdot 10^{-9} \text{ m}$$

$$A_i := \frac{r_c(60)^2}{\lambda^2} \quad A_i = 2.284 \cdot 10^{-7} \quad \text{Determining an initial area fraction of decohesion}$$

$$f(A) := \frac{1}{\sqrt{A} \left[\frac{1}{2} \ln \left(\frac{1}{A} \right) - \frac{3}{4} + A \cdot \left(1 - \frac{A}{4} \right) \right]} \cdot \left[1 - \frac{\frac{2 \cdot \gamma}{\sigma_e(55)}}{\left(\frac{A \cdot \pi \cdot \lambda^2}{4 \cdot F_b} \right)^{\frac{1}{2}}} \right] \cdot (1 - A)$$

$$A_{\text{val}} := \int_{A_i}^{0.15} \frac{1}{f(A)} dA$$

$$A_{\text{val}} = 0.026$$

So the damage level that corresponds to 15% decohesion is 0.026

$$\int_{60}^{66.42} G(t) \cdot 2629800 \cdot \text{sec} dt = 0.02602$$

$$\int_{60}^{71.4} G_1(t) \cdot 2629800 \cdot \text{sec} dt = 0.02594$$

$$\int_{60}^{102} G_2(t) \cdot 2629800 \cdot \text{sec} dt = 0.02603$$

$$\int_{60}^{540} G_3(t) \cdot 2629800 \cdot \text{sec} dt = 0.01814$$

$$t_f := 65, 70, \dots, 220$$

plotting variable and plotting functions

$$a(t_f) := \int_{60}^{t_f} G(t) \cdot 2629800 \cdot \text{sec} dt$$

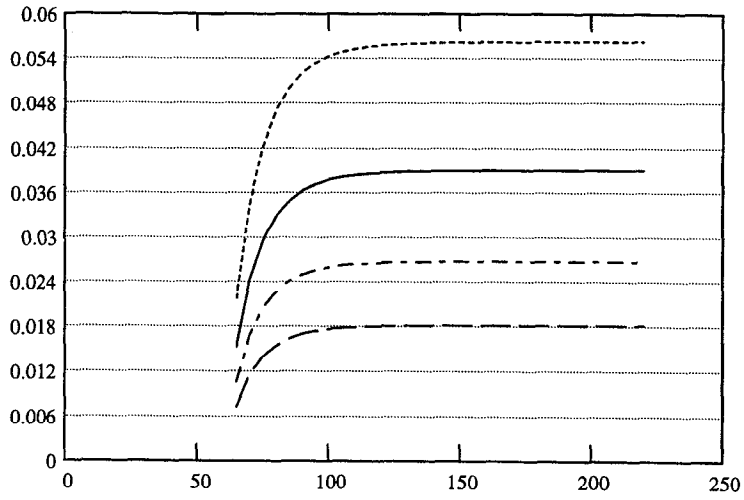
$$a_1(t_f) := \int_{60}^{t_f} G_1(t) \cdot 2629800 \cdot \text{sec} dt$$

$$a_2(t_f) := \int_{60}^{t_f} G_2(t) \cdot 2629800 \cdot \text{sec} dt$$

$$a_3(t_f) := \int_{60}^{t_f} G_3(t) \cdot 2629800 \cdot \text{sec} dt$$

a max = 0.05623 99%=0.05567 =60mth
a1 max = 0.03923 99%=0.03884 =58mth
a2 max = 0.02676 99%=0.02649 =57mth
a3 max = 0.01814 99%=0.01796 =56mth

Plot for Figure 4



Mathcad Document for Figure 6

Defining a stress and temperature range

$$x := 1.932$$

$$T(t) := \left[x \cdot 10^3 \cdot \left(t \cdot \frac{12}{100} \right)^{-0.282} \right] \cdot K$$

Temperature decay profile (PNNL), where t is in hundredths of a year

$$T(500) - 273 \text{ K} = 335.932 \text{ K}$$

$$i := 160$$

$$\sigma := i \cdot 10^6 \cdot \text{Pa}$$

Defining the time (temp) dependent stress term
 $\sigma(500)$ =initial stress at time of insertion into dry storage
 (5 years)

$$\sigma(t) := \frac{T(t)}{T(500)} \cdot \sigma$$

Constants (From Chin 1989 [73])

$$T(500) - 273 \text{ K} = 335.932 \text{ K}$$

$$R := 8.3144 \frac{\text{joule}}{\text{mole} \cdot \text{K}}$$

gas constant

$$k := 1.38 \cdot 10^{-23} \frac{\text{joule}}{\text{K}}$$

Boltzmann's constant

$$b := 3.23 \cdot 10^{-10} \cdot \text{m}$$

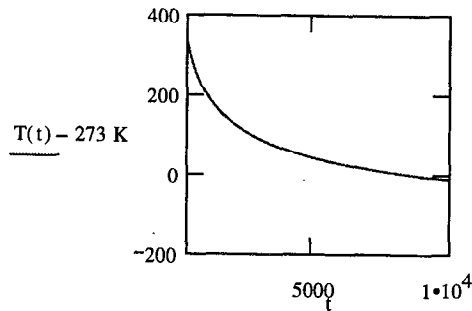
Burgers vector

$$d := 5 \cdot 10^{-6} \cdot \text{m}$$

grain size

$$T_m := 2125 \cdot \text{K}$$

melting temperature



$$E(t) := \text{if} \left[\frac{T_m}{T(t)} > 4.06, \left(11.81 - 14.59 \cdot \frac{T(t)}{T_m} \right) \cdot 10^{10} \cdot \text{Pa}, \left(11.09 - 11.61 \cdot \frac{T(t)}{T_m} \right) \cdot 10^{10} \cdot \text{Pa} \right]$$

elastic modulus

$$n := 5$$

power law exponent

$$Q_L := 250 \cdot 10^3 \frac{\text{joule}}{\text{mole}}$$

$$Q_{gb} := 175 \cdot 10^3 \frac{\text{joule}}{\text{mole}}$$

activation energies

$$Q_c := 180 \cdot 10^3 \frac{\text{joule}}{\text{mole}}$$

$$D_{oL} := 2 \cdot 10^{-4} \frac{\text{m}^2}{\text{sec}}$$

$$D_{ogb} := 3.89 \cdot 10^{-6} \frac{\text{m}^2}{\text{sec}}$$

diffusivity coefficients

$$D_{oc} := 2.26 \cdot 10^{-6} \frac{\text{m}^2}{\text{sec}}$$

$$A_L := 7.4 \cdot 10^7$$

$$A_{CO} := 5.362 \cdot 10^2$$

$$A_{GBS} := 8.85 \cdot 10^6$$

strain rate coefficients

$$A_{NH} := 0.92$$

$$A_{GBL} := 5 \cdot 10^2$$

$$\sigma_o(t) := 2.4 \cdot 10^{-2} \cdot E(t)$$

cutoff stress $\sigma_o(500) = 1.863 \cdot 10^9 \cdot \text{Pa}$

$$l := 2.6 \cdot 10^{-6} \cdot \text{m}$$

average cavity spacing

$$S(t) := \frac{E(t) \cdot b}{3 \cdot l}$$

$$\delta := 1.6 \cdot 10^{-8} \cdot \text{m}$$

grain boundary width (diffusion zone width)

$$\varepsilon_n := 0.08$$

hole nucleation strain

$$P_o := 10 \cdot 10^{-9} \cdot \text{m}$$

average particle diameter

$$l_o := 2 \cdot 10^{-6} \cdot \text{m}$$

average particle spacing along gb

$$\zeta := 0.2$$

$= \dot{\varepsilon}(\text{gbs}) / \dot{\varepsilon} = \text{contribution of gb strain to total strain}$

$$\gamma_f := 35 \frac{\text{joule}}{\text{m}^2}$$

free surface energy created by fracture

$$f_v := 0.025$$

volume fraction of intergranular inclusions

Full and Reduced Deformation equations

$$\varepsilon_{DG} := 0$$

stress is always lower than the cutoff stress in dry storage
(dislocation glide controlled creep)

$$\varepsilon_{HT}(t) := A_L \cdot D_{oL} \cdot \exp\left(\frac{-Q_L}{R \cdot T(t)}\right) \cdot \left(\frac{E(t) \cdot b}{k \cdot T(t)}\right) \cdot \left(\frac{\sigma(t)}{E(t)}\right)^n \quad \text{high temperature climb (full and reduced)}$$

$$\varepsilon_{HT}(500) = 5.896 \cdot 10^{-10} \text{ sec}^{-1}$$

$$\varepsilon_{HT}(t) := \exp\left[5 \cdot \ln\left(\frac{\sigma(t)}{E(t)}\right) + 55.75 - 14.15 \cdot \left(\frac{T_m}{T(t)}\right) + \ln\left(\frac{T_m}{T(t)}\right) + \ln\left(\frac{E(t)}{10^{10} \cdot \text{Pa}}\right)\right] \cdot \text{sec}^{-1}$$

$$\varepsilon_{HT}(500) = 5.887 \cdot 10^{-10} \text{ sec}^{-1}$$

$$\varepsilon_{LT}(t) := 50 \cdot A_L \cdot D_{oc} \cdot \exp\left(\frac{-Q_c}{R \cdot T(t)}\right) \cdot \left(\frac{E(t) \cdot b}{k \cdot T(t)}\right) \cdot \left(\frac{\sigma(t)}{E(t)}\right)^{n+2} \quad \text{low temperature climb}$$

$$\varepsilon_{LT}(500) = 1.43 \cdot 10^{-9} \text{ sec}^{-1}$$

$$\varepsilon_{LT}(t) := \exp\left[7 \cdot \ln\left(\frac{\sigma(t)}{E(t)}\right) + 55.18 - 10.19 \cdot \left(\frac{T_m}{T(t)}\right) + \ln\left(\frac{T_m}{T(t)}\right) + \ln\left(\frac{E(t)}{10^{10} \cdot \text{Pa}}\right)\right] \cdot \text{sec}^{-1}$$

$$\varepsilon_{LT}(500) = 1.42 \cdot 10^{-9} \text{ sec}^{-1}$$

grain boundary sliding (gb diffusion)

$$\varepsilon_{GBS}(t) := A_{GBS} \cdot D_{ogb} \cdot \exp\left(\frac{-Q_{gb}}{R \cdot T(t)}\right) \cdot \left(\frac{E(t) \cdot b}{k \cdot T(t)}\right) \cdot \left(\frac{b}{d}\right)^3 \cdot \left(\frac{\sigma(t)}{E(t)}\right)^2 \quad \varepsilon_{GBS}(500) = 1.146 \cdot 10^{-10} \text{ sec}^{-1}$$

$$\varepsilon_{GBS}(t) := \exp\left[2 \cdot \ln\left(\frac{\sigma(t)}{E(t)}\right) + 20.74 - 9.9036 \cdot \left(\frac{T_m}{T(t)}\right) + \ln\left(\frac{T_m}{T(t)}\right) + \ln\left(\frac{E(t)}{10^{10} \cdot \text{Pa}}\right)\right] \cdot \text{sec}^{-1}$$

$$\varepsilon_{GBS}(500) = 1.145 \cdot 10^{-10} \text{ sec}^{-1}$$

grain boundary sliding (lattice diffusion)

$$\varepsilon_{GBL}(t) := A_{GBL} \cdot D_{oL} \cdot \exp\left(\frac{-Q_L}{R \cdot T(t)}\right) \cdot \left(\frac{E(t) \cdot b}{k \cdot T(t)}\right) \cdot \left(\frac{b}{d}\right)^2 \cdot \left(\frac{\sigma(t)}{E(t)}\right)^2$$

$$\varepsilon_{GBL}(500) = 1.899 \cdot 10^{-15} \text{ sec}^{-1}$$

$$\varepsilon_{NH}(t) := A_{NH} \cdot D_{oL} \cdot \exp\left(\frac{-Q_L}{R \cdot T(t)}\right) \cdot \left(\frac{E(t) \cdot b}{k \cdot T(t)}\right) \cdot \left(\frac{b}{d}\right)^2 \cdot \left(\frac{\sigma(t)}{E(t)}\right) \quad \text{Nabarro-Herring creep}$$

$$\varepsilon_{NH}(500) = 1.695 \cdot 10^{-15} \text{ sec}^{-1}$$

$$\varepsilon_{NH}(t) := \exp \left[\ln \left(\frac{\sigma(t)}{E(t)} \right) + 18.25 - 14.15 \cdot \left(\frac{T_m}{T(t)} \right) + \ln \left(\frac{T_m}{T(t)} \right) + \ln \left(\frac{E(t)}{10^{10} \cdot \text{Pa}} \right) \right] \cdot \text{sec}^{-1}$$

$$\varepsilon_{NH}(500) = 1.689 \cdot 10^{-15} \text{ sec}^{-1}$$

$$\varepsilon_{CO}(t) := A_{CO} \cdot D_{ogb} \cdot \exp \left(\frac{-Q_{gb}}{R \cdot T(t)} \right) \cdot \left(\frac{E(t) \cdot b}{k \cdot T(t)} \right) \cdot \left(\frac{b}{d} \right)^3 \cdot \left(\frac{\sigma(t)}{E(t)} \right) \quad \text{Coble creep}$$

$$\varepsilon_{CO}(500) = 3.368 \cdot 10^{-12} \text{ sec}^{-1}$$

$$\varepsilon_{CO}(t) := \exp \left[\ln \left(\frac{\sigma(t)}{E(t)} \right) + 11.03 - 9.9036 \cdot \left(\frac{T_m}{T(t)} \right) + \ln \left(\frac{T_m}{T(t)} \right) + \ln \left(\frac{E(t)}{10^{10} \cdot \text{Pa}} \right) \right] \cdot \text{sec}^{-1}$$

$$\varepsilon_{CO}(500) = 3.37 \cdot 10^{-12} \text{ sec}^{-1}$$

$$\varepsilon_{\text{dot}}(t) := \text{if} \left(\varepsilon_{HT}(t) > \varepsilon_{LT}(t), \varepsilon_{HT}(t), \varepsilon_{LT}(t) \right)$$

$$\varepsilon_{\text{dott}}(t) := \text{if} \left(\varepsilon_{\text{dot}}(t) > \varepsilon_{GBS}(t), \varepsilon_{\text{dot}}(t), \varepsilon_{GBS}(t) \right)$$

$$\varepsilon_{\text{dottt}}(t) := \text{if} \left(\varepsilon_{\text{dott}}(t) > \varepsilon_{GBL}(t), \varepsilon_{\text{dott}}(t), \varepsilon_{GBL}(t) \right)$$

$$\varepsilon_{\text{dotttt}}(t) := \text{if} \left(\varepsilon_{\text{dottt}}(t) > \varepsilon_{NH}(t), \varepsilon_{\text{dottt}}(t), \varepsilon_{NH}(t) \right) \quad \text{finding the fastest creep rate}$$

$$\varepsilon_{\text{dottttt}}(t) := \text{if} \left(\varepsilon_{\text{dotttt}}(t) > \varepsilon_{CO}(t), \varepsilon_{\text{dotttt}}(t), \varepsilon_{CO}(t) \right) \quad \varepsilon_{\text{dottttt}}(500) = 1.42 \cdot 10^{-9} \text{ sec}^{-1}$$

Reduced and Full Fracture Equations (From PNNL Report - 1987 [4])

Transgranular Fracture

$$t_{FTG}(t) := \exp \left(-1.797 - \ln \left(\varepsilon_{\text{dottttt}}(t) \cdot \text{sec} \right) \right)$$

$$t_{FTG}(500) = 1.168 \cdot 10^8$$

$$t_{FTG}(t) := \left[\varepsilon_n + \left(\frac{1}{4.937} \right) \cdot \left(\frac{n}{n-1} \right) \cdot \ln \left(\frac{0.38}{\frac{1}{f_v^2}} - 1 \right) \right] \cdot \varepsilon_{\text{dottttt}}(t)^{-1} \cdot \text{sec}^{-1}$$

$$t_{FTG}(500) = 1.168 \cdot 10^8$$

Triple-point cracking

$$t_{FTP}(t) := \exp \left[\left(-5.655 - \ln \left(\varepsilon_{\text{dottttt}}(t) \cdot \text{sec} \right) \right) - \ln \left(\frac{\sigma(t)}{E(t)} \right) - \ln \left(\frac{E(t)}{10^{10} \cdot \text{Pa}} \right) \right]$$

$$t_{FTP}(500) = 1.541 \cdot 10^8$$

$$t_{FTP}(t) := \frac{\gamma_f}{E(t) \cdot d \cdot \zeta} \cdot \left(\frac{\sigma(t)}{E(t)} \right)^{-1} \cdot \varepsilon_{\text{dottttt}}(t)^{-1} \cdot \text{sec}^{-1}$$

$$t_{FTP}(500) = 1.541 \cdot 10^8$$

Cavitation -- Diffusional growth

$$t_{fDC}(t) := \exp\left(4.15 - \ln(\epsilon_{GBS}(t) \cdot \text{sec}) + \ln\left(\frac{\sigma(t)}{E(t)}\right)\right)$$

$$t_{fDC}(500) = 1.142 \cdot 10^9$$

$$t_{fDC}(t) := \frac{2.525 \cdot 10^{-3} \cdot i^3}{\delta \cdot D_{ogb} \cdot b^2 \cdot \exp\left(\frac{-Q_{gb}}{R \cdot T(t)}\right)} \cdot \left(\frac{k \cdot T(t)}{E(t) \cdot b}\right) \cdot \left(\frac{\sigma(t)}{E(t)}\right)^{-1} \cdot \text{sec}^{-1}$$

$$t_{fDC}(500) = 1.141 \cdot 10^9$$

Cavitation -- Power law growth

$$t_{fCP}(t) := \exp\left(-1.587 - \ln(\epsilon_{dotttt}(t) \cdot \text{sec})\right)$$

$$t_{fCP}(500) = 1.441 \cdot 10^8$$

$$t_{fCP}(t) := \left(\frac{1 - 0.78 \cdot \frac{P_o}{I_o}}{4.87}\right) \cdot \epsilon_{dotttt}(t)^{-1} \cdot \text{sec}^{-1}$$

$$t_{fCP}(500) = 1.441 \cdot 10^8$$

Recovery factor from Chin [28] Appendix 9

Stepwise (as reported in [28])

Continuous

$$F(t) := 7.36 \cdot 10^{24} \cdot \frac{1}{100} \cdot \exp\left[-\frac{40000K}{\left(\frac{T(t) + T(t-1)}{2}\right)}\right]$$

$$F1(t) := 8.4 \cdot 10^{20} \cdot 365.25 \cdot 24 \cdot \frac{1}{100} \cdot \exp\left(-\frac{40000K}{T(t)}\right)$$

$$A_1 := F(500)$$

$$i := 1..1500$$

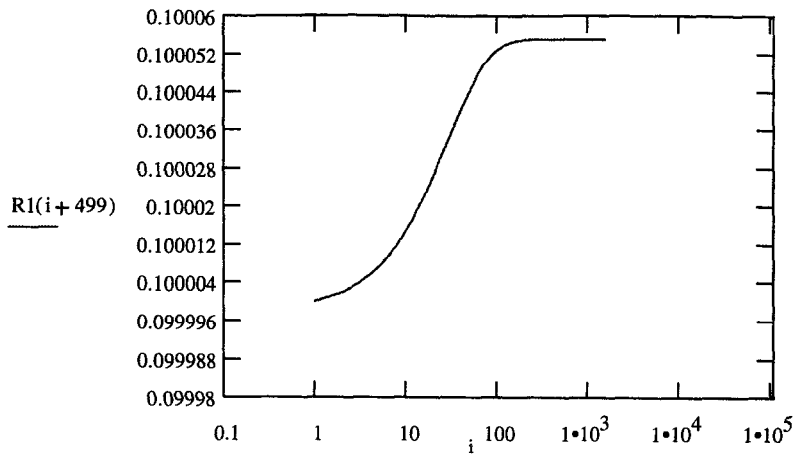
$$A_i := A_{i-1} + F(i + 499)$$

$$R_i := 1 - \left[\frac{1}{(1 + A_i)}\right] \cdot 0.9$$

$$R_1 := 1 - \left[\frac{1}{(1 + A_1)}\right] \cdot 0.9$$

$$A1(t) := \int_{500}^t F1(t) dt$$

$$R1(t) := 1 - 0.9 \cdot \left[\frac{1}{1 + \int_{500}^t F1(t) dt}\right]$$



$$\text{Damage1}(t) := \int_{500}^t \left(\frac{315576}{t_{fDC}(t)} \right) \frac{1}{R1(t)} dt$$

$T(500) - 273K = 335.932 \text{ K}$
 $x = 1.932$
 $\sigma(500) = 1.6 \cdot 10^8 \text{ kg} \cdot \text{m}^{-1} \cdot \text{sec}^{-2}$

Determining the controlling fracture mechanism (assuming that the shortest fracture time is the controlling mechanism and acting independently -- as assumed by PNNL [4])

Only the most relevant fracture mechanisms are compared to save computational time

$$R_2 = 0.1$$

$$t_f(t) := \text{if}(t_{fCP}(t) < t_{fDC}(t), t_{fCP}(t), t_{fDC}(t))$$

$$R_{500} = 0.1$$

$$t_{fff}(t) := \text{if}(t_f(t) < t_{fTG}(t), t_f(t), t_{fTG}(t))$$

$$t_{fDC}(60) = 200.215$$

$$t_{fDC}(140) = 3.386 \cdot 10^4$$

$$\text{Damage}(t) := \sum_{m=501}^t \left(\frac{315576}{t_{fff}(m)} \right) \frac{1}{R_{m-500}}$$

$$\sigma(500) = 1.6 \cdot 10^8 \cdot \text{Pa}$$

$$T(500) - 273K = 335.932 \text{ K}$$

$$x = 1.932$$

$$T(61) - 273 \text{ K} = 829.085 \text{ K}$$

Damage after 1 year $\text{Damage}(600) = 1.014$

Damage after 5 years

$$\sigma(500) = 1.6 \cdot 10^8 \cdot \text{Pa}$$

Damage after 40 years

tabulated results
for 5, 40 year failure results as of 3.18.99

T_i	σ_i	x
487	10	2.411
463	20	2.335
424	30	2.212
406	40	2.155
398	50	2.13
393	60	2.113
389	70	2.101
386	80	2.091
382	90	2.079
377	100	2.062
371	110	2.044
365	120	2.025
358	130	2.002
349	140	1.974
341	150	1.948
334	160	1.925

tabulated results
for 1 year failure

T_i	σ_i	x
496	10	2.44
474	20	2.37
452	30	2.3
415	40	2.186
405	50	2.151
399	60	2.132
395	70	2.12
392	80	2.11
386	90	2.091
379	100	2.074
373	110	2.05
367	120	2.032
360	130	2.009
351	140	1.98
343	150	1.955
336	160	1.932

Mathcad Document for Figures 7, 8 and 9

$$\alpha := .8727 \cdot \text{rad}$$

Angle formed at junction of cavity and G.B.

$$F_b := \pi \cdot \sin(\alpha)^2$$

$$F_v := \frac{2 \cdot \pi}{3} \cdot (2 - 3 \cdot \cos(\alpha) + \cos(\alpha)^3)$$

$$k := 1.38 \cdot 10^{-23} \frac{\text{joule}}{\text{K}}$$

Boltzmann's Constant

$$\Omega := 3.37 \cdot 10^{-29} \cdot \text{m}^3$$

Atomic Volume by PNNL -- LLNL
suggested a value of $2.312 \cdot 10^{-29} \text{m}^3$

$$R := 8.314 \frac{\text{joule}}{\text{K} \cdot \text{mole}}$$

Gas Constant

$$t_2 := 10..500$$

plotting variable

Creep temperature

$$T_1(t) := 2.09 \cdot 10^3 \cdot t^{-0.282} \cdot \text{K}$$

$$T_2(t) := 1.91 \cdot 10^3 \cdot t^{-0.260} \cdot \text{K}$$

$$T_3(t) := 1.76 \cdot 10^3 \cdot t^{-0.24} \cdot \text{K}$$

$$T_4(t) := 1.622 \cdot 10^3 \cdot t^{-0.22} \cdot \text{K}$$

$$T_5(t) := 1.494 \cdot 10^3 \cdot t^{-0.2} \cdot \text{K}$$

$$T_1(60) = 658.73 \text{ K}$$

$$T_1(180) = 483.236 \text{ K}$$

$$T_2(60) = 658.74 \text{ K}$$

$$T_3(60) = 658.804 \text{ K}$$

$$T_4(60) = 658.958 \text{ K}$$

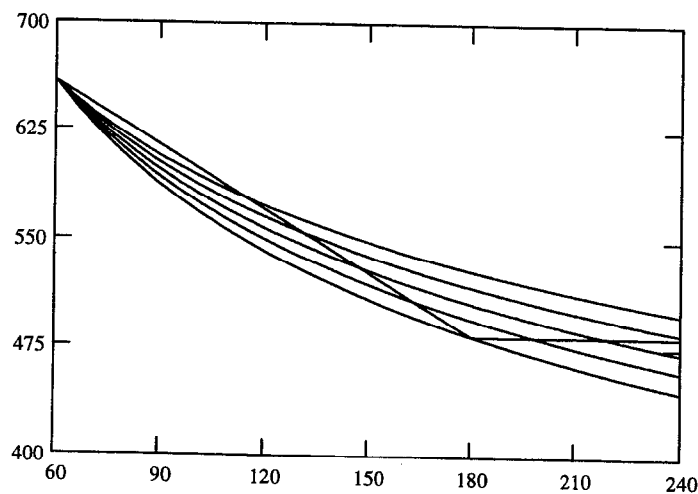
$$T_5(60) = 658.75 \text{ K}$$

$$\text{slope} := \frac{T_1(60) - T_1(180)}{120}$$

defining linear temp profile

$$T_6(t) := \text{if}(t < 180, 746.48 \text{K} - 1.46 \cdot t \cdot \text{K}, 484 \text{K})$$

$$T_6(t) := \text{if}[t < 180, (T_1(60) + \text{slope} \cdot 60) - \text{slope} \cdot t, T_1(180)]$$



Defining diffusion coefficients for each temperature profile

$$D_{gb1}(t) := 5.9 \cdot 10^{-6} \cdot e^{-\frac{131 \cdot 10^3 \frac{\text{joule}}{\text{mole}}}{R \cdot T_1(t)}} \frac{\text{m}^2}{\text{sec}} \quad D_{gb4}(t) := 5.9 \cdot 10^{-6} \cdot e^{-\frac{131 \cdot 10^3 \frac{\text{joule}}{\text{mole}}}{R \cdot T_4(t)}} \frac{\text{m}^2}{\text{sec}}$$

$$D_{gb2}(t) := 5.9 \cdot 10^{-6} \cdot e^{-\frac{131 \cdot 10^3 \frac{\text{joule}}{\text{mole}}}{R \cdot T_2(t)}} \frac{\text{m}^2}{\text{sec}} \quad D_{gb5}(t) := 5.9 \cdot 10^{-6} \cdot e^{-\frac{131 \cdot 10^3 \frac{\text{joule}}{\text{mole}}}{R \cdot T_5(t)}} \frac{\text{m}^2}{\text{sec}}$$

$$D_{gb3}(t) := 5.9 \cdot 10^{-6} \cdot e^{-\frac{131 \cdot 10^3 \frac{\text{joule}}{\text{mole}}}{R \cdot T_3(t)}} \frac{\text{m}^2}{\text{sec}} \quad D_{gb6}(t) := 5.9 \cdot 10^{-6} \cdot e^{-\frac{131 \cdot 10^3 \frac{\text{joule}}{\text{mole}}}{R \cdot T_6(t)}} \frac{\text{m}^2}{\text{sec}}$$

$$\delta := 9.69 \cdot 10^{-10} \cdot \text{m}$$

Grain Boundary Thickness (approximated by 3b)

$$\lambda := 10 \cdot 10^{-6} \cdot \text{m}$$

Cavity spacing as suggested by LLNL

Defining stresses for each temperature profile

$$\sigma_{e1}(t) := 100 \cdot 10^6 \cdot \text{Pa} \cdot \frac{T_1(t)}{T_1(60)} \quad \sigma_{e4}(t) := 100 \cdot 10^6 \cdot \text{Pa} \cdot \frac{T_4(t)}{T_4(60)}$$

$$\sigma_{e2}(t) := 100 \cdot 10^6 \cdot \text{Pa} \cdot \frac{T_2(t)}{T_2(60)} \quad \sigma_{e5}(t) := 100 \cdot 10^6 \cdot \text{Pa} \cdot \frac{T_5(t)}{T_5(60)}$$

$$\sigma_{e3}(t) := 100 \cdot 10^6 \cdot \text{Pa} \cdot \frac{T_3(t)}{T_3(60)} \quad \sigma_{e6}(t) := 100 \cdot 10^6 \cdot \text{Pa} \cdot \frac{T_6(t)}{T_6(60)}$$

$$b := 3.2 \cdot 10^{-10} \cdot \text{m}$$

Burgers vector for Zircaloy

Defining the G(t) function for each temperature profile

$$G_1(t) := \frac{32}{3 \cdot \pi^{\frac{1}{2}}} \cdot \frac{F_b^{\frac{3}{2}} \cdot \Omega \cdot \delta \cdot \sigma_{e1}(t) \cdot D_{gb1}(t)}{F_v \cdot k \cdot \lambda^3 \cdot T_1(t)} \quad G_4(t) := \frac{32}{3 \cdot \pi^{\frac{1}{2}}} \cdot \frac{F_b^{\frac{3}{2}} \cdot \Omega \cdot \delta \cdot \sigma_{e4}(t) \cdot D_{gb4}(t)}{F_v \cdot k \cdot \lambda^3 \cdot T_4(t)}$$

$$G_2(t) := \frac{32}{3 \cdot \pi^{\frac{1}{2}}} \cdot \frac{F_b^{\frac{3}{2}} \cdot \Omega \cdot \delta \cdot \sigma_{e2}(t) \cdot D_{gb2}(t)}{F_v \cdot k \cdot \lambda^3 \cdot T_2(t)} \quad G_5(t) := \frac{32}{3 \cdot \pi^{\frac{1}{2}}} \cdot \frac{F_b^{\frac{3}{2}} \cdot \Omega \cdot \delta \cdot \sigma_{e5}(t) \cdot D_{gb5}(t)}{F_v \cdot k \cdot \lambda^3 \cdot T_5(t)}$$

$$G_3(t) := \frac{32}{3 \cdot \pi^{\frac{1}{2}}} \cdot \frac{F_b^{\frac{3}{2}} \cdot \Omega \cdot \delta \cdot \sigma \cdot e^{3(t)} \cdot D_{gb3}(t)}{F_v \cdot k \cdot \lambda^3 \cdot T_3(t)}$$

$$G_6(t) := \frac{32}{3 \cdot \pi^{\frac{1}{2}}} \cdot \frac{F_b^{\frac{3}{2}} \cdot \Omega \cdot \delta \cdot \sigma \cdot e^6(t) \cdot D_{gb6}(t)}{F_v \cdot k \cdot \lambda^3 \cdot T_6(t)}$$

Defining integrals for each temperature function

$$\int_{60}^{119} G_1(t) \cdot 2629800 \cdot \text{sec} \, dt = 0.0477 \quad \text{max1}=0.04817; \text{99\%}=0.04769$$

reached after 59 months=4.9yrs

$$\int_{60}^{127} G_2(t) \cdot 2629800 \cdot \text{sec} \, dt = 0.05244 \quad \text{max2}=0.05297; \text{99\%}=0.05244$$

reached after 67 months=5.6yrs

$$\int_{60}^{136} G_3(t) \cdot 2629800 \cdot \text{sec} \, dt = 0.05777 \quad \text{max}=0.05836; \text{99\%}=0.05778$$

reached after 76 months=6.3yrs

$$\int_{60}^{149} G_4(t) \cdot 2629800 \cdot \text{sec} \, dt = 0.0645 \quad \text{max}=0.06514; \text{99\%}=0.06449$$

reached after 89 months=7.4

$$\int_{60}^{165} G_5(t) \cdot 2629800 \cdot \text{sec} \, dt = 0.0719 \quad \text{max}=0.07264; \text{99\%}=0.07191$$

reached after 105 months=8.75yrs

$$\int_{60}^{134} G_6(t) \cdot 2629800 \cdot \text{sec} \, dt = 0.08421 \quad \text{max}=0.08504 \text{ (40yrs)}; \text{99\%}=0.08419$$

reached after 74 months=6.17yrs

The series of decreasingly concave temperature decay profile is bounded by a straight line curve anchored at 5 and 10 years by the temperatures given by PNNL. This was thought to be plenty conservative as after 10 years in storage using this linear decay profile, more than 99.95% of the damage has occurred in the material, even for initial temperatures as high as 525C, which is higher than any maximum predicted storage limit. The temperature based on the linear decay profile is higher at all times than the PNNL power law decay.

$t_f := 60..200$ defining plot variable

defining plot functions

$$g_1(t_f) := \int_{60}^{t_f} G_1(t) \cdot 2629800 dt$$

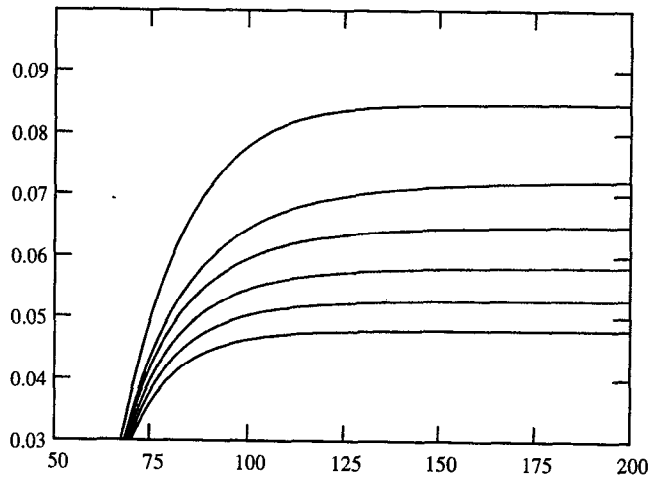
$$g_2(t_f) := \int_{60}^{t_f} G_2(t) \cdot 2629800 dt$$

$$g_3(t_f) := \int_{60}^{t_f} G_3(t) \cdot 2629800 dt$$

$$g_4(t_f) := \int_{60}^{t_f} G_4(t) \cdot 2629800 dt$$

$$g_5(t_f) := \int_{60}^{t_f} G_5(t) \cdot 2629800 dt$$

$$g_6(t_f) := \int_{60}^{t_f} G_6(t) \cdot 2629800 dt$$



plot of the initial temperature vs. the fracture time for each of the functions $g(t)$

Mathcad Document for Figures 10, 11

$\alpha := .8727 \cdot \text{rad}$ Angle formed at junction of cavity and G.B.

$$F_b := \pi \cdot \sin(\alpha)^2$$

$$F_v := \frac{2 \cdot \pi}{3} \cdot (2 - 3 \cdot \cos(\alpha) + \cos(\alpha)^3)$$

$k := 1.38 \cdot 10^{-23} \frac{\text{joule}}{\text{K}}$ Boltzmann's Constant

$\Omega := 3.37 \cdot 10^{-29} \cdot \text{m}^3$ Atomic Volume by PNNL -- LLNL suggested a value of $2.312 \cdot 10^{-29} \text{m}^3$

$R := 8.314 \frac{\text{joule}}{\text{K} \cdot \text{mole}}$ Gas Constant

$t_2 := 0..1200$

$t_1 := 40..1200$

plotting variables

Creep temperature

$T_{10}(t) := 2.4038 \cdot 10^3 \cdot t^{-0.282} \cdot \text{K}$ adjusted PNNL temperature profile

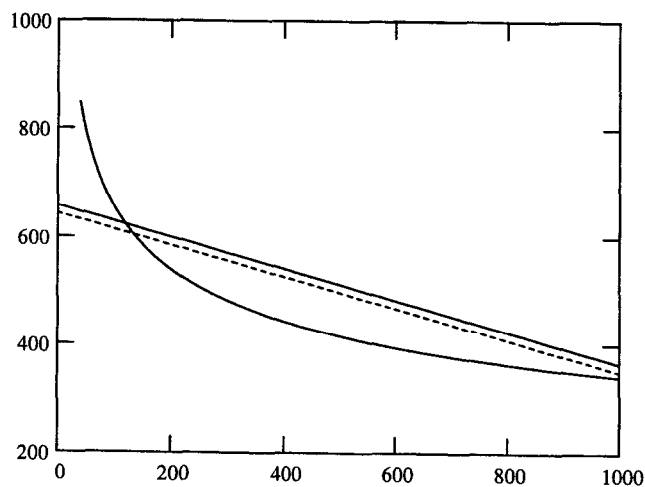
$T_{10}(120) = 623.116 \text{ K}$

$T_{10p}(t) := 658.15 \text{ K} - 0.2917 \cdot t \cdot \text{K}$ upper BNL profile

$T_{10p}(120) = 623.146 \text{ K}$

$T_{10pL}(t) := 643.15 \cdot \text{K} - 0.2917 \cdot t \cdot \text{K}$ lower BNL profile

$T_{10pL}(120) = 608.146 \text{ K}$



Grain boundary diffusion coefficients

$$D_{gb10}(t) := 5.9 \cdot 10^{-6} \cdot e^{-\frac{131 \cdot 10^3 \frac{\text{joule}}{\text{mole}}}{R \cdot T_{10}(t)}} \cdot \frac{\text{m}^2}{\text{sec}} \quad D_{gb10p}(t) := 5.9 \cdot 10^{-6} \cdot e^{-\frac{131 \cdot 10^3 \frac{\text{joule}}{\text{mole}}}{R \cdot T_{10p}(t)}} \cdot \frac{\text{m}^2}{\text{sec}}$$

$$\delta := 9.69 \cdot 10^{-10} \cdot \text{m}$$

Grain Boundary Thickness (approximated by 3b)

$$\lambda := 10 \cdot 10^{-6} \cdot \text{m}$$

Cavity spacing as suggested by LLNL

Creep stress as a function of temperature

$$\sigma_{e10}(t) := 100 \cdot 10^6 \cdot \text{Pa} \cdot \frac{T_{10}(t)}{T_{10}(120)} \quad \sigma_{e10p}(t) := 100 \cdot 10^6 \cdot \text{Pa} \cdot \frac{T_{10p}(t)}{T_{10p}(120)}$$

$$\sigma_{e10p}(120) = 1 \cdot 10^8 \text{ kg} \cdot \text{m}^{-1} \cdot \text{sec}^{-2}$$

$$\sigma_{e10}(120) = 1 \cdot 10^8 \text{ kg} \cdot \text{m}^{-1} \cdot \text{sec}^{-2}$$

$$b := 3.2 \cdot 10^{-10} \cdot \text{m}$$

Burgers vector for zircaloy

Defining the G(t) function

$$G_{10}(t) := \frac{32}{3 \cdot \pi^2} \cdot \frac{F_b^{\frac{3}{2}} \cdot \Omega \cdot \delta \cdot \sigma_{e10}(t) \cdot D_{gb10}(t)}{F_v \cdot k \cdot \lambda^3 \cdot T_{10}(t)}$$

$$G_{10p}(t) := \frac{32}{3 \cdot \pi^2} \cdot \frac{F_b^{\frac{3}{2}} \cdot \Omega \cdot \delta \cdot \sigma_{e10p}(t) \cdot D_{gb10p}(t)}{F_v \cdot k \cdot \lambda^3 \cdot T_{10p}(t)}$$

Damage integrals

$$\int_{120}^{228} G_{10}(t) \cdot 2629800 \cdot \text{sec} \, dt = 0.0242$$

max=0.0244; 99%=0.0242
reached after 108 months=9yrs

$$\int_{120}^{432} G_{10p}(t) \cdot 2629800 \cdot \text{sec} \, dt = 0.102$$

max=0.1030; 99%=0.1020
reached after 312 months=26yrs

Mathcad Document for Figure 12

$\alpha := .8727 \cdot \text{rad}$ Angle formed at junction of cavity and G.B.

$$F_b := \pi \cdot \sin(\alpha)^2$$

$$F_v := \frac{2 \cdot \pi}{3} \cdot (2 - 3 \cdot \cos(\alpha) + \cos(\alpha)^3)$$

$k := 1.38 \cdot 10^{-23} \frac{\text{joule}}{\text{K}}$ Boltzmann's Constant

$\Omega := 3.37 \cdot 10^{-29} \cdot \text{m}^3$ Atomic Volume by PNNL -- LLNL
suggested a value of $2.312 \cdot 10^{-29} \text{m}^3$

$R := 8.314 \frac{\text{joule}}{\text{K} \cdot \text{mole}}$ Gas Constant

$t_2 := 10..1000$ plotting variable

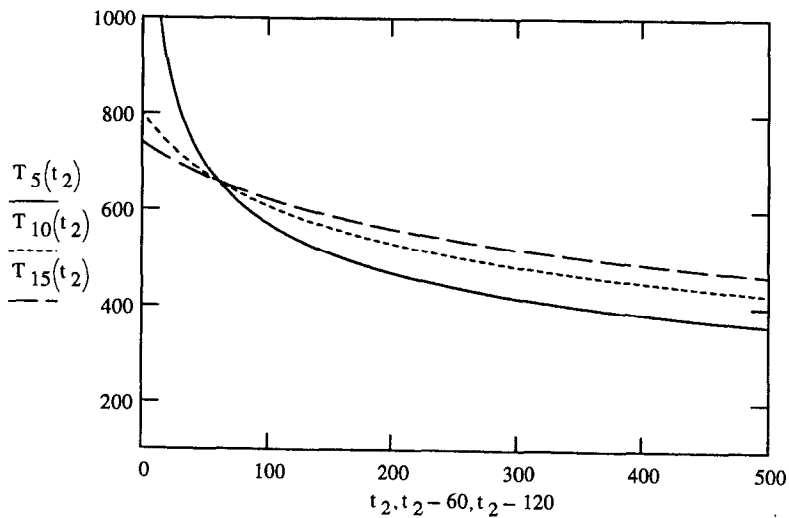
Creep temperature

$$T_{10}(t) := 2.54 \cdot 10^3 \cdot t^{-0.282} \cdot \text{K} \quad T_{10}(120) = 658.422 \text{ K}$$

$$T_5(t) := 2.09 \cdot 10^3 \cdot t^{-0.282} \cdot \text{K} \quad T_5(60) = 658.73 \text{ K}$$

$$T_{15}(t) := 2.85 \cdot 10^3 \cdot t^{-0.282} \cdot \text{K} \quad T_{15}(180) = 658.958 \text{ K}$$

Plot of temperature profiles normalized to one time reference frame



Diffusion coefficients

$$D_{gb5}(t) := 5.9 \cdot 10^{-6} \cdot e^{-\frac{131 \cdot 10^3 \frac{\text{joule}}{\text{mole}}}{R \cdot T_5(t)}} \cdot \frac{\text{m}^2}{\text{sec}}$$

$$D_{gb10}(t) := 5.9 \cdot 10^{-6} \cdot e^{-\frac{131 \cdot 10^3 \frac{\text{joule}}{\text{mole}}}{R \cdot T_{10}(t)}} \cdot \frac{\text{m}^2}{\text{sec}}$$

$$D_{gb15}(t) := 5.9 \cdot 10^{-6} \cdot e^{-\frac{131 \cdot 10^3 \frac{\text{joule}}{\text{mole}}}{R \cdot T_{15}(t)}} \cdot \frac{\text{m}^2}{\text{sec}}$$

$$\delta := 9.69 \cdot 10^{-10} \cdot \text{m}$$

Grain Boundary Thickness (approximated by 3b)

$$\lambda := 10 \cdot 10^{-6} \cdot \text{m}$$

Cavity spacing as suggested by LLNL

$$\sigma_{e5}(t) := 100 \cdot 10^6 \cdot \text{Pa} \cdot \frac{T_5(t)}{T_5(60)}$$

Stress as a function of temperature

$$\sigma_{e10}(t) := 100 \cdot 10^6 \cdot \text{Pa} \cdot \frac{T_{10}(t)}{T_{10}(120)}$$

$$\sigma_{e15}(t) := 100 \cdot 10^6 \cdot \text{Pa} \cdot \frac{T_{15}(t)}{T_{15}(180)}$$

$$b := 3.2 \cdot 10^{-10} \cdot \text{m}$$

Burgers vector for zircaloy

$$G_5(t) := \frac{32}{3 \cdot \pi^{\frac{1}{2}}} \cdot \frac{F_b^{\frac{3}{2}}}{F_v} \cdot \frac{\Omega \cdot \delta \cdot \sigma_{e5}(t) \cdot D_{gb5}(t)}{k \cdot \lambda^3 \cdot T_5(t)}$$

Defining G(t) function for each temp profile

$$G_{10}(t) := \frac{32}{3 \cdot \pi^{\frac{1}{2}}} \cdot \frac{F_b^{\frac{3}{2}}}{F_v} \cdot \frac{\Omega \cdot \delta \cdot \sigma_{e10}(t) \cdot D_{gb10}(t)}{k \cdot \lambda^3 \cdot T_{10}(t)}$$

$$G_{15}(t) := \frac{32}{3 \cdot \pi^{\frac{1}{2}}} \cdot \frac{F_b^{\frac{3}{2}}}{F_v} \cdot \frac{\Omega \cdot \delta \cdot \sigma_{e15}(t) \cdot D_{gb15}(t)}{k \cdot \lambda^3 \cdot T_{15}(t)}$$

Damage integrals

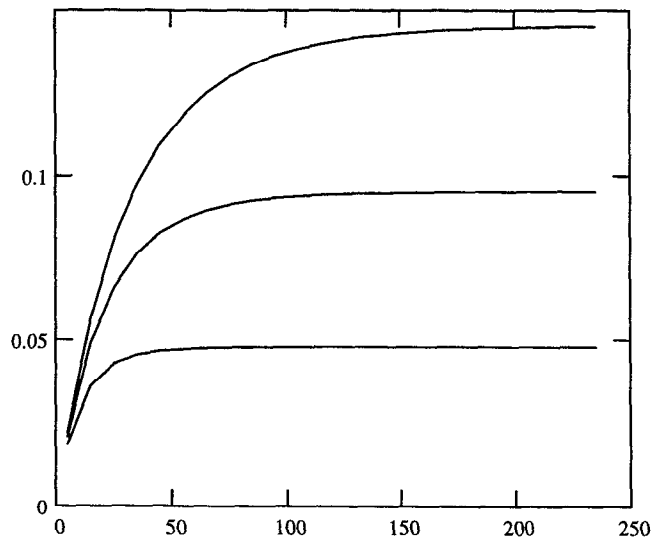
\int_{60}^{119}	$G_5(t) \cdot 2629800 \cdot \text{sec dt} = 0.0477$	max(5)=0.04817; 99%=0.04769 reached after 59 months=5years
\int_{120}^{237}	$G_{10}(t) \cdot 2629800 \cdot \text{sec dt} = 0.0943$	max=0.09526; 99%=0.0943 reached after 117 months=9.75yrs
\int_{180}^{356}	$G_{15}(t) \cdot 2629800 \cdot \text{sec dt} = 0.14425$	max=0.1457; 99%=0.14425 reached after 176 months=15yrs

Plotting variables

$t_{f5} := 65, 75.. 300$ $t_{f15} := 185, 195.. 420$ $t_{f10} := 125, 135.. 360$

$r := 0.01, 0.02.. 0.05$

$f(r) := r$



This document is a calculation of the failure time (or initial temp) that would be predicted if the least conservative values were chosen for all the constants put into the SW equations

$\alpha := .8727 \cdot \text{rad}$ $\alpha = 50.002 \cdot \text{deg}$ Angle formed at junction of cavity and G.B.

$F_b := \pi \cdot \sin(\alpha)^2$ Functions of the cavity dihedral angle (Raj and Ashby)

$F_v := \frac{2 \cdot \pi}{3} \cdot (2 - 3 \cdot \cos(\alpha) + \cos(\alpha)^3)$

$k := 1.38 \cdot 10^{-23} \cdot \frac{\text{joule}}{\text{K}}$ Boltzmann's Constant

$\Omega := 3.37 \cdot 10^{-29} \cdot \text{m}^3$ conservative (PNNL)

$\Omega := 2.312 \cdot 10^{-29} \cdot \text{m}^3$ non-conservative (LLNL's initial suggested value)
Gas Constant

$R := 8.314 \cdot \frac{\text{joule}}{\text{K} \cdot \text{mole}}$

Creep test temperature

$\delta := 1.6 \cdot 10^{-8} \cdot \text{m}$ PNNL Grain Boundary Thickness (more conservative)

$\delta := 9.69 \cdot 10^{-10} \cdot \text{m}$ LLNL Grain Boundary Thickness (less conservative)

$x := 2.938$ NRC profile

$T(t) := x \cdot 10^3 \cdot t^{-.282} \cdot \text{K}$

$T(60) - 273.15\text{K} = 652.855 \text{ K}$

$T(60) - 373 \text{ K} = 553.005 \text{ K}$

$D_{gb}(t) := 5.9 \cdot 10^{-6} \cdot e^{-\frac{131 \cdot 10^3 \cdot \frac{\text{joule}}{\text{mole}}}{R \cdot T(t)}} \cdot \frac{\text{m}^2}{\text{sec}}$

LLNL

$D_{gb}(60) = 2.405 \cdot 10^{-13} \text{ m}^2 \cdot \text{sec}^{-1}$

$D_{gb}(t) := 0.9 \cdot 10^{-4} \cdot e^{-\frac{183 \cdot 10^3 \cdot \frac{\text{joule}}{\text{mole}}}{R \cdot T(t)}} \cdot \frac{\text{m}^2}{\text{sec}}$

Least conservative (slowest) estimate based on bulk diffusion measurements in the literature (0.6Qsd=Qgb)

$D_{gb}(60) = 4.277 \cdot 10^{-15} \text{ m}^2 \cdot \text{sec}^{-1}$

$D_{gb}(t) := 4.2 \cdot \frac{10^{-13}}{\delta} \cdot e^{-\frac{167 \cdot 10^3 \cdot \frac{\text{joule}}{\text{mole}}}{R \cdot T(t)}} \cdot \frac{\text{m}^2}{\text{sec}}$

average estimate based on gb diffusion study

$D_{gb}(60) = 1.646 \cdot 10^{-13} \text{ m} \cdot \text{sec}^{-1}$

$$D_{gb}(t) := 3.4 \cdot 10^{-11} \cdot e^{-\frac{55.2 \cdot 10^3 \frac{\text{joule}}{\text{mole}}}{R \cdot T(t)}} \frac{\text{m}^2}{\text{sec}}$$

Most conservative (fastest) estimate based on bulk diffusion measurements in the literature (0.6Qsd=Qgb) [Borisov et al. 1958]

$$D_{gb}(60) = 2.616 \cdot 10^{-14} \text{ m}^2 \cdot \text{sec}^{-1}$$

$$D_{gb}(t) := 3.89 \cdot 10^{-6} \cdot e^{-\frac{175 \cdot 10^3 \frac{\text{joule}}{\text{mole}}}{R \cdot T(t)}} \frac{\text{m}^2}{\text{sec}}$$

PNNL (least conservative diffusion coefficient)

$$D_{gb}(60) = 5.225 \cdot 10^{-16} \text{ m}^2 \cdot \text{sec}^{-1}$$

$$\lambda := 2.6 \cdot 10^{-6} \cdot \text{m} \quad \text{PNNL (more conservative)}$$

$$\lambda := 10 \cdot 10^{-6} \cdot \text{m} \quad \text{LLNL (less conservative)}$$

$$\sigma_e(t) := 100 \cdot 10^6 \cdot \text{Pa} \cdot \frac{T(t)}{T(60)} \quad \text{100MPa stress used for SW analysis}$$

$$G(t) := \frac{32}{3 \cdot \pi^{0.5}} \frac{F_b^{\frac{3}{2}} \Omega \cdot \delta \cdot \sigma_e(t) D_{gb}(t)}{F_v k \cdot \lambda^3 T(t)}$$

Integration function

$$b := 3.2 \cdot 10^{-10} \cdot \text{m} \quad \text{Burgers vector}$$

$$T_m := 2125 \cdot \text{K} \quad \text{Melting temperature}$$

$$E(t) := \left(11.09 - 11.61 \frac{T(t)}{T_m} \right) \cdot 10^{10} \cdot \text{Pa} \quad \text{Elastic modulus from PNL}$$

$$\gamma := \frac{E(55) \cdot b}{100}$$

Free surface energy of silver (D.R. Askeland, "The Science and Engineering of Materials," Brooks/Cole Engineering Division, A Division of Wadsworth, Inc., pg 154)

$$\gamma = 0.189 \frac{\text{joule}}{\text{m}^2} \quad \text{Surface free energy}$$

$$r_c(t) := \frac{2 \cdot \gamma}{\sigma_e(t)}$$

Determination of the critical radius necessary for stable cavity formation

$$A_i := \frac{r_c(55)^2}{\lambda^2} \quad A_i = 1.36 \cdot 10^{-7} \quad \text{Determining the minimum area fraction of decohesion}$$

$$r_c(t) := \frac{2 \cdot \gamma}{\sigma_e(t)}$$

Initial cavity radius or critical cavity radius

$$f(A) := \frac{1 - A \cdot \left[\frac{\frac{2 \cdot \gamma}{\sigma_e(55)}}{\left(\frac{A \cdot \pi \cdot \lambda^2}{4 \cdot F_b} \right)^{\frac{1}{2}}} \right] \cdot (1 - A)}{\sqrt{A} \cdot \frac{1}{2} \cdot \ln\left(\frac{1}{A}\right) - \frac{3}{4} + A \cdot \left(1 - \frac{A}{4}\right)}$$

Area function defined by SW (this one was used for this analysis)

$$A_{val} := \int_{A_i}^{0.15} \frac{1}{f(A)} dA$$

$$T(60) - 273 \text{ K} = 653.005 \text{ K}$$

$$A_{val} = 0.026001$$

This document is a calculation of the failure time (or initial temp) that would be predicted if the most conservative values were chosen for all the constants put into the SW equations

$\alpha := .8727 \cdot \text{rad}$ $\alpha = 50.002 \cdot \text{deg}$ Angle formed at junction of cavity and G.B.

$F_b := \pi \cdot \sin(\alpha)^2$ Functions of the cavity dihedral angle (Raj and Ashby)

$F_v := \frac{2 \cdot \pi}{3} \cdot (2 - 3 \cdot \cos(\alpha) + \cos(\alpha)^3)$

$k := 1.38 \cdot 10^{-23} \frac{\text{joule}}{\text{K}}$ Boltzmann's Constant

$\Omega := 2.312 \cdot 10^{-29} \cdot \text{m}^3$ non-conservative (LLNL's initial suggested value)

$\Omega := 3.37 \cdot 10^{-29} \cdot \text{m}^3$ conservative (PNNL)

$R := 8.314 \frac{\text{joule}}{\text{K} \cdot \text{mole}}$ Gas Constant

$\delta := 9.69 \cdot 10^{-10} \cdot \text{m}$ LLNL Grain Boundary Thickness (less conservative)

$\delta := 1.6 \cdot 10^{-8} \cdot \text{m}$ PNNL Grain Boundary Thickness (more conservative)

Creep test temperature

$x := .937$ NRC profile

$T(t) := x \cdot 10^3 \cdot t^{-.282} \cdot \text{K}$

$T(60) - 273.15 \text{K} = 22.175 \text{K}$

$D_{gb}(t) := 5.9 \cdot 10^{-6} \cdot e^{-\frac{131 \cdot 10^3 \frac{\text{joule}}{\text{mole}}}{R \cdot T(t)}} \frac{\text{m}^2}{\text{sec}}$ LLNL $T(60) - 273 \text{K} = 22.325 \text{K}$

$D_{gb}(60) = 3.98 \cdot 10^{-29} \text{m}^2 \cdot \text{sec}^{-1}$

$D_{gb}(t) := 3.89 \cdot 10^{-6} \cdot e^{-\frac{175 \cdot 10^3 \frac{\text{joule}}{\text{mole}}}{R \cdot T(t)}} \frac{\text{m}^2}{\text{sec}}$ PNNL $D_{gb}(60) = 4.328 \cdot 10^{-37} \text{m}^2 \cdot \text{sec}^{-1}$

$D_{gb}(t) := 0.9 \cdot 10^{-4} \cdot e^{-\frac{183 \cdot 10^3 \frac{\text{joule}}{\text{mole}}}{R \cdot T(t)}} \frac{\text{m}^2}{\text{sec}}$ Least conservative (slowest) estimate based on bulk diffusion measurements in the literature (0.6Qsd=Qgb)

$D_{gb}(60) = 3.851 \cdot 10^{-37} \text{m}^2 \cdot \text{sec}^{-1}$

$$D_{gb}(t) := \frac{(4.2 \cdot 10^{-13})}{\delta} \cdot e^{-\frac{167 \cdot 10^3 \frac{\text{joule}}{\text{mole}}}{R \cdot T(t)}} \cdot \frac{\text{m}^2}{\text{sec}}$$

average estimate based on one gb diffusion study

$$D_{gb}(60) = 7.595 \cdot 10^{-35} \text{ m} \cdot \text{sec}^{-1}$$

$$D_{gb}(t) := 3.4 \cdot 10^{-11} \cdot e^{-\frac{55.2 \cdot 10^3 \frac{\text{joule}}{\text{mole}}}{R \cdot T(t)}} \cdot \frac{\text{m}^2}{\text{sec}}$$

Most conservative (fastest) estimate based on bulk diffusion measurements in the literature (0.6Qsd=Qgb) [Borisov et al. 1958]

$$D_{gb}(60) = 5.859 \cdot 10^{-21} \text{ m}^2 \cdot \text{sec}^{-1}$$

$$\lambda := 10 \cdot 10^{-6} \cdot \text{m} \quad \text{LLNL (less conservative)}$$

$$\lambda := 2.6 \cdot 10^{-6} \cdot \text{m} \quad \text{PNNL (more conservative)}$$

$$\sigma_e(t) := 100 \cdot 10^6 \cdot \text{Pa} \cdot \frac{T(t)}{T(60)} \quad \text{100MPa stress used for SW analysis}$$

$$G(t) := \frac{32}{3 \cdot \pi^{0.5}} \cdot \frac{F_b^{\frac{3}{2}}}{F_v} \cdot \frac{\Omega \cdot \delta \cdot \sigma_e(t) \cdot D_{gb}(t)}{k \cdot \lambda^3} \cdot \frac{1}{T(t)}$$

Integration function

$$b := 3.2 \cdot 10^{-10} \cdot \text{m} \quad \text{Burgers vector}$$

$$T_m := 2125 \cdot \text{K} \quad \text{Melting temperature}$$

$$E(t) := \left(11.09 - 11.61 \cdot \frac{T(t)}{T_m} \right) \cdot 10^{10} \cdot \text{Pa} \quad \text{Elastic modulus from PNL}$$

$$\gamma := \frac{E(55) \cdot b}{100}$$

Free surface energy of silver (D.R. Askeland, "The Science and Engineering of Materials," Brooks/Cole Engineering Division, A Division of Wadsworth, Inc., pg 154)

$$\gamma = 0.302 \frac{\text{joule}}{\text{m}^2}$$

Surface free energy

$$r_c(t) := \frac{2 \cdot \gamma}{\sigma_e(t)}$$

Determination of the critical radius necessary for stable cavity formation

$$A_i := \frac{r_c(55)^2}{\lambda^2}$$

$$A_i = 5.137 \cdot 10^{-6}$$

Determining the minimum area fraction of decohesion

$$r_c(t) := \frac{2 \cdot \gamma}{\sigma_e(t)} \quad \text{Initial cavity radius or critical cavity radius}$$

$$f(A) := \frac{1 - A}{\sqrt{A} \cdot \frac{1}{2} \cdot \ln\left(\frac{1}{A}\right) - \frac{3}{4} + A \cdot \left(1 - \frac{A}{4}\right)} \cdot \left[\frac{\frac{2 \cdot \gamma}{\sigma_e(55)}}{\left(\frac{A \cdot \pi \cdot \lambda^2}{4 \cdot F_b}\right)^{\frac{1}{2}}} \right] \cdot (1 - A)$$

Area function defined by SW (this one was used for this analysis)

$$A_{val} := \int_{A_i}^{.15} \frac{1}{f(A)} dA$$

$$A_{val} = 0.026349$$

$$G(t) := \frac{32 \cdot F_b^{\frac{3}{2}} \cdot \Omega \cdot \delta \cdot \sigma_e(t) \cdot D_{gb}(t)}{3 \cdot \pi \cdot \frac{1}{2} \cdot F_v \cdot k \cdot \lambda^3 \cdot T(t)} \quad \frac{A_{val}^{\frac{1}{3}} \cdot \pi^{\frac{1}{2}} \cdot F_v}{F_b^{\frac{3}{2}} \cdot 32} = 1.23543 \cdot 10^{-3}$$

$$T(60) = 295.325 \text{ K}$$

$$T(60) - 273.15 \text{ K} = 22.175 \text{ K}$$

$$T(63) = 291.29 \text{ K}$$

$$x = 0.937$$

$$\int_{60}^{150} G(t) \cdot 2629800 \cdot 10 \cdot \text{sec} dt = 0.02618$$

Failure as defined by S&W at 15% area fraction of decohesion occurs at 0.026

Failure predicted with an initial temperature of 56C (x=1.043 if not using recovery factor)

Failure predicted with an initial temperature of 22C (x=0.937 using recovery factor)

multiplied by a factor of 10 to account for recovery factor for low initial temperatures

Mathcad Document for LLNL + Herzig most/least conservative

$\alpha := .8727 \cdot \text{rad}$ Angle formed at junction of cavity and G.B.

$$F_b := \pi \cdot \sin(\alpha)^2 \qquad F_v := \frac{2 \cdot \pi}{3} \cdot (2 - 3 \cdot \cos(\alpha) + \cos(\alpha)^3)$$

$k := 1.38 \cdot 10^{-23} \frac{\text{joule}}{\text{K}}$ Boltzmann's Constant

$\Omega := 3.37 \cdot 10^{-29} \cdot \text{m}^3$ Atomic Volume by PNNL -- LLNL suggested a value of $2.312 \cdot 10^{-29} \text{m}^3$

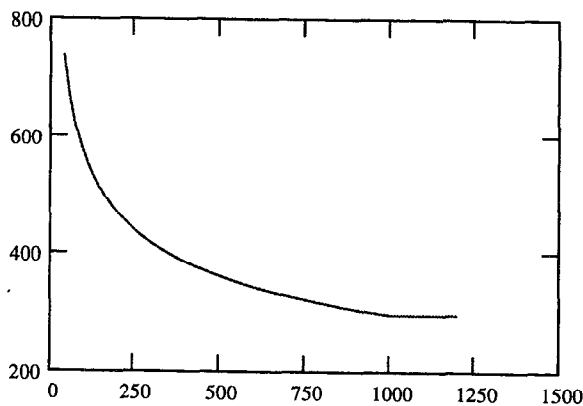
$R := 8.314 \frac{\text{joule}}{\text{K} \cdot \text{mole}}$ Gas Constant

Creep temperature

$T(t) := 2.09 \cdot 10^3 \cdot t^{-0.282} \cdot \text{K}$ PNNL temp profile

$T(t) := \text{if}(t < 1000, 2.09 \cdot 10^3 \cdot t^{-0.282} \cdot \text{K}, T(999.9))$

$t_2 := 40.. 1200$ plotting variable



Defining a range of temperature profiles based on PNNL profile (changing the initial temp by changing the coefficient)

$T(t) := 2.0705 \cdot 10^3 \cdot t^{-.282} \cdot \text{K}$ $T(60) - 273 \text{ K} = 379.584 \text{ K}$

$T_1(t) := 2.403 \cdot 10^3 \cdot t^{-.282} \cdot \text{K}$ $T_1(60) - 273 \text{ K} = 484.382 \text{ K}$

if constant temp

$T(t) := 570.5 \text{ K}$

$T_1(t) := 658 \cdot \text{K}$

temperature in Celcius

$$\delta := 9.69 \cdot 10^{-10} \cdot \text{m}$$

Grain Boundary Thickness (approximated by 3b)

Grain boundary diffusion coefficients (based on Herzig and Vieregge)

most conservative

least conservative

$$D_{gb}(t) := \frac{1.01 \cdot 10^{-12}}{\delta} \cdot e^{-\frac{160 \cdot 10^3 \frac{\text{joule}}{\text{mole}}}{R \cdot T(t)}} \cdot \frac{\text{m}^3}{\text{sec}}$$

$$D_{gb1}(t) := \frac{1.7 \cdot 10^{-13}}{\delta} \cdot e^{-\frac{174 \cdot 10^3 \frac{\text{joule}}{\text{mole}}}{R \cdot T_1(t)}} \cdot \frac{\text{m}^3}{\text{sec}}$$

Hoop stress in fuel cladding

$$\sigma_e(t) := 100 \cdot 10^6 \cdot \text{Pa} \cdot \frac{T(t)}{T(60)}$$

$$\sigma_{e1}(t) := 100 \cdot 10^6 \cdot \text{Pa} \cdot \frac{T_1(t)}{T_1(60)}$$

$$\lambda := 10 \cdot 10^{-6} \cdot \text{m}$$

Cavity spacing as suggested by LLNL

defining integration function G(t)

$$G(t) := \frac{32}{3 \cdot \pi^{0.5}} \cdot \frac{F_b^{\frac{3}{2}} \cdot \Omega \cdot \delta \cdot \sigma_e(t) \cdot D_{gb}(t)}{F_v \cdot k \cdot \lambda^3 \cdot T(t)}$$

$$G_1(t) := \frac{32}{3 \cdot \pi^{0.5}} \cdot \frac{F_b^{\frac{3}{2}} \cdot \Omega \cdot \delta \cdot \sigma_{e1}(t) \cdot D_{gb1}(t)}{F_v \cdot k \cdot \lambda^3 \cdot T_1(t)}$$

$$b := 3.2 \cdot 10^{-10} \cdot \text{m}$$

Burgers vector for zircaloy

$$T_m := 2125 \cdot \text{K}$$

Melting temperature for zircaloy

$$E(t) := \left(11.09 - 11.61 \cdot \frac{T(t)}{T_m} \right) \cdot 10^{10} \cdot \text{Pa}$$

Elastic modulus in temperature range of interest as suggested by Chin

The following exercise is only to verify that the damage level (integral of G(t)) should be 0.026 after 15% area fraction of decohesion

$$\gamma := \frac{E(60) \cdot b}{100} \quad \text{Free surface approximation}$$

$$\gamma = 0.255 \frac{\text{joule}}{\text{m}^2}$$

$$r_c(t) := \frac{2 \cdot \gamma}{\sigma_e(t)} \quad \text{Determining the critical cavity radius (initial cavity radius)}$$

$$r_c(60) = 5.103 \cdot 10^{-9} \text{ m}$$

$$A_i := \frac{r_c(60)^2}{\lambda^2} \quad A_i = 2.604 \cdot 10^{-7} \quad \text{Determining an initial area fraction of decohesion}$$

$$f(A) := \frac{1}{\sqrt{A} \left[\frac{1}{2} \ln \left(\frac{1}{A} \right) - \frac{3}{4} + A \cdot \left(1 - \frac{A}{4} \right) \right]} \left[1 - \frac{\frac{2 \cdot \gamma}{\sigma_e(55)}}{\left(\frac{A \cdot \pi \cdot \lambda^2}{4 \cdot F b} \right)^{\frac{1}{2}}} \right] \cdot (1 - A)$$

$$A_{\text{val}} := \int_{A_i}^{0.15} \frac{1}{f(A)} dA$$

$$A_{\text{val}} = 0.026$$

So the damage level that corresponds to 15% decohesion is 0.026

$$\int_{60}^{540} G(t) \cdot 2629800 \cdot \text{sec} dt = 0.02605$$

$$T(60) - 273 \text{ K} = 297.5 \text{ K}$$

$$\int_{60}^{540} G_1(t) \cdot 2629800 \cdot \text{sec} dt = 0.02611$$

$$T_1(60) - 273 \text{ K} = 385 \text{ K}$$

Using the profile suggested by PNNL (power decay), the maximum temperature for the most conservative Herzig GB diffusion coefficient is

$$T_{\text{max}} = 380\text{C}$$

and the least conservative is

$$T_{\text{max}} = 484\text{C}$$